DEVELOPMENT OF A NOVEL METHOD IN ELECTROLESS COPPER PLATING

SENG SWEE SONG

NATIONAL UNIVERSITY OF SINGAPORE

2004

DEVELOPMENT OF A NOVEL METHOD IN ELECTROLESS COPPER PLATING

SENG SWEE SONG
(B.Eng. (Hons), NUS)

A THESIS SUBMITTED

FOR THE DEGREE OF MASTER OF ENGINEERING

DEPARTMENT OF CHEMICAL AND BIOMOLECULAR

ENGINEERING

NATIONAL UNIVERSITY OF SINGAPORE

2004

ACKNOWLEDGEMENTS

TABLE OF CONTENTS

SUMMARY

This study examines the effect of chelating agents, stabilizers and surfactants on the electroless copper plating process with emphasis in the surface morphology of the plated copper. The reducing agent was formaldehyde and the substrate was a acrylonitrile-butadiene-styrene (ABS) film formed from a plate casting method. Electroless plating was performed at room temperature (25 $^{\circ}$C) and a constant stirring rate was provided with a magnetic stirrer.

Structurally similar chelating agents: sodium potassium tartrate, trisodium citrate and potassium sodium salt of malic acid were used separately in each of the plating solution as the main chelating agent. A fine grain copper structure was exhibited by the sodium potassium tartrate and trisodium citrate, while potassium sodium salt of malic acid forms coarse grain structures. Plating rate of the structurally similar chelating agent are in the increasing order of sodium potassium tartrate, potassium sodium salt of malic acid and trisodium citrate. All the plated copper were found to contain 111 and 200 crystallographic planes. Cyclic voltammetry suggests that the dual chelating agent system of sodium potassium tartrate and disodium EDTA are electrochemically favourable as compared the single chelating agent.

Amino acids, such as L-methionine and glycine, were selected to replace the bi-pyridine. The function of the bi-pyridine as the stabilizer was verified as the absence of bi-pyridine decreases the decomposition time of the plating solution. L-methionine, a sulphur containing amino acid, results in high plating rate. However, its concentration is not proportional to the plating rate. L-methionine also induces fine grain copper structures similar to those obtained using bi-pyridine. Glycine does not

result in a high plating rate and coarse grain structure was formed. Sulphur containing amino acids can affect the plating rate and grain size to a certain extent.

One special class of surfactant, polyethylene glycol (PEG) was selected for the purpose of investigating the effect of surfactant on the surface morphology of the electrolessly plated copper. Various molecular weights of PEG in 2.0 g/L were added separately to the electroless copper plating solution containing sodium potassium tartrate as the main chelating agent. Highly uniform copper grain structures of about 100-200 nm in size were formed. Higher molecular weight of PEG results in a smaller copper grain size and however, above 10,000 g/mol, this trend was not obvious. Thermal properties of the ABS film are also affected when PEG was introduced to the plating solution. The second glass transition temperature (Tg) generally increases with the molecular weight of the PEG. This may due to the strong Cu-CN bonding at the copper-ABS interface, which results in a more orderly structure of the ABS polymer. Cyclic voltammetry shows that addition of PEG favours electroless copper deposition.

NOMENCLATURE

γ	Surface tension of the metal-solution interface
A	Amperes
E_{mp}^{o}	Equilibrium potential
e^{-}	Electrons
E_o	Standard redox potential at $25^{o}C$
E_{Me}	Potential of the metal in the solution containing metal ions
E_{Red}	Potential of the metal in the solution containing reducing agents
F	Faraday's constant
H_{ads}	Adsorbed hydrogen
IC	Integrated circuit
i_a	Anodic current density
i_c	Cathodic current density
i_{total}	Total current density
K	Observed rate constant at a given temperature
K_a	Anodic reaction rates
K_c	Cathodic reaction rates
M	Metal
n	Number of electrons
Ox	Oxidizing agent
R	Reductant
R_{ads}	Electroactive species originated from Red

RDS	Rate determining step
Red	Reducing agent
r	Reaction rate
r*	Critical nuclei radius
Tg	Glass transition temperature
V	Volts

LIST OF FIGURES

LIST OF TABLES

Chapter 1

Introduction

Electroless plating uses a redox reaction to deposit metal on an object without the passage of an electric current. It is autocatalytic in nature as after the first few atomic layers of metal are deposited on the activated substrate, subsequent reduction of metal occurs on the plated metal surface by itself, which means that the catalyst plays no part in the electroless plating process after that. A chemical reducing agent is responsible for supplying electrons for the conversion of metal ions to elemental form. The overall reaction of metal deposition can be represented as follows:

$$M^{n+}_{solution} + \text{Re}\,d_{solution} \xrightarrow{\quad catalytic.surface \quad} M_{lattice} + Ox_{solution} \qquad (1.1)$$
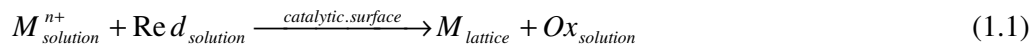
where Ox is the oxidation product of the reducing agent, Red. The catalytic surface can be the substrate or catalytic nuclei of metal M' dispersed on a noncatalytic substrate. The above redox reaction only proceeds on a catalytic surface. Thus, the above equation is a heterogeneous catalytic electron-transfer reaction and can only proceed provided that the homogeneous reaction between the M^{n+} and Red in the bulk solution is suppressed. Metals that can be electrolessly deposited include silver, gold, cobalt, copper, nickel, palladium, platimum, ruthenium and tin. Commonly used reducing agents consist of formaldehyde (HCHO), sodium phosphinate monohydrate (NaH_2PO_2), potassium borohydride (KBH_4) and boron hydride dimethylamine ($(CH_3)_2NH.BH_3$) (Murphy et al., 1992). Electroless plating offers many advantages over electroplating, but it is not without its drawbacks. Table 1.1 shows some of the advantages and disadvantages of electroless plating (Hajdu, 1996), (Decker, 1995a), (Lowenheim, 1974).

Table 1.1 Advantages and disadvantages of electroless plating

Advantages	Disadvantages
Uniformity of coverage	High operating costs due to more expensive chemical reducing agents
Ability to plate selectively	Shorter plating bath
Less porous deposits compared to electrodeposits	
Absence of power supplies, electrical contacts and electrical measuring instruments	
Unique chemical, mechanical or magnetic properties of deposit	

The history of electroless plating dates back to 1946 where Brenner and Riddel discovered the electroless nickel-phosphorous plating during their nickel electroplating experiments. Subsequently, electroless copper plating was reported in 1947 by Narcus. The early electroless plating solution was commonly plagued by problems such as "triggering"(spontaneous decomposition of the bath), "plate-out" (decomposition over a prolonged period), dark deposit colour, rough deposit, coarse grain size etc. The modern electroless plating is more stable due to well characterized and controlled trace additives.

Applications of electroless plating encompass a wide range of areas with electroless copper and nickel as the two most widely used plating metals. Electroless copper plating is commonly used in printed circuit board (PCB) industries, plating on plastic industries (POP) and electro magnetic interference (EMI) shielding. The electroless nickel plating is used extensively for decorative, engineering and electroforming purposes (Decker, 1995b), (Baudrand, 1995).

Since electroless copper plating has such diverse applications, it would be interesting and useful to investigate the effect of the plating solution chemistry on the type of electrolessly plated copper, so as to cater the needs for the many applications. As such, the primary aim of this research is to examine the effects of chelating agents, stabilizers and surfactants on the electrolessly deposited copper and as well as the plating process, so as to establish relationship between the composition of the plating solution and the quality of the deposited copper.

Chapter 2

Literature Review

Many aspects of electroless copper plating have been reported. It would be voluminous to describe all of them is this chapter. Selected studies that are relevant to the fundamental research of electroless copper plating solution chemistry are presented.

2.1 Fundamentals of electroless copper plating

2.1.1 Electroless copper plating bath chemistry

The overall electroless copper plating reaction is theoretically given as:

$$Cu^{2+} + 2HCHO + 4OH^- \rightarrow Cu^o + H_2 + 2H_2O + 2HCO_2^-$$ (2.1)

This equation employs formaldehyde (HCHO) as the reducing agent. Theoretically, it requires 4 moles of hydroxyl ions and 2 moles of formaldehyde to produce 1 mole of deposited copper. Actually, other side reactions do occur, the Cannizzaro reaction is a good example, in which formaldehyde disproportionates and is given as follows:

$$2HCHO + OH^- \leftrightarrow CH_3OH + HCOO^-$$ (2.2)

The above Cannizaro reaction consumes additional formaldehyde and base. Also, formaldehyde may reduce the cupric ions to form cuprous oxide, which is an unwanted product:

$$2Cu^{2+} + HCHO + 5OH^- \rightarrow Cu_2O + HCOO^- + 3H_2O$$ (2.3)

With only the copper ions and formaldehyde do not therefore ensure electroless copper deposition on the substrate. The modern electroless copper plating bath consists

of complexing agents, a buffer, a stabilizer, accelerators and surfactants (Decker, 1995a).

Complexing agent

The electroless copper plating solution favours an alkaline medium (i.e. high pH) to acidic medium (i.e. low pH) because the thermodynamic driving force for copper deposition is greater. Complexing agents are added to prevent precipitation within the plating solution at high pH. Commonly used complexing agents include ethylenediaminetraacetic acid (EDTA), malic acid (Mal), succinic acid (Suc), tartrate (Tart), citrate (Cit), triethanolamine (TEA) and ethylenediamine (En) (Mallory and Haju, 1990), (Shacham-Diamand et al, 1995).

Buffer

During the plating process, pH of the plating solution changes as oxidation of the reducing agent involves the formation of either hydrogen (H^+) or hydroxide (OH^-) ions. Therefore, buffers are added to stabilize the plating solution pH. Sodium carbonate is a commonly used buffer (Mallory and Haju, 1990).

Stabilizer

Stability of electroless metal plating solution depends on the probability and the rate of nucleation in the solution, i.e. its growth or dissolution. The critical radius of nuclei (r^*) can be expressed by Equation 2.4.

$$r^* = \frac{2\gamma v}{[nF(E_{Me} - E_{\mathrm{Re}d})]} \qquad (2.4)$$

where γ = surface tension of the metal-solution interface

v = molar volume of the metal

n = number of electrons in the redox reaction

F = Faraday's constant

$E_{Me}, E_{\mathrm{Re}d}$ = potential of the metal in the solution containing metal ions and reducing agents, respectively

When the nuclei in the plating solution is larger than r* in Equation 2.4, the solution becomes unstable and spontaneously decomposes. The probability that the solution will decompose increases with the decrease in nuclei critical radius. From Equation 2.4, it is easily seen that by reducing the difference between E_{Me} and E_{Red}, the stability of the electroless plating bath is increased. Decreasing the solution pH (a more positive E_{Red}) will also have the same effect.

Stabilizers can be used to prevent spontaneous decomposition, as they are known to competitively adsorb on the active nuclei, which block its growth and shield them from the reducing agent in the plating solution. Since, the stabilizers can also adsorb on the activated substrate, its concentration must not be in excess. Suitable stabilizers are metal-containing compounds (V, Mo, Nb, W, Re, Sb, Bi, Ce, U, Hg, Ag, As), sulphur-containing compounds (sylphites, thiosulphates, sylphates, etc.), nitrogen-containing compounds (tetracyanoethylene, cyanides, pyridines, 2,2'-dipyridil, etc.), and sulphur- and nitrogen-containing compounds (cycteines, cystines, diethlditiocarbamates, thiosemicarbazide, etc.)

Some stabilizers may also form complexes with Cu(I) and prevent reduction to Cu^{o} in the bulk solution. Examples of Cu (I) complexing agents are cyanides, 2,2'-dipyridyl and 1,10-phenanthrolines. In addition, oxidizing agents such as chromates, Fe(III), chlorates, iodates, molybdates, hydrogen peroxide, or oxygen can be introduced to the solution by stirring or air agitation to oxidize Cu(I) to Cu(II) (Mallory and Haju, 1990), (Shacham-Diamand et al, 1995).

<u>Accelerators</u>

The introduction of complexing agents retard the plating rate, accelerators which are generally anions, such as cynide, are added to increase the plating rate to an acceptable level without causing plating bath instability. The plating rate of common electroless plating bath ranges from 1-5 µm/hr. With the introduction of additives, the plating rate can increase by a few folds. Typical additives are pyridine, 2-mercaptobenzothiazole sodium salt, guanidine hydrochloride and cytosine (Coombs, 1996), (Nuzzi, 1983). Possible reasons to explain the action of the additives include activation of the catalyst and formation of labile copper complexes (Bielinski, 1987).

<u>Surfactants</u>

The role of surfactants is to decrease the surface tension of the plating solution and helps to remove the hydrogen bubbles formed on the surface of electroless copper deposits by inhibiting the dehydrogenation reaction. Anionic, non-ionic, amphoteric or cationic surfactants may be used. The selection of surfactants depends on the operating temperature, the pH and ionic strength of the electroless plating bath. Popular surfactants include complex organic phosphate esters, anionic perfluoroalkyl sulfonates and carboxylates, non-ionic fluorinated alkyl alkoxylates and cationic fluorinated quaternary ammonion compounds (Shacham-Diamand et al, 1995).

2.1.2   Mixed potential of electroless metal deposition

The principle of superposition of the partial electrochemical processes was proposed by Wager and Traud in the 1930s and is commonly known as mixed potential. Subsequently, Paunovic and Saito applied the mixed potential concepts to interpret the process of electroless deposition of metal. The mixed potential states that the rate of a faradaic process is independent of other faradaic processes occurring at the electrode

and depends only on the electrode potential. In this manner, polarization curves for independent anodic and cathodic processes can be added to predict the overall rates and potentials which may exist when more than one reaction occurs simultaneously at an electrode. The overall reaction can be represented by considering a redox reaction occurring on an inert electrode given in (2.5):

$$Ox + ne \underset{K_a}{\overset{K_c}{\Longleftrightarrow}} \mathrm{Re}\,d \qquad (2.5)$$
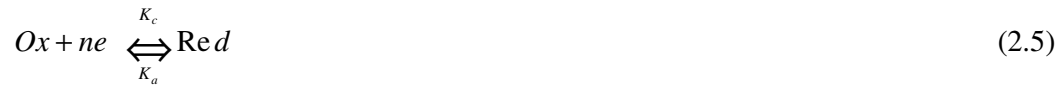
where Ox is the oxidation product of the reducing agent, Red

      ne is the n number of electrons

      K_c and K_a is the rates of the cathodic and anodic reactions respectively

There are two direct consequences of the above redox equation.

1. At any point, the total current density, i_{total} can be expressed by the following equation:

$$i_{total} = i_c + i_a \qquad (2.6)$$

    where i_{total} represents the total current density

        i_c and i_a represent the cathodic and anodic current densities respectively

Initially, the two opposing reactions occur at different rates, leading to a non-zero total current density. After some time, the two reactions proceed at the same rates and the total current density, i_{total} becomes zero. Equilibrium is established at this point.

2. The potential at which this equilibrium occurs is described as the equilibrium potential (A.K.A steady-state mixed potential), E_{mp}^0. This equilibrium potential can be determined in the thermodynamic sense using the Nernst equation.

Consider a case where two or more reactions occur simultaneously at the electrode surface. A good example is the copper/formaldehyde electroless plating process. In this set of reaction, the anodic reaction is the oxidation of the reducing agent (formaldehyde):

$$HCHO + 3OH^- \Leftrightarrow HCOO^- + 2H_2 + 2e^- \quad (\text{pH=14, } E_o = -1.07) \tag{2.7}$$

or simply $R^o \rightarrow R^{z+} + ze^-$ (2.8)
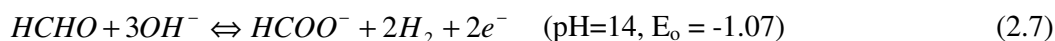
The cathodic reaction is the reduction of the metal(copper) complex

$$[CuL_6]^{(6n-2)-} \Leftrightarrow Cu^{2+} + 6L^{n-} \tag{2.9}$$

$$Cu^{2+} + 2e^- \rightarrow Cu^o \tag{2.10}$$

or simply $M^{Z+} + ze^- \rightarrow M^0$ (2.11)

where R and M represent the reductant and the metal respectively.

Therefore, the overall reaction can be represented by

$$M^{z+} + R^o \rightarrow M^o + R^{z+} \tag{2.12}$$

The above equation can be electrochemically described in terms of three current-potential (i-V) curves shown in Fig. 2.1. The overall reaction, $i_{total} - V$ is represented by a dashed curve in Fig. 2.1. The current-potential curve, $i_c - V$ for the reduction of M^{z+} ions in the absence of the reducing agent lies below the dashed curve, and the current-potential curve, $i_a - V$ for the oxidation of the reducing agent in the absence of the M^{z+} ions lies above the dashed curve. The point where the dashed line

crosses the potential axis is known as the equilibrium potential, E_{mp}^0 described earlier, and it corresponds to a zero current density. From Fig. 2.1, it can be seen that the equilibrium potential of the reducing agent, $E_{eq,\mathrm{Re}d}$, must be more negative than the metal electrode, $E_{eq,M}$ in order for Red to be function as an electron donor and M^{z+} as an electron acceptor.
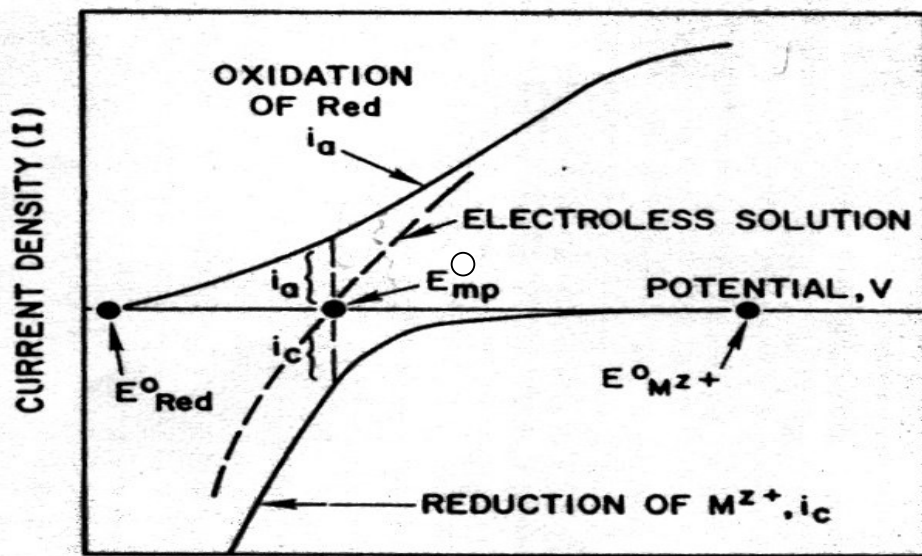
Fig 2.1 Total and component current-potential curves for the overall electroless deposition reaction (Murphy et al., 1992)

In addition, according to the mixed potential theory, the partial reduction and oxidation electrochemical processes occurs at the same time, but spatially separated on the substrate. This means the catalytic sites on the substrate consists of a mixture of cathodic and anodic sites (Mallory and Haju, 1990), (Murphy et al., 1992).

2.1.2.1 The cathodic half reaction

The mechanism of the partial cathodic reaction involves at least two basic elementary steps (Paunovic, 1977):

1. Formation of the electroactive species

2. Charge transfer from the catalytic surface to the electroactive species (electron capture)

The electroactive species, M^{z+} are formed by dissociation of the metal complex, $[ML_x]^{z\ +\ xp}$ and shown in Equation 2.13. In general, the metal ions in the electroless metal deposition are complexed with at least one ligand.

$$\left[ML_x\right]^{z+xp} \rightarrow M^{z+} + xL^{P} \tag{2.13}$$

where p is the charge of the ligand L

z is the charge of the noncomplexed metal ion

z + xp is the charge of the complexed metal ion

The transfer of z electrons from the catalytic surface to the electroactive species, M^{z+} proceeds in steps. The first charge transfer or the one electron transfer is usually the rate-determining step(RDS):

$$M^{z+} + e^- \xrightarrow{\quad RDS \quad} M^{(z-1)+} \tag{2.14}$$

2.1.2.2 The anodic half reaction

Similar to the cathodic partial reaction, the mechanism of the anodic partial reaction proceeds in at least two elementary steps (Murphy et al., 1992):

1. Formation of the electroactive species

11

2. Charge transfer from the electroactive species to the catalytic surface(electron injection)

A general mechanism for the formation of electroactive species of the reducing agent, Red is given by Murphy et al. (1992):

$$R - H \xrightarrow{breaking.RH.bond} R_{ads} + H_{ads}$$ (2.15)

where R-H is the reducing agent, Red

R_{ads} is the electroactive species originating from Red

H_{ads} is the adsorbed hydrogen

According to the above mechanism, the electroactive species, R_{ads} is formed in the process of dissociative adsorption (dehydrogenation) of the reducing agent Red, represented as R-H on the catalytic surface. This process usually proceeds through an intermediate, R'. For example, if the reducing agent is formaldehyde (HCHO), the intermediate, R' is $H_2C(OH)O^-$ and the electroactive species, R_{ads} is $[HC(OH)^-]_{ads}$.

The H_{ads} can be either desorbed by a chemical reaction shown in Equation 2.16a or by an electrochemical reaction shown in Equation 2.16b.

$$H_{ads} \rightarrow \frac{1}{2} H_2$$ (2.16a)

$$H_{ads} \rightarrow H^+ + e^-$$ (2.16b)

For example, in electroless deposition of copper, when the reducing agent is formaldehyde. Initially, when the substrate is covered with palladium or platinum, H_{ads} desorbs via an electrochemical reaction 2.16b. After the substrate is covered with copper, H_{ads} desorbs via a chemical reaction 2.16a.

The charge transfer from the electroactive species, R_{ads} to the catalytic surface (electron injection) in an alkaline medium is given by:

$$R_{ads} + OH^- \rightarrow ROH + e^- \qquad (2.17)$$

2.1.3   Kinetics of electroless copper deposition

Since most of the electroless copper plating solutions consist of four essential components: copper ions, alkalinity, formaldehyde and ligands, a number of studies on the effect of these four components on the rate of copper deposition have been performed (Donahue, 1980), (Dumesic et al. 1974), (Schmacher et al. 1985), (El-Raghy and Abo-Salama, 1979). Generally, the overall rate law for electroless copper deposition can be written as:

$$r = k[Cu^{2+}]^a[OH^-]^b[HCHO]^c[Ligand]^d \qquad (2.18)$$

where k is the observed rate constant at a given temperature

a, b, c and d are the reaction orders for the reactants

Some experimentally determined reaction orders for the four components are given in Table 2.1. As shown in Table 2.1, the reaction orders are quite diverse. A number of factors have contributed to this phenomenon. Firstly, the substrates used in each electroless copper plating solution are made of different materials, and thus have varying degrees of catalytic activity. Some subtrates are metal, while others are catalyzed dielectrics. Secondly, the time frame at which measurements were taken is critical. Dumesic et al. (1974) reported that the rate of initial copper deposition depends strongly on formaldehyde concentration, but not on copper concentration, whereas the final rate is independent of the formaldehyde concentration. The third reason is due to mass transfer effects. In the absence of forced convection, the primary

means of mass transfer is from the microconvection of hydrogen bubbles and evolution from the reaction surface (Donahue, 1980). The observed rate constant k is a function of temperature and it obeys the Arrhenius equation. From the slope of an Arrhenius plot, an activation energy of 60.9 KJ mol^{-1} was estimated.

Table 2.1 Experimentally determined reaction orders for electroless copper plating solution (Mallory and Haju, 1990)

Cu^{2+}	OH-	HCHO	Ligand
0.47	0.18	0.07	- (tartrate)
0.37	0.25	0.08	0.19 (tartrate)
0.78	<0.02	0.13	<0.02 (tartrate)
0.43	-0.70	0.16	-0.04 (EDTA)
1.00	0.37	0.00	- (EDTA)[a]
0.00	1.00	0.68	- (EDTA)[b]
0.00	0.00	1.00	0 (EDTA)

[a] refers to the final deposition rate
[b] refers to the initial deposition rate

Presently, most electroless copper plating solutions contain additional components to enhance the properties of copper deposits and improve the plating solution stability. These additional components will affect the plating kinetics, but it is too complicated to study these systems. Therefore, kinetic studies are largely restricted to the four essential components.

A variety of measurement techniques have been employed to obtain kinetic data for electroless copper plating. Dumesic et al. (1974) described an optical method, which is based on the monochromatic light at a sensitized transparent rotating cylinder. They were successful in distinguishing the changes in the initial plating rate and the final rate region and reported that the reaction order for formaldehyde changed from 0.68 in the initial stages of plating to 0 during the final stages. Schumacher et al. (1985) utilized a quartz crystal microbalance to measure the deposition rate of electroless copper plating. This technique offers the advantage of in-situ measurement

compared to the macroscopic weight measurements. Using a resistance probe, in which the cathode comprises one arm of a wheatstone bridge, Vitkavage et al. (1983) reported that the plating rate may be monitored by observing changes in resistance with time.

2.1.4   Alkaline-free electroless copper plating bath

The conventional electroless copper plating baths are usually alkaline-based, because it is more favourable in a thermodynamic sense. However, acid-based electroless copper deposition is still thermodynamically feasible. Tseng et al. (2001) studied the electroless copper deposition on a SiO_2/Ta/TaN substrate using an acid-based plating bath. The plating bath consists of copper chloride ($CuCl_2$), nitric acid (HNO_3), ammonia fluoride (NH_4F) and hydrogen fluoride (HF) and is maintained at a pH of 4.5. The NH_4F and HF serve as the buffer in the plating solution. The role of $CuCl_2$ is not limited to the supply of copper ions, the Cl^- ion can help to prevent the formation of nitrogen dioxide gas by suppressing the reduction of nitric acid. In addition, Cl^- and F^- act as complexing agents and transmit electrons from silicon, Si to Cu^{2+}, where Si act as the reducing agent. The presence of nitric acid ensures that shining reddish copper is deposited, omission of nitric acid results in dark-reddish dots.

Shacham-Diamand et al. (1995) outlined an alkaline-free electroless copper plating bath suitable for integrated circuit (IC) fabrication. The composition and various functions of the components in the plating bath are given in Table 2.2. Another type of alkaline-free electroless plating bath was proposed by Hung (1988). The plating bath consists of 0.024 M copper sulphate ($CuSO_4$), 0.052 M sodium citrate ($C_6H_5Na_3O_7$), 0.27 M sodium hypophosphate ($NaH_2PO_2.H_2O$), 0.5M boric acid

(H$_3$BO$_3$) and 0.002 M nickel sulphate (NiSO$_4$). The pH was maintained at 9.2 and the plating temperature was set at 65 $^{\circ}$C. The substrate was a copper sheet, which is activated by 0.1% palladium chloride (PdCl$_2$) solution for 1 minute. Nickel ions were added as nickel sulphate to promote autocatalysis and continuous plating.

Table 2.2 Components of alkali-free electroless copper plating bath (Shacham-Diamand et al., 1995)

Component	Quantity (Range only)	Function
Copper sulphate (CuSO$_4$.5H$_2$O)	0.05-0.1 M	Supply copper ions
Tetraethylammonium hydroxide [N(C$_2$H$_5$)$_4$OH]	0.5-1.0 M	Supply electrons
Ethylenediaminetetraacetic acid, EDTA [C$_{10}$H$_{14}$N$_2$O$_8$]	0.1 M	Complexing agent
Formaldehyde (HCOH) (or alternatively glyoxylic acid)	0.01-0.1 M	Reducing agent
Tetramethyammonium cyanide [N(CH$_3$)$_4$CN]	0-0.01 M	Complexing agent (Affects morphology)
GAF RE-610	0.5-2 %	Surfactant (Reduces surface tension)

Alkaline-free electroless copper plating solution is generally preferred in IC manufacturing. This is because alkali metal ions such as sodium and potassium from the hydroxides can drift quickly into silicon dioxide under an electric field, which causes the accumulation of positive ion charges near the silicon-silicon dioxide interface. This extra charge alters the device characteristics, possibly resulting in a circuit failure (Sze, 1981).

2.2   General processes and principles of plating plastics

Since the research was originally undertaken on electroless copper plating on acrylonitrile-butadiene-styrene(ABS), which is a plastic, it is useful to briefly discuss the general processes and practices in the plastic plating industry. Plating on plastics is generally classified under two broad stages: pretreatment and electroplating.

2.2.1 Introduction

Plating of plastics has been around for forty over years since the early 1960s. Industries at that time saw the need to develop the plastic plating technology due to the following reasons:

- Better resistance to corrosion

- Lower cost

- No secondary operations (i.e., no deflashing or buffing)

- Design freedom (i.e., the ability to mold large and complex parts)

- Weight reduction

Of the above reasons, weight reduction is one of the most important reasons for the increase in popularity of plating on plastics. This greatly benefits the automobile industry, which reduces the fuel usage (Mallory and Haju, 1990).

Many grades of plastics have been proven to be electrolessly platable. They include ABS, polypropylene, polysulfone, polyethersulfone, polyetherimide, teflon, polyarylether, polycarbonate, polyphenylene oxide (modified), polyacetal, urea formaldehyde, diallyl phthalate, mineral-reinforced nylon (MRN) and phenolic. One of the earliest plastics plated on a large scale was polypropylene. ABS is the most widely used plastics for plating. It is a thermoplastic that has a acrylonitrile-styrene matrix

with butadiene rubber uniformly distributed in it. This quality makes ABS unique for plating, as the butadiene can be selectively etched out of the matrix, leaving microscopic holes that are used as bonding sites for electroless plating and also promote adhesion between the substrate and metallic film. ABS was chosen as the substrate for electroless copper plating in this study as it is the most easily plated plastics (Mallory and Haju, 1990).

```
                    ┌──────────────┐
                    │   Plastic    │
                    └──────┬───────┘
                           ▼
                    ┌──────────────┐
                    │Stress Relieve│──────┐
                    └──────┬───────┘      │
                           ▼              │
                    ┌──────────────┐      │
                    │  Degreasing  │      │
                    └──────┬───────┘      │
                           ▼              │
                    ┌──────────────┐      │
                    │Chemical Etching│    ├── Pretreatment
                    └──────┬───────┘      │
                           ▼              │
                    ┌──────────────┐      │
                    │ Neutralizing │      │
                    └──────┬───────┘      │
                           ▼              │
                    ┌──────────────┐      │
                    │  Sensitizing │      │
                    └──────┬───────┘      │
                           ▼              │
                    ┌──────────────┐      │
                    │  Activating  │──────┘
                    └──────┬───────┘
                           ▼
                    ┌──────────────┐
                    │Electroless Metal│── Electroless
                    │  Deposition  │    Plating
                    └──────────────┘
```
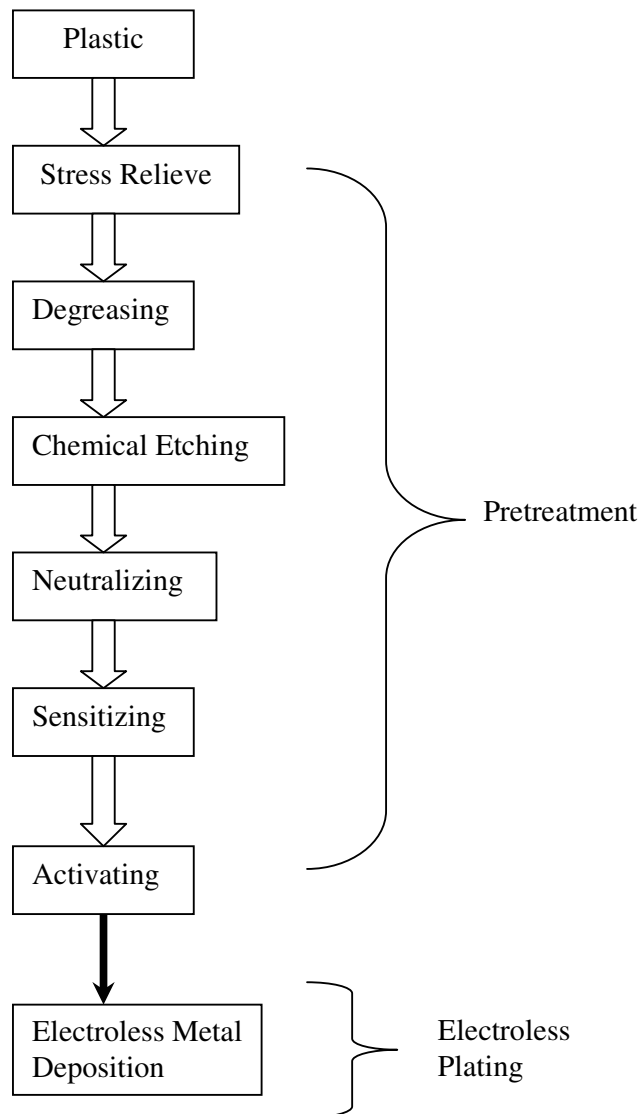
Fig 2.2 Flow chart on the general operation of plastic plating (Mallory and Haju, 1990)

2.2.2 Pretreatment of plastics plating

The general operation on electroless plating of plastics is shown in Fig. 2.2. The objective of the pretreatment stage is to ensure electroless metal deposition on the plastics substrate which is non-conductive initially, and also reasonably good adhesion between the deposited metal and substrate. As seen in Fig. 2.2, the pretreatment stage consists of many stages in which some are more important for certain plastics, while others can be completely omitted.

Stress Relieve

Polysulphone and other highly stressed plastics require this step to prevent cracking during the subsequent processing and to obtain a more uniform etching. This step consists of holding the plastics mouldings in a forced air circulated oven at a high temperature such that the plastics will stand without softening and distorting until the surface stresses have been suffucuently reduced (Muller and Baudrand, 1971).

Degreasing

Degreasing is not required if the plastics substrates are free of grease. If required, silicon-free cleaner is used.

Chemical Etching

This step increase the roughness of the plastics surface, which will facilitate the subsequent electroless plating step. Etching composition typically consists of aqueous chromic acid/sulphuric acid or a mixture of both. The etching composition is best determined experimentally. A typical etch composition is as follows by Muller and Baufrand. (1971):

Sulphuric acid: 100mL

Potassium dichromate: 15mL

Water: 30mL

Neutralizing

Neutralizing solution usually contains reducing agents, such as sodium hydrogen sulfite ($NaHSO_3$). This neutralizing step prevents the carry over of the hexavalent chromium (Cr^{6+}) ions from the etching solution to the sensitizing solution, as Cr^{6+} are known to oxidize Sn^{2+} to Sn^{4+} in the sensitizing solution, thus making the solution ineffective. This step is usually run at 70 to 110 ^oF for 1 to 3 minutes with air agitation (Mallory and Haju, 1990).

Sensitizing

The previous step discussed above optimized the sensitizing step and this step is important for the success of the electroless plating process. The sensitizing solution typically consists of 10-20 g/L tin(II) chloride ($SnCl_2$) and 15-50 g/L concentrated hydrochloric acid (HCl). The colour of the sensitizing solution can be used as a guide for the amounts of HCl required for a fixed amount of $SnCl_2$. When $SnCl_2$ was dissolved in a calculated amount of deionised water, a milky-grey solution is formed. Concentrated HCl was added with constant stirring until the solution becomes clear again. At this point, the $SnCl_2$ and HCl concentrations are in correct balance (Muller and Baudrand, 1971).

Activating

As the name implies, this step is supposed to activate the plastics surface with catalyst. Suitable catalysts include precious metals such as gold, silver and palladium. Palladium is the most common used catalyst for electroless plating. A suitable activating formulation consists of palladium chloride (0.25-0.5 g/L) and concentrated

hydrochloric acid (10 mL/L). In the previous sensitizing step, Sn^{2+} from the tin(II) chloride/hydrochloric acid solution was adsorbed onto the surface. The adsorbed Sn^{2+} reduced the Pd^{2+} to Pd^0 according to Equation 2.18 in the subsequent activating step.

$$Sn^{2+} + Pd^{2+} \rightarrow Sn^{4+} + Pd^o \tag{2.18}$$

Thus, the palladium sites for the catalytic surfaces needed for metal deposition was formed. It is possible to combine the sensitizing and activating step together by mixing the tin(II) chloride, palladium chloride and concentrated hydrochloric acid together. A palladium-tin hydrosol, which is a solution of complex ions and the tin ions is formed. Its activity and stability depend very much on the chloride and tin ions concentrations (Mallory and Haju, 1990).

Rinsing

The rinsing steps are omitted in Fig. 2.2 for simplicity. In fact, rinsing is needed in between every step. This is to prevent any undesirable chemicals from the previous step to carry over to the subsequent step. Proper rinsing ensures the success of the electroless plating process (Muller and Baudrand, 1971).

2.2.3 Electroless metal deposition

This step simply deposits metal on the activated plastics surface. In Section 2.1.1, the fundamental aspects of the electroless plating solution have been discussed and will not be repeated in this section. Before the activated plastics substrate is immersed in the plating solution, the plating solution is still stable, only after the substrate is immersed, chemical reduction of metal occurs on the palladium-bearing plastics surface. Commercially, the electroless plating bath is closely monitored by an automatic controller, whereby the pH and concentrations of chemicals are constantly analyzed. Whenever necessary, plating reagents and other reagents will be replenished.

Electroless copper plating solution are reported to cause more problems than electroless nickel plating solution (Mallory and Haju, 1990).

2.3 Voltammetry analysis of electroless copper plating solution

There are two common types of voltammetry: linear sweep and cyclic. Voltammetry is an electroanalytical technique for the study of electroactive species and frequently used in the field of electrochemistry, inorganic chemistry, organic chemistry and biochemistry (Kissinger and Heineman, 1983). Cyclic voltammetry is an extension of linear sweep voltammetry with the voltage scan reversed after the maximum/minimum voltage is reached. This technique can provide more information about the properties and characteristics of the electrochemical process and also gives insight to complicating processes involving pre- and post-electron transfer reactions as well as kinetic considerations. The voltammogram is a display of current (vertical axis) versus potential (horizontal axis) (Sawyer et al., 1995).

Cyclic/linear sweep voltammetry analysis of electroless copper plating solution are rarely reported. Voltammetry analysis on copper electrode immersed in basic solution containing reducing agent and additives are more common. Fig 2.3 shows a typical voltammogram of a copper electrode in pure base at 25 $^{\circ}$C represented by a dashed line (Burke et al., 1998). A total of two anodic and two cathodic peaks are shown in this figure. Anodic peak, A_1 represents the conversion of Cu to Cu_2O and anodic peak, A_2 reflects the conversion of Cu_2O (and some additional Cu) to a mixture of CuO and $Cu(OH)_2$. The cathodic peak, C_2 is the reduction of Cu(II) to Cu(I) species in the surface layer of copper electrode and lastly the cathodic peak, C_1 is the further

reduction of Cu(I) to Cu. The copper equilibria data involving two solid substances are given as follows:

$$2Cu + H_2O \Leftrightarrow Cu_2O + 2H^+ + 2e^- \quad E^o=0.471V \qquad (2.19)$$

$$Cu + H_2O \Leftrightarrow CuO + 2H^+ + 2e^- \quad E^o=0.570V \ (0.609V) \qquad (2.20)$$

$$Cu_2O + H_2O \Leftrightarrow 2CuO + 2H^+ + 2e^- \quad E^o=0.669V \ (0.747V) \qquad (2.21)$$
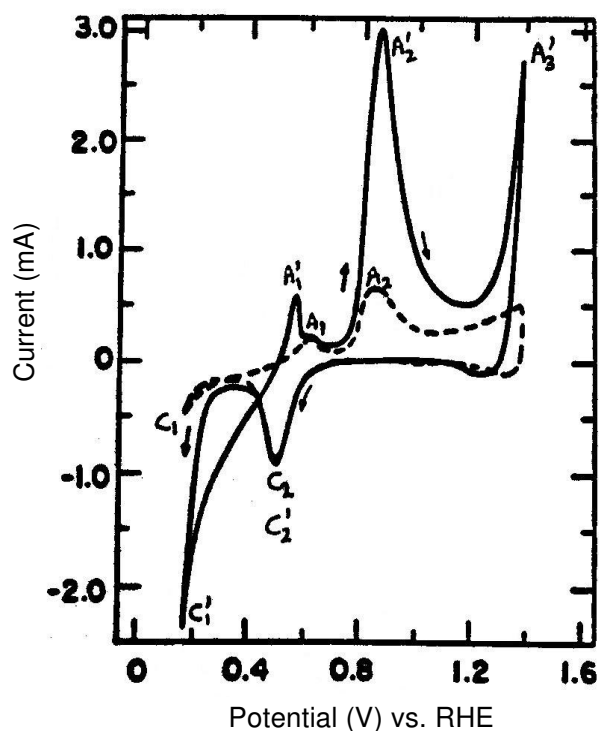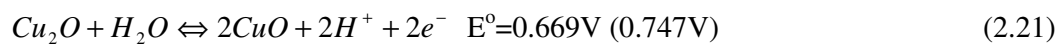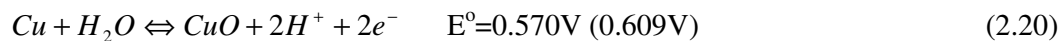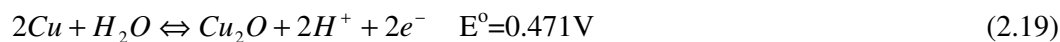
Fig 2.3 Cyclic voltammetry curves for Cu in 1M NaOH (dashed curve) and 1M NaOH + 0.1M HCHO (solid curve). Electrode area = 0.458 cm^2; Scan rate = 0.1 V/S; Temperature = 25°C (Burke et al., 1998)

The potential values in parenthesis refer to hydrated copper(II) oxide. Equation (2.19) is applicable for peak A_1 and C_1 and formation of peak A_2 is probably due to a combination of processes shown in Equations 2.20 and 2.21. Thus, the behaviour of copper in base is complicated because of the multiple oxidation states of copper and its oxides can exist in both anhydrous and hydrated form (Burke et al., 1998), (Burke and Ryan, 1990).

For the case where formaldehyde (HCHO) was added, the resulting voltammogram (in solid curve in Fig. 2.3) was quite similar. The anodic peak, $A_1^{'}$ occurs as a result of the reaction of HCHO on the freshly reducing copper surface. The large increase of the anodic current at peak $A_2^{'}$ is due to the interaction of formaldehyde with Cu(OH)$_2$. There is an additional anodic peak $A_3^{'}$ at around 1.4 V, this peak occurs after the CuO has been removed by dissolution and the oxidation of the formaldehyde on the fresh copper surface appears again. Addition of HCHO have no effect on the cathodic peak $C_2^{'}$ (as the cathodic current is the same as without formaladehyde), however the peak $C_1^{'}$ reveals a large cathodic current which is due to formaldehyde reduction (Bindra and Roldan, 1985).

Based on the cyclic voltammogram on the copper electrode immersed in a mixture of NaOH and HCHO, Burke et al. (1998) proposed a interfacial redox mechasnism for aldehyde oxidation and reduction. Fig. 2.4 and 2.5 shows the actual proposed reaction mechanism. Due to energy fluctuations, the copper atoms at an active site in a low lattice coordination state, may be oxidised to Cu(I) state at around -0.1 V. The oxidised copper atoms can rapidly react with an aldehyde molecule to form Cu* in nascent (or very active) form as shown in Fig. 2.4. The Cu* is immediately oxidized as shown in Fig. 2.5 and the cycle continues. In the course of reaction, if some of the excess energy of the nascent Cu* atoms is transferred to other metal atoms at the active sites, the aldehyde oxidation will be observed below 0.0 V.

$$2Cu^* + 2nH_2O \Leftrightarrow 2[Cu^{+1}.nH_2O]_{ads} + 2e(\rightarrow i_a)$$

$$RCOO^- + 2H_2O \qquad RCHO + 3OH^-$$
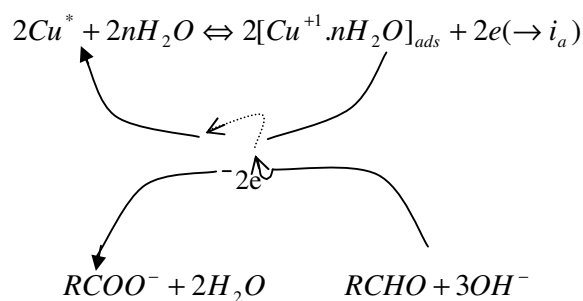
Fig 2.4 Interfacial cyclic redox mechanism for aldehyde oxidation at a copper electrode in aqueous base (Burke et al., 1998)

$$(\rightarrow i_c)2[Cu^{+1}.nH_2O]_{ads} + 2e \Leftrightarrow 2Cu^* + 2nH_2O$$

$$RCHO + 2H_2O \qquad RCH_2OH + 2OH^-$$
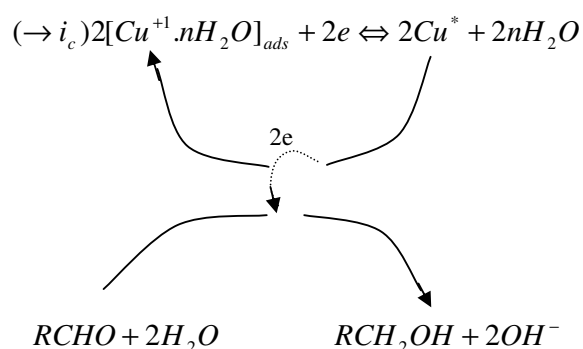
Fig 2.5 Interfacial cyclic redox mechanism for aldehyde reduction at a copper electrode in aqueous base (Burke et al., 1998)

Linear sweep voltammetry are performed on electroless copper plating solution containing $CuSO_4.5H_2O$, ethylenediaminetetraacetic acid (EDTA), triethanolamine (TEA) and HCHO. The anodic linear sweep voltammogram shared close resemblance with the ones in Burke et al. (1998) and Bindra and Roldan. (1985). It was expected as the plating solution only contains additional chelating agents. The voltammograms revealed that EDTA plays an important role in chelating, while TEA adsorbs onto the copper surface to inhibit HCHO oxidation, if the plating solution contains sufficient EDTA. In addition, traces of ethylenediamine were found to affect the morphology of the plated copper. This is due to the high adsorption capability of ethylenediamine, which makes it a prominent refining agent (Lin and Yen, 2001).

Cyclic voltammetry experiments were performed on a new type of electroless copper plating solution using cobalt(II)-ethylenediamine complex as reducing agent. The electroless plating solution of pH 6-8 contains $CuCl_2$, $CoCl_2$ and ethylenediamine (En). From the voltammograms, complicated electrochemical behaviour was observed as both the anodic and cathodic processes are occurring simultaneously on the same metal surface at the same potential. The current measured corresponds to the algebraic sum of anodic Co(II) oxidation and cathodic Cu(II) reduction currents. The Cu(II) reduction and Co(II) oxidation takes place at around 0.15 V and the pH of solution was 7. Furthermore, chloride ions were found to play a crucial role in accelerating both the partial reactions of Co(II) oxidation and Cu(II) reduction, by electron transfer through the Cl^- bridge in Fig. 2.6 and Fig. 2.7 (Vaskelis et al., 1999).
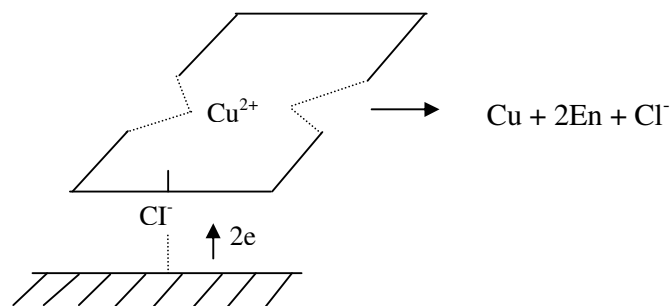
Fig 2.6 Reduction of mixed Cu(II)-En-chloride complexe through a chloride 'bridge' (Vaskelis et al., 1999)
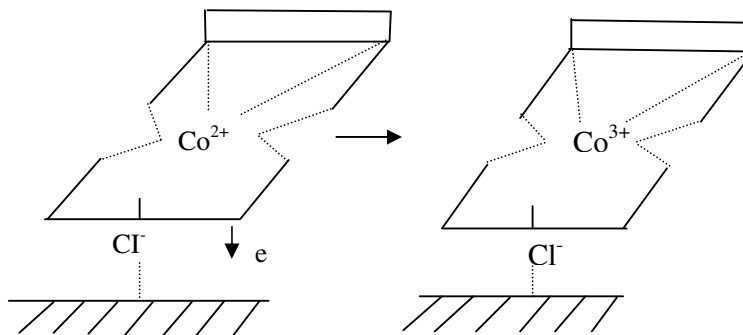
Fig 2.7 Electrooxidation of $CoEn_3Cl^+$ complex through the chloride 'bridge' (Vaskelis et al., 1999)

Chapter 3

Materials and methods

3.1 Preparation of acrylonitrile-butadiene-styrene (ABS) film

3.1.1 Materials

The acrylonitrile-butadiene-styrene (ABS) { [-$CH_2CH(CN)$-]$_x$ (-$CH_2CH=CHCH_2$-)$_y$ [-$CH_2CH(C_6H_5)$-]$_z$ has a acrylonitrile/butadiene/styrene molar ratio of 2:1:2. Melt index (230 °C/3.8 kg, ASTM D 1238). Glass transition temperature is 103 °C. It exists in pellet form obtained from Aldrich. Toluene, acetronitrile and chlorform were used as the organic solvent for the ABS pellets. All the organic solvents used are of analytical grade. Glass slides (15x15 mm) of 2 mm thickness were used as the base material for coating of organic solvents containing ABS.

3.1.2 Methods

A transparent thin film of ABS about 0.2 mm was prepared. Chloroform, toluene and acetonitrile weight % of 40, 50 and 10 respectively were mixed together. The ABS pellets were then dissolved in the mixture of organic solvents with the aid of a IKA Labortechnik KS250 mechanical shaker. The concentration of ABS is 5% by weight. The dissolved ABS solution was then ultrasonicated for 5 minutes.

Coating of ABS onto the glass slides was carried out in a laboratory fume cupboard. Each time, a fixed amount of organic solvents containing ABS was deposited on the glass slides using a deposable glass dropper. This is to ensure that the thickness of ABS film on every glass slides is constant. The coated glass slides were subsequently left inside the fume cupboard where the organic solvents were allowed to evaporate, leaving behind the ABS film. Fig. 3.1 illustrates the process of ABS film coating on the glass slide.
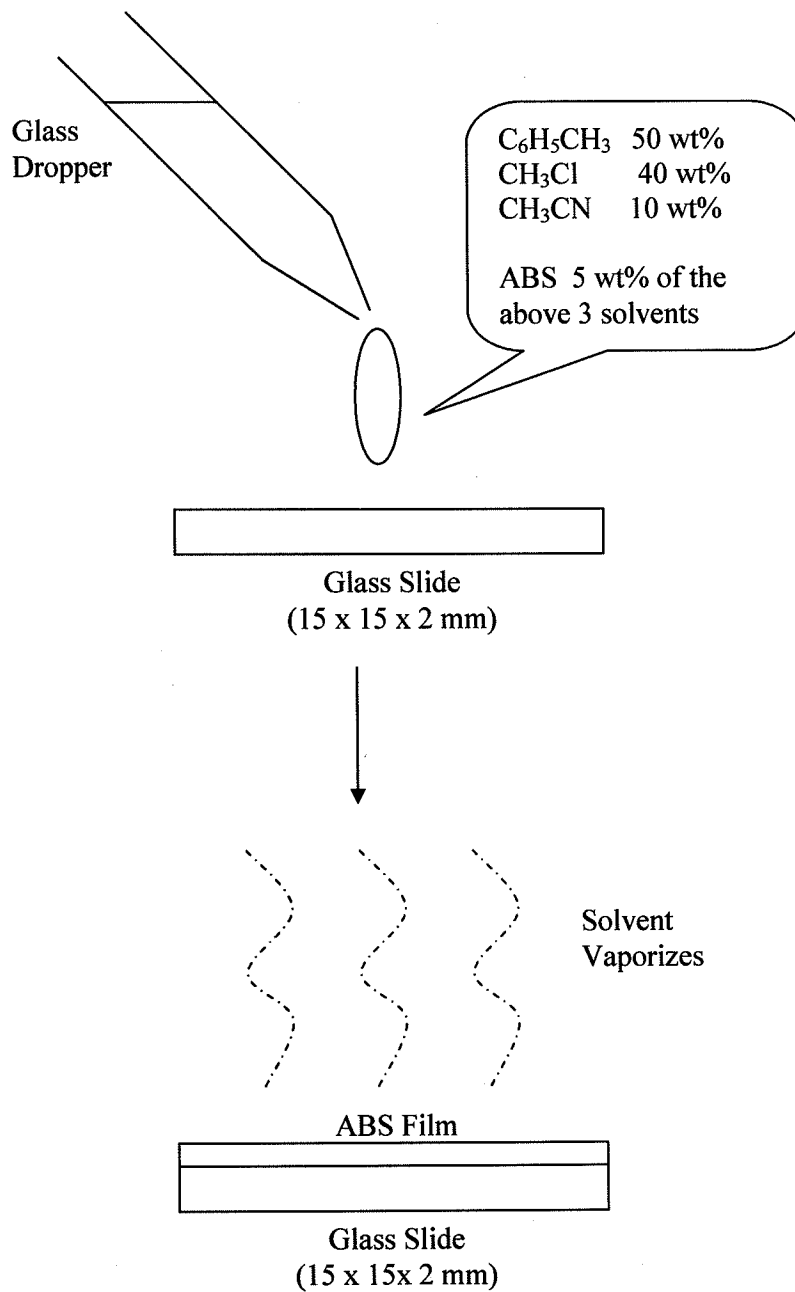
Fig 3.1 Coating of ABS film on a glass slide

3.2 Electroless deposition of copper on acrylonitrile-butadiene-styrene (ABS) film

3.2.1 Materials

Tin (II) chloride dihydrate ($SnCl_2.2H_2O$), palladium chloride ($PdCl_2$) and concentrated hydrochloric acid, 37 wt% (HCl) constitute the activating solutions. The reference copper plating solution consists of copper(II) sulphate pentahydrate ($CuSO_4.5H_2O$), potassium sodium tartrate tetrahydrate ($KNaC_4H_4O_6.4H_2O$), EDTA Disodium salt, dihydrate crystal ($C_{10}H_{14}N_2Na_2O_8.2H_2O$), triethanolamine ($N[CH_2CH_2OH]_3$),sodium hydroxide (NaOH), sodium carbonate (Na_2CO_3), potassium ferrocyanide(II) trihydrate ($K_4Fe[CN]_6.3H_2O$), bi-pyridine and 37 wt% formaldehyde (CH_2O). Additional chemicals include tri-sodium citrate dehydrate ($C_6H_5Na_3O_7.2H_2O$), malic acid ($C_4H_6O_5$), potassium hydroxide, L-cystein ($C_3H_7SNO_2$), glycine ($C_2H_5NO_2$), L-Methionine ($C_4H_9SNO_2$), polyethylenglycol of molecular weights 600, 4000, 10000 and 35000 g/mol [$HO(C_2H_4O)_nH$]. The chemicals used are of analytical grade. Water used are of deionised form unless otherwise stated. Binder clips (15mm) were used to hold the ABS film firmly on the glass slides.

3.2.2 Methods

Electroless copper plating consists of activating and electroless plating step. Figures 3.2 and 3.3 shows the schematic diagram of the activating and electroless copper plating step respectively.

3.2.2.1 Activating Step

The activating step performs on the acrylonitrile-butadiene-styrene (ABS) surface and involves two separate activating solutions. They are acidic tin(II) chloride solution and

acidic palladium(II) chloride solution. The composition of the activating solutions is given in Table 3.1-2.

Table 3.1 Composition of acidic tin(II) chloride solution

	g/L	mol/L (10^{-1})
$SnCl_2$	2.42	0.13
HCl	12.82	3.52

Table 3.2 Composition of acidic palladium(II) chloride solution

	g/L	mol/L (10^{-2})
$PdCl_2$	0.99	0.56
HCl	4.36	12.00

The acidic tin(II) chloride solution was prepared by dissolving tin(II) chloride dihydrate in distilled water, followed by addition of concentrated hydrochloric acid until the solution turns from milky to clear. The acidic palladium(II) chloride solution was prepared by dissolving palladium chloride in distilled water with the aid of a 2.5 cm magnetic stirrer. After 70-80 % of the palladium chloride has dissolved, a certain amount of concentrated hydrochloric acid was added. Stirring continues until all of the palladium chloride dissolves in the solution.

The ABS film is attached firmly to the glass slide by binder clips. The glass slide provides mechanical support and ensures that the ABS film is flat. The ABS film was dipped into the acidic tin(II) chloride solution for 1 minute and followed by another minute of rinsing. The ABS film was then immersed in acidic palladium(II) chloride solution for 1 minute and then rinsed again for another minute. This cycle repeats another two times. There is a total of 3 cycles for this activating step.

Binder Clip

Rinsing

1min
0.01276M SnCl$_2$,
0.3517M HCl

Rinsing

1 min
0.005583M PdCl$_2$,
0.1196M HCl

Rinsing
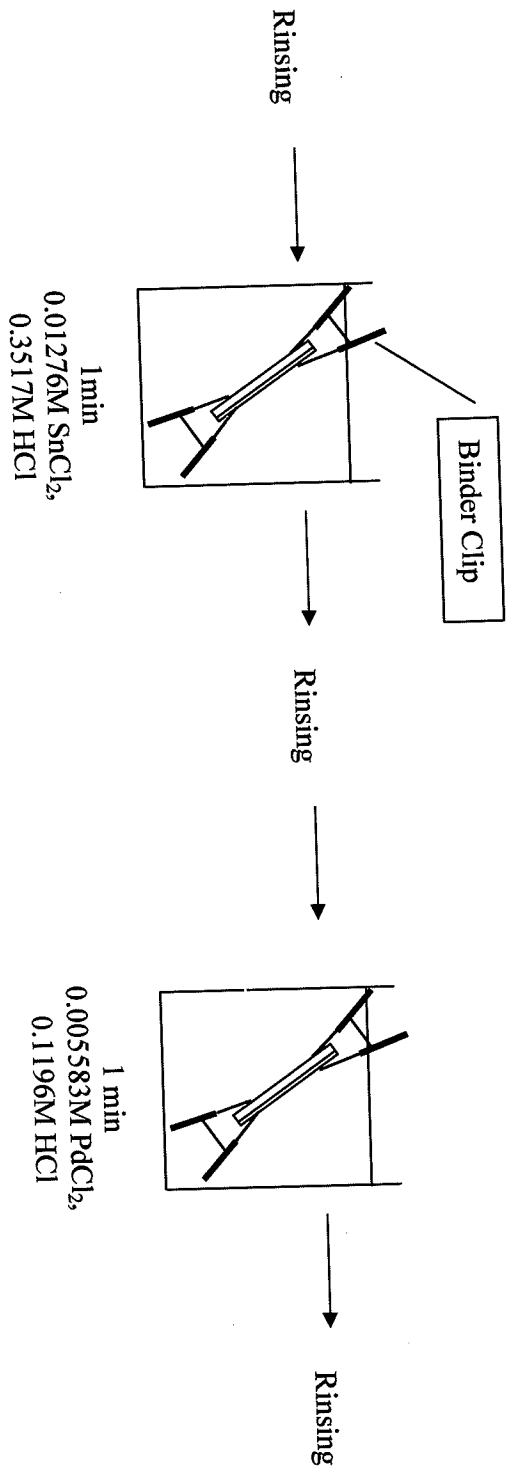
Fig 3.2 Schematic diagram of electroless copper plating activating step (1 cycle)

3.2.2.2 Electroless copper plating step

In this step, copper is electrolessly plated onto the ABS film. The composition of the reference plating solution is given in Table 3.3.

Table 3.3 Composition of electroless copper plating solution

Components	mol/L	g/L
$CuSO_4.5H_2O$	0.1161	29.00
$KNaC_4H_4O_6.4H_2O$	0.5031	142.00
$C_{10}H_{14}N_2Na_2O_8.2H_2O$	0.03224	12.00
$N[CH_2CH_2OH]_3$	0.03351	5.00
NaOH	1.048	42.00
Na_2CO_3	0.2359	25.00
$K_4Fe[CN]_6.3H_2O$	0.000118	0.05
Bi-pyridine	0.00064	0.10
CH_2O	2.058	61.79

The required amount of $CuSO_4.5H_2O$, $KNaC_4H_4O_6.4H_2O$, $C_{10}H_{14}N_2Na_2O_8.2H_2O$, Na_2CO_3 and bi-pyridine were weighted in a Mettler Toledo College balance B204-S (220 g - 0.001 g) and placed in a 50 mL beaker. This is followed by the addition of 29.31 mL of distilled water, 1.68 g of NaOH, 4.16 mL of $N[CH_2CH_2OH]_3$ (48.08 g/L) and 0.4 mL of $K_4Fe[CN]_6.3H_2O$ (5 g/L). The plating solution was then stirred using a spetula to accelerate the dissolution rate. A clear dark blue solution was obtained. The pH of the plating solution was measured using a ATI Orion 525A pH meter.

After the activating step, 6.13 mL of 37 wt% CH_2O was added to the plating solution to make the total volume to 40 mL and stirred using a spetula. The pH of the solution was then measured. A 15 mm long magnetic stirrer bar was immersed in the plating solution and subsequently placed onto a Torrey Pines Scientific HS10-2 stirring hot plate at room temperature ($\approx$ 25 °C). The ABS coated glass slide bounded by 2 binder clips was suspended in the plating solution 5 minutes after 37 wt% CH_2O was

added with the help of a retort stand as shown in Fig. 3.3. The plating solution was constantly stirred throughout the plating process and placed in a fume cupboard. The copper plated ABS coated glass slide was removed from the plating solution after 15 minutes of immersion. To prevent any possible reaction on the freshly plated copper surface, millipore water (0.22 μm) was used to rinse the plated ABS coated glass slide. This is followed by washing with 99.8 % ethanol in a Cole-Parmer 8891 ultrasonicator for 10 seconds with a 5 seconds break in between to ensure the plated copper surface is clean. The copper plated ABS coated glass slide was left to dry at room temperature for 30 minutes and then preserved in a nitrogen filled Scienceware dessicator (F42022).

3.3   Method of determining the plated copper thickness

The substrate for electroless copper plating is a ABS film casted on a (1.5 x 1.5) cm^2 glass slide. Let the surface area be S cm^2. Before activating and electroless copper plating, the ABS film together with the glass slide are weighted. Let the initial weight be W_i, in grams. After the ABS film was plated with copper, the unwanted copper which is coated on the glass surfaces are gently removed using a task wiper. The plated copper ABS film is then left to dry at room temperature for 1.5 hours before the final weight, W_f, in grams, is taken. Density of copper, ρ_{Cu} at 20 °C is taken to be 8.92 g/cm^3 (Dean, 1979).

$$\text{Mass of plated copper metal} = W_f - W_i \text{ g} \qquad (3.1a)$$

$$\text{Volume of plated copper metal} = \frac{W_f - W_i}{\rho_{Cu}} \; \frac{g}{gcm^{-3}} = cm^3 \qquad (3.1b)$$

$$\text{Thickness of plated copper metal} = \frac{W_f - W_i}{\rho_{Cu}S} \; \frac{cm^3}{cm^2} = \frac{cm}{1} = \frac{10^4 \, \mu m}{cm}$$

$$= \frac{W_f - W_i}{\rho_{Cu}S} \times 10^4 \, \mu m \qquad (3.1c)$$

Magnetic
Stirrer
Bar

6.13 mL of 37 wt %
CH_2O added 5 mins
before the ABS
coated glass slide is
immersed

≈ 15 min
Copper Plating Bath

Magnetic Stirrer

Retort
Stand

Rinse with
Millipore water
(0.22 μm)

Ultrasonicated in
industrial grade
ethanol for 10 s
with a 5 s break in
between

Preserved in
nitrogen filled
dessicator
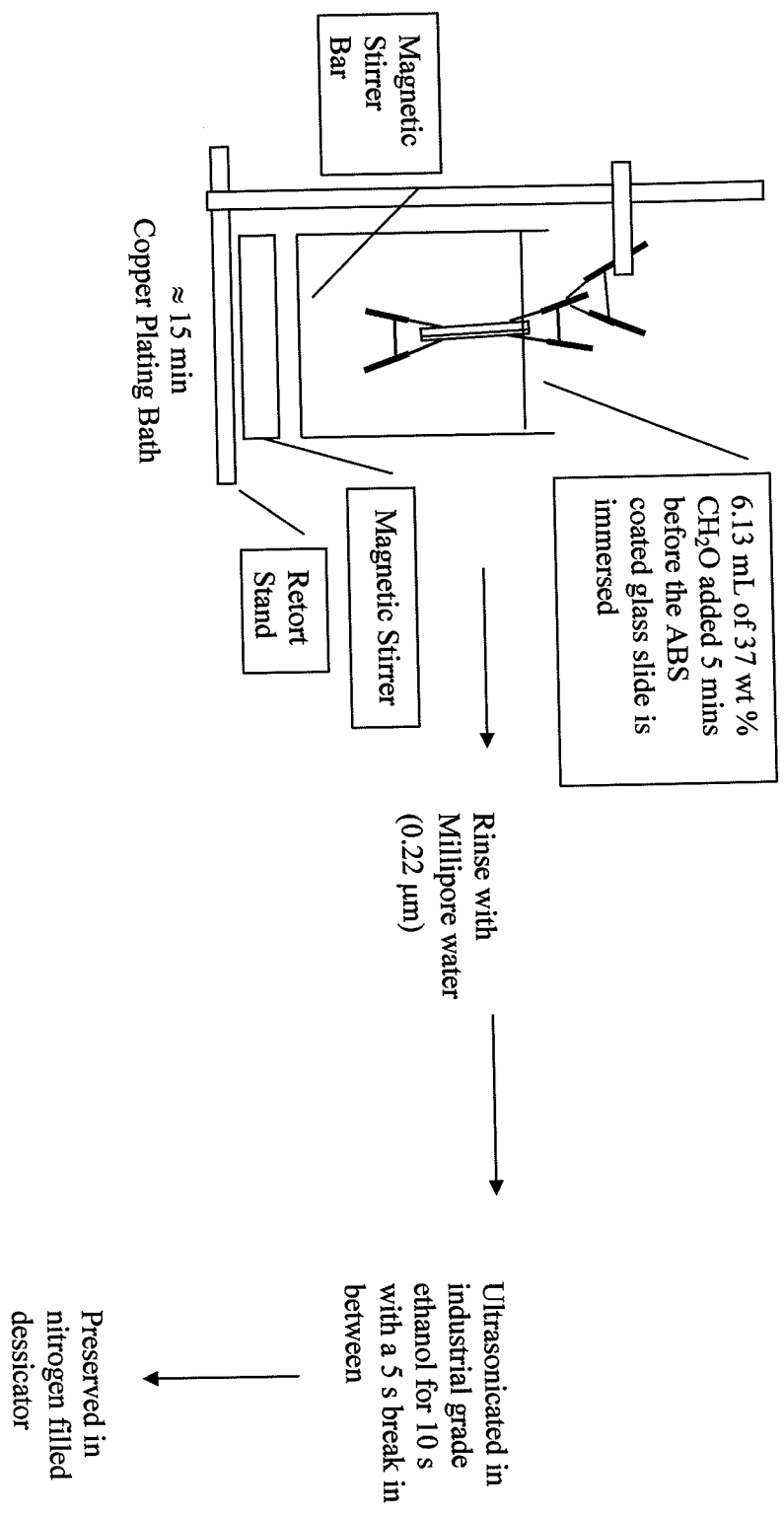
Fig 3.3 Schematic diagram of electroless copper plating

34

3.4   Method of determining the plating rate of copper

The copper thickness at each plating time is calculated using Equation 3.1 and the copper thickness versus plating time is plotted. Since the relationship between the copper thickness and plating time is linear, the plating rate can be easily obtained from the gradient of the fitted linear line through the points.

3.5   Analytical techniques

A variety of analytical instruments was used for the surface analysis of plated copper. The atomic force microscope (AFM) MultiMode^{TM} scanning probe microscope MM-SPM was used for surface topography measurements and was operated in tapping mode with an insulating Si_3N_4 tip cantilever with a spring constant of about 0.12 Nm^{-1}. The scanning electron microscope (SEM) JEOL JSM-5600LV was used to reveal two dimensional surface morphology of the plated copper at a micro level. Transmission electron microscope (TEM) performed on a Jeol system with a tension voltage of 100kV was also used to view the surface morphology of plated copper at a higher magnification.

For the characterization of crystalline planes, X-ray diffraction (XRD) Philips diffractometer PW1710 equipped with a CuK_α source (45 kV and 40 mA) was used. Mettler Toledo Differential scanning colorimetry (DSC) 822e was used to reveal the thermal motion of ABS film from measurement of the glass transition temperature, melting temperature of the plated and unplated film.

Cyclic voltammetry analysis on electroless plating solutions was performed by Autolab Potentiostat/Galvanostat PGSTAT12. A platinum electrode was used as counter electrode, Ag/AgCl electrode filled with a 3 M KCl was used as reference

electrode and the working electrode was made of brass (1.5x1.7 cm^2). The distance among the three electrodes in the plating solutions were fixed.

Chapter 4

Effects of Chelating Agents in the Electroless Copper Plating Solution

This chapter examines the effects of changing the main chelating agent in the electroless copper plating solution. The reference plating solution employs a dual chelating agent where the main chelating agent is tartrate salt and the side chelating agent is EDTA disodium salt. Analytical instruments such as scanning electron microscope (SEM), atomic force microscope (AFM) and X-ray diffraction (XRD) were used extensively in order to gain a more in-depth understanding of the plated copper structures.

4.1   The influence of varying the concentration of potassium sodium tartrate

Tartrate salts serve as a chelating agent in electroless copper plating solution and its primary role is to prevent precipitation of copper into the bulk solution during the plating process. Hence, the mole ratio of tartrate salts to copper salts will have a direct consequence on the type of copper plated. The plating time was held constant at 15 minutes and the mole ratio of sodium potassium tartrate to copper (II) sulphate was made to vary from 2.5 to 4.3 and the surface morphology of the plated copper was observed by AFM and SEM.

Figures 4.1a-c show the 3-dimensional surface image generated by AFM at different mole ratios of potassium sodium tartrate to copper (II) sulfate and Table 4.1 shows the corresponding selected results from the roughness analysis. The 3-dimensional surface images clearly shows that at the molar ratio of 3.5, the 'cone' structures of copper are more closely packed and the roughness analysis shown in Table 4.1 confirmed that it has the smoothest surface.
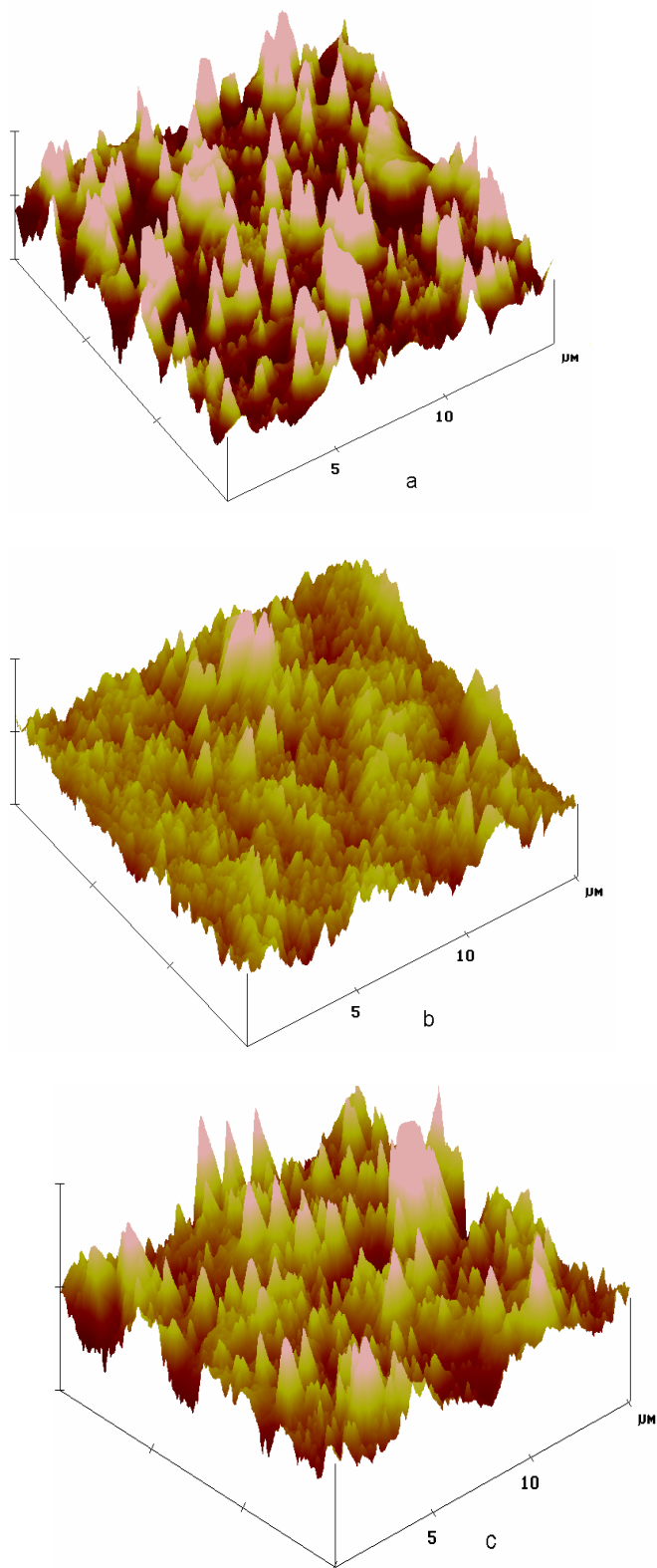
Fig 4.1 Atomic force microscope 3-dimensional surface images (15 x 15 µm) when the molar ratio of sodium potassium tartrate to copper (II) sulphate is a) 4.3 b) 3.5 c) 2.5 (Z axis 250 nm/div)

Table 4.1 Selected roughness analysis results on various molar ratios of sodium
potassium tartrate to copper (II) sulphate

Mole ratio of sodium potassium tartrate to copper (II) sulphate	Img. RMS (Rq) /nm
4.3	67.0
3.5	32.5
2.5	48.3

Img. Rms (Rq) refers to the root mean square of height deviations taken from the mean

data plane, expressed as $\sqrt{\dfrac{(Z_1^2 + Z_2^2 + Z_3^2 + ... + Z_n^2)}{N}}$

Figures 4.2a-c shows the scanning electron microscope images at 5000 magnification at various mole ratios of potassium sodium tartrate to copper (II) sulphate. From these electron micrographs, only the 2-dimensional surface morphology was revealed. Fine grains of copper structures were seen and form clusters of about 4 µm in size. The clusters of copper structures formed in Fig. 4.2b are more uniform than the others, which probably explains the resulting lowest surface roughness. The scanning electron microscope images can be still considered as consistent with the corresponding 3-dimensional atomic force microscope surface image. Therefore, the optimum ratio of 3.5 was selected.

a   b

c
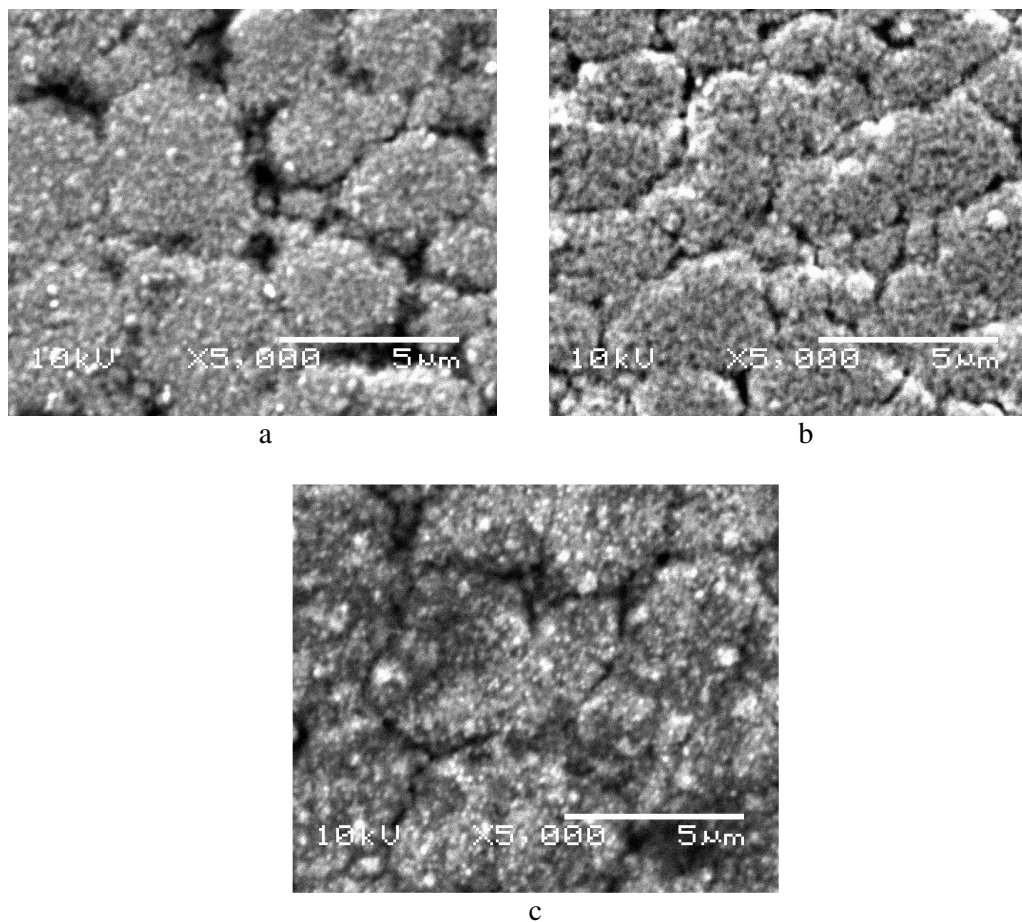
Fig 4.2 Scanning electron microscope images when the molar ratio of sodium potassium tartrate to copper (II) sulphate is a) 4.3 b) 3.5 c) 2.5. Magn. X5000

4.2   The influence of varying the concentration of trisodium citrate

Trisodium citrate is a common citric salt and its chemical structure is similar to potassium sodium tartrate, except that it contains an additional carboxylic group, and one less hydroxyl group. In this section, potassium sodium tartrate was replaced by trisodium citrate. The function of the citric salt is still the same as the tartaric salt, which serves as a chelating agent. Similar to Section 4.1, this section seeks to obtain the optimal concentration of citric salt in the electroless copper plating solution. Again, the plating time was fixed at 15 minutes.

The 3-dimensional surface images generated by AFM at different mole ratios of trisodium citrate to copper (II) sulphate are shown in Figures 4.3a-d and Table 4.2 shows the corresponding selected results from the roughness analysis. The 'cone' copper structures of various heights are distributed unevenly on the 15x15 µm area when the mole ratio is 5.5, 4.3 and 2.5. At a molar ratio of 3.5, the copper 'cone' structures appear to be more uniform in size and height and the roughness analysis also revealed that it has the smoothest surface.

The scanning electron microscope images at 5000 magnification at various mole ratios of trisodium citrate to copper (II) sulphate are shown in Figures 4.4a-d. Similar to tartaric salts, citric salts also offer fine grains of copper structures, which form clusters ranging from 2 to 6 µm in size. But it was observed that at a low molar ratio of 2.5, bigger grains of copper are formed. This may be associated with the higher plating rate, when the concentration of chelating agent is reduced. The scanning electron microscope images are quite consistent with the corresponding 3-dimensional atomic force microscope surface image. In view of the roughness analysis and surface morphologies of the four plated copper, the optimum ratio of 3.5 was selected.
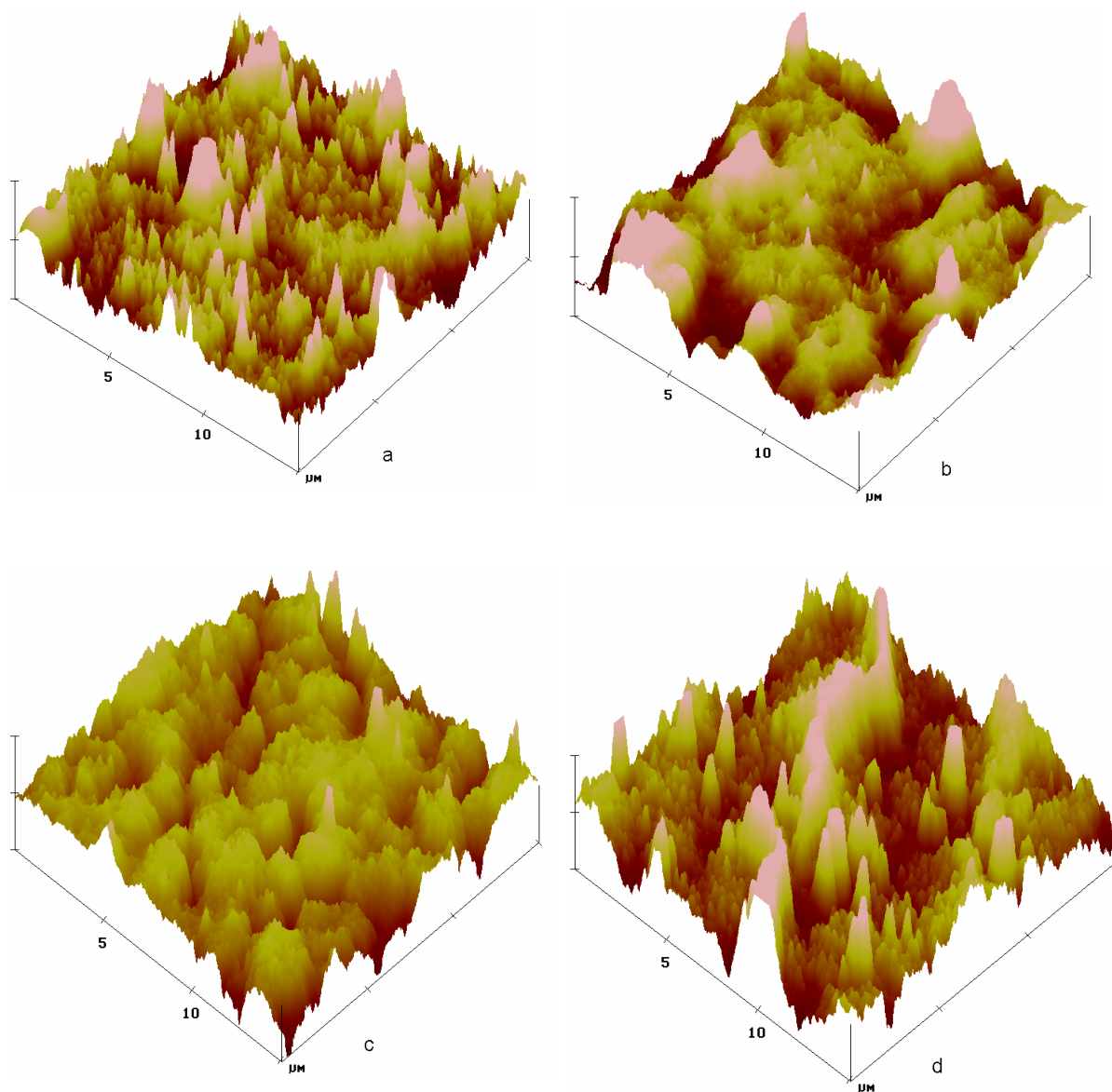
Fig 4.3 Atomic force microscope 3-dimensional surface images (15 x 15 µm) when the molar ratio of trisodium citrate to copper (II) sulphate is a) 5.5 b) 4.3 c) 3.5 d) 2.5 (Z axis 250 nm/div)

Table 4.2 Selected roughness analysis results on various molar ratios of trisodium citrate to copper (II) sulphate

Mole ratio of trisodium citrate to copper (II) sulphate	Img. RMS (Rq) /nm
5.5	62.0
4.3	60.3
3.5	58.8
2.5	96.8

Img. Rms (Rq) refers to the root mean square of height deviations taken from the mean

data plane, expressed as $\sqrt{\dfrac{(Z_1^2 + Z_2^2 + Z_3^2 + ... + Z_n^2)}{N}}$
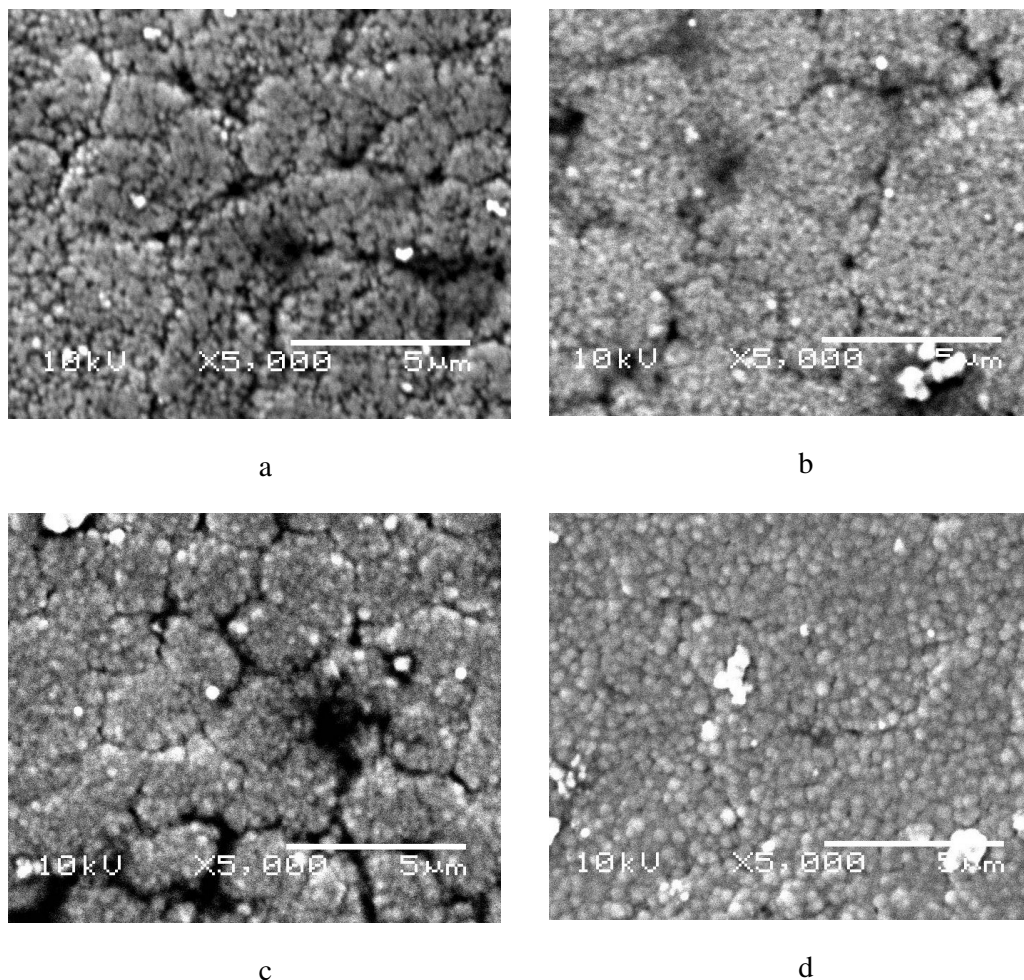
Fig 4.4 Scanning electron microscope images when the molar ratio of trisodium citrate to copper (II) sulphate is a) 5.5 b) 4.3 c) 3.5 d) 2.5. Magn. X5000

4.3   The influence of varying the concentration of potassium sodium salt of malic acid

The malic acid is not available in the form of salt. In the preparation of electroless copper plating solution, a malic salt is desired. The method of preparation involves simple titration of potassium hydroxide and sodium hydroxide with malic acid. Theoretically, one mole of malic acid will react with one mole of sodium hydroxide and one mole of potassium hydroxide to form one mole of a salt of a malic acid and two moles of water. Sodium hydroxide solution was added dropwise to the solution of malic acid until the pH of the solution reaches the first pK_a value of the malic acid at 3.4. Then, potassium hydroxide solution was added dropwise to the solution until the pH of the solution reaches the second pK_a value of 5.05 (Dean, 1979). At this point, the bulk of the malic acid should be in its salt form. Similar to the Section 4.2, potassium sodium tartrate was replaced by potassium sodium salt of malic acid, which are both structurally similar. The only difference is that potassium sodium tartrate has an additional hydroxyl ion. The purpose is to obtain the optimal concentration of malic salt in the electroless copper plating solution. A plating time of 15 minutes was selected.

Figures 4.5a-d shows the 3-dimensional surface image generated by AFM at different mole ratios of potassium sodium salt of malic acid to copper (II) sulfate pentahydrate and Table 4.3 shows the corresponding selected results from the roughness analysis. The surface images shared close resemblance with the tartaric and citric salts counterparts. At the molar ratio of 5.5, a mixture of thick and thin 'cone' structures were seen. At the molar ratio of 4.3, the scan area was largely made up of thick 'cone' structures. When the mole ratio is further reduced to 3.5, many thin 'cone' structures of about the same height were seen. Lastly, a mixture of 'cone' structures

were seen when the mole ratio is 2.5. The roughness values shown in Table 4.3 indicate that the surface of the plated copper appears to be rougher than the tartaric and citric salts.
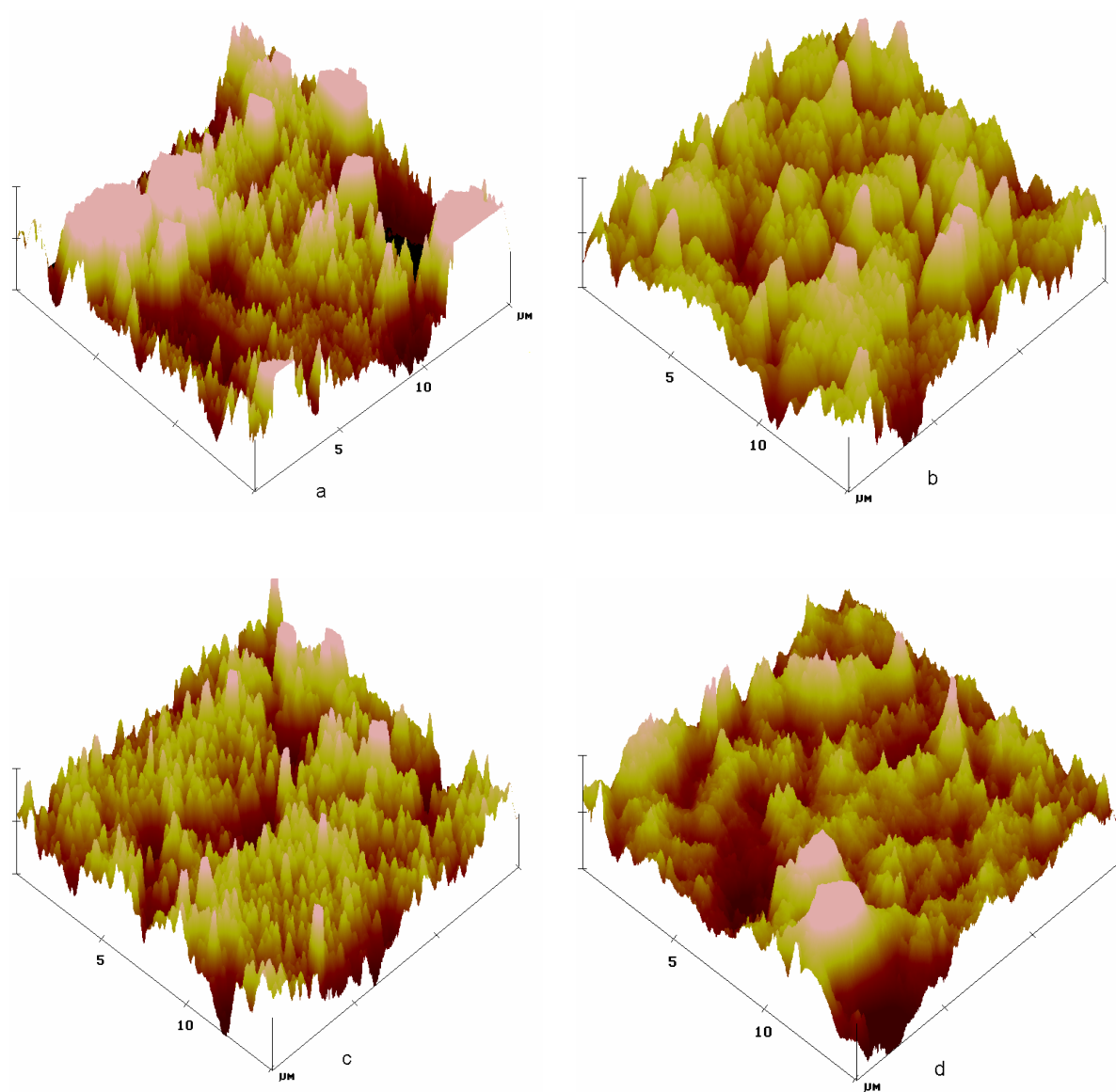

Fig 4.5 Atomic force microscope 3-dimensional surface images (15 x 15 μm) when the molar ratio of potassium sodium salt of malic acid to copper (II) sulphate is a) 5.5 b) 4.3 c) 3.5 d) 2.5 (Z axis 250 nm/div)

Table 4.3 Selected roughness analysis results on various molar ratios of potassium sodium salt of malic acid to copper (II) sulphate

Mole ratio of potassium sodium salt of malic acid to copper (II) sulphate	Img. RMS (Rq) /nm
5.5	200.5
4.3	85.6
3.5	89.2
2.5	78.7

Img. Rms (Rq) refers to the root mean square of height deviations taken from the mean data plane, expressed as $\sqrt{\dfrac{(Z_1^2 + Z_2^2 + Z_3^2 + ... + Z_n^2)}{N}}$

Figures 4.6a-d show the scanning electron microscope images at 5000 magnification at various mole ratios of potassium sodium salt of malic acid to copper (II) sulphate pentahydrate. The copper grains in all the four microscope images were noticeably larger than the copper grains deposited by using tartaric and citric acid salts as the chelating agents. Copper clusters of 2-6 µm in size were observed in all the microscope images, except in Fig. 4.6b. Changing the molar ratio of malic acid within the range of 5.5 to 2.5 does not have a great impact on the surface morphology as suggested by the electron microscope images. Only the copper grains at a molar ratio of 4.3 were much larger and was confirmed by the corresponding AFM 3-dimensional surface image. The ideal molar ratio of potassium sodium salt of malic acid to copper (II) sulphate pentahydrate was chosen to be 2.5 as it has the lowest roughness value. Again, the scanning electron microscope images and the corresponding 3-dimensional atomic force microscope surface images are in agreement.
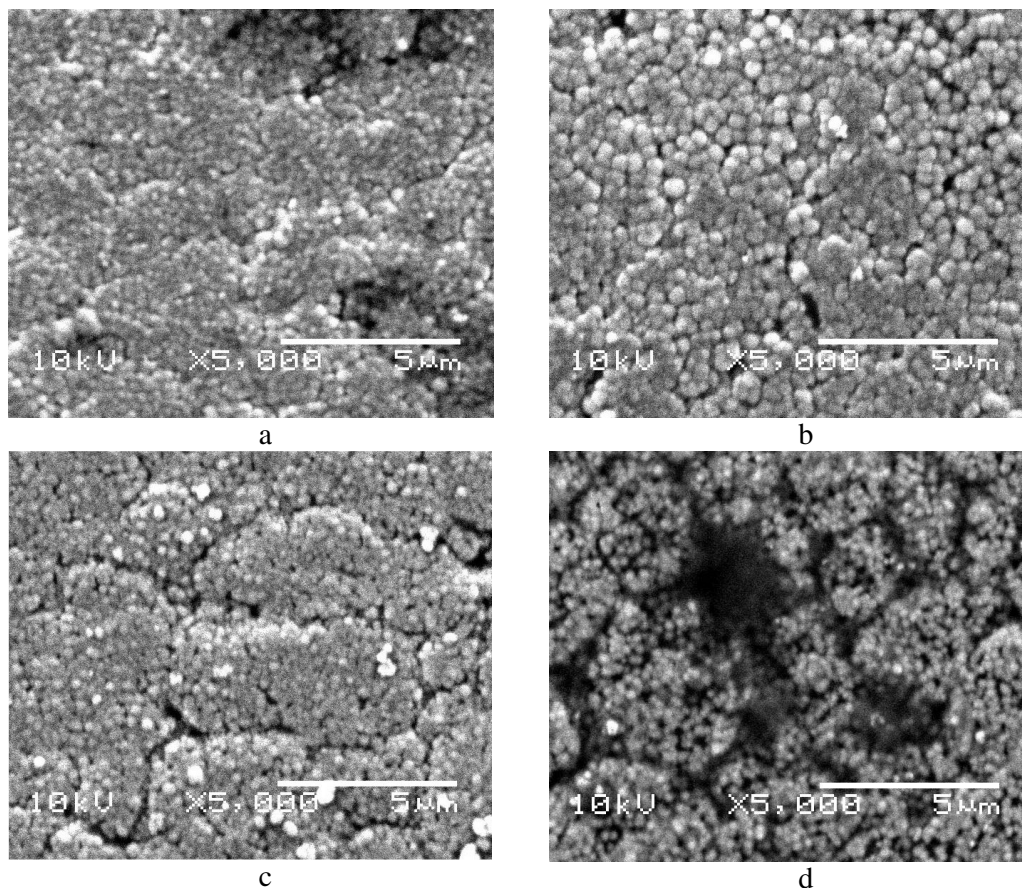
Fig 4.6 Scanning electron microscope images when the molar ratio of potassium sodium salt of malic acid to copper (II) sulphate is a) 5.5 b) 4.3 c) 3.5 d) 2.5. Magn. X5000

4.4 Kinetics analysis of structurally similar chelating agents

Different chelating agents will result in various copper plating rates. This could be due to its different stability formation constants and complex structures. It would be interesting to examine the plating rates of structurally similar chelating agents. Plating rate is an important factor in electroless plating as it has a direct impact on the morphology of plated metal and of course, time needed to plate a certain thickness. This section examines and discusses the various plating rates of the chelating agents and also the changes in the plated copper surface during the plating process.

4.4.1 Calculated plating rates of the structurally similar chelating agents

Figures 4.7-9 shows the graph of the increase of plated copper with plating time for tartaric, citrate and malic salts, respectively. The plating experiments for the similar chelating agents were repeated twice or more for each plating time in order to minimize any possible experimental error. The plating bath and conditions are the same for all the plating experiments except the main chelating agent and plating time were changed when required. Table 4.4 shows the plating rate of the respective chelating agents calculated from Figures 4.7-9. The pH of the plating solution of the various chelating agents is highly basic and maintain at a close range of 12.10 to 12.30. Since the structurally similar chelating agents are added to the electroless plating solution in the form of salt, the predominant form for the tartaric, citric and malic salts exists as $[C_4H_4O_6]^{2-}$, $[C_6H_5O_7]^{3-}$, $[C_4H_4O_5]^{2-}$ respectively. The chemical structures of the predominant form of the structurally similar chelating agents are given in Table 4.5.

Copper Thickness with Plating Time
(Chelating Agent: Potassium Sodium Tartrate)
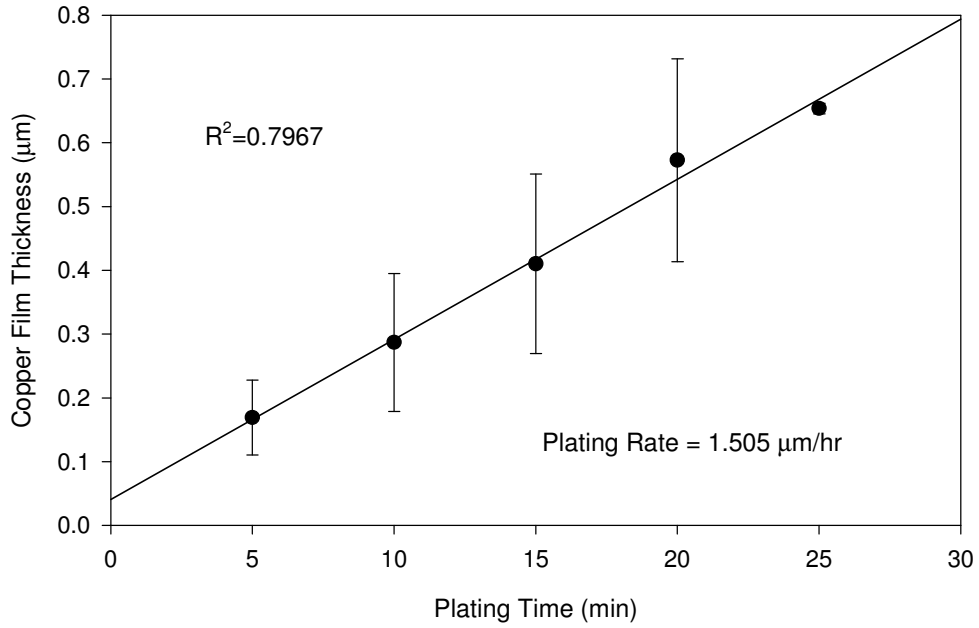
Fig 4.7 Plated copper thickness with time with sodium potassium tartrate as the chelating agent

Copper Thickness with Plating Time
(Chelating Agent: Trisodium Citrate)
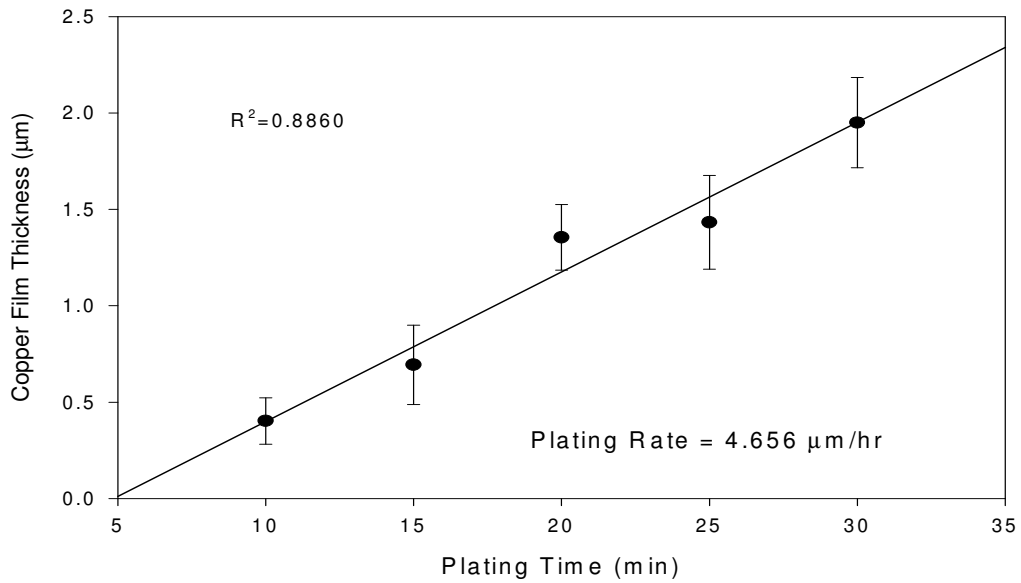
Fig 4.8 Plated copper thickness with time with trisodium citrate as the chelating agent
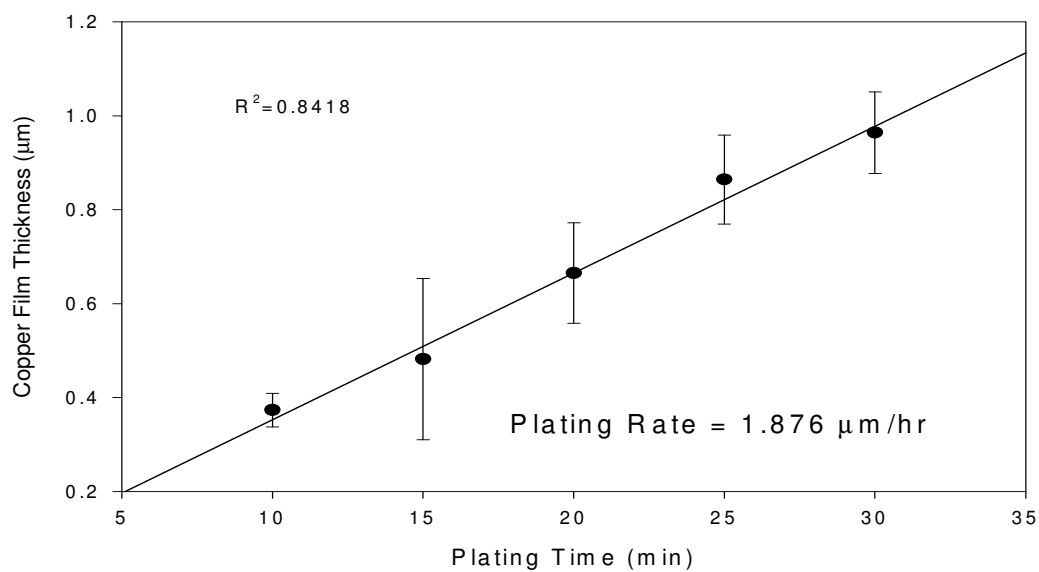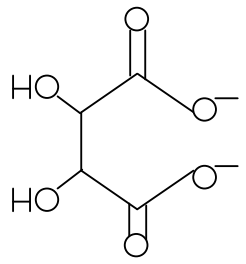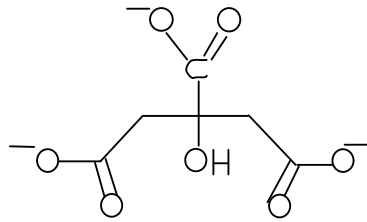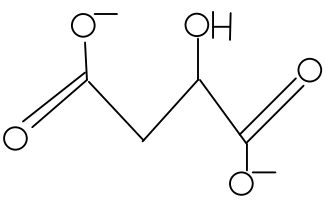
Fig 4.9 Plated copper thickness with time with potassium sodium salt of malic acid as the chelating agent

Table 4.4 Plating rates of structurally similar chelating agents

Chelating agents	Plating rate / μmhr^{-1}
Sodium potassium tartrate	1.51
Trisodium citrate	4.66
Potassium sodium salt of malic acid	1.88

Table 4.5 Structurally similar chelating agents in deprotonated form

Chelating agents	Deprotonated form
Tartaric acid $(C_4H_4O_6^{2-})$	
Citric acid $(C_6H_5O_7^{3-})$	
Malic acid $(C_4H_4O_5^{2-})$	

The chelating agents were added individually to the plating solutions in salt form and the pH of the plating solutions of the various chelating agents ranges from 12.10 to 12.30, so it is safe to assume that the three chelating agents in the plating solutions exists in deprotonated form. Hung and Chen. (1989) compared the plating rate of hypophosphite-reduced electroless copper plating bath using trisodium citrate, sodium potassium tartrate and malic acid respectively as the sole chelating agent. The results of plating rate and stability constant of the chelating agents with Cu^{2+} are shown

in Table 4.6. From the electron paramagnetic resonance (EPR) analysis, the above three chelating agents do not form a characteristics structure with Cu^{2+} unlike EDTA, which forms an octahedral structure. They suggested dimeric structures are formed instead and presence of dicupric complex ions resulted in high plating rate. However, the exact reason for this phenomenon is still unknown.

Table 4.6 Plating rates and stability constants with copper(II) ion for various chelating agents

Chelating agent	Stability constant with Cu^{2+} Log K	Plating rate pH=9.2, 65°C mg/cm^2.h
Trisodium citrate	ML (5.9) M_2L_2 (13.2)	7.6
Sodium potassium tartrate	ML (3.42) M_2L_2 (8.24)	6.6
Malic acid	ML (3.42) M_2L_2 (8.0)	4.2

From Table 4.6, it can be seen that there is no relationship between the stability constants and the plating rate. This also applies to the dual chelating agents system when Table 4.4 is compared with Table 4.6. A high stability constant implies that the chelating agent is bound strongly to the metal ion. The plating rate of sodium potassium tartrate and malic acid in the dual chelating system seems to agree with the corresponding stability constants of the dicupric complex (M_2L_2). The plating rate of malic acid is slightly faster than the sodium potassium tartrate as the stability constant of the dicupric complex of sodium potassium tartrate is slightly higher. The sodium citrate has an exceptionally high stability constant and this is because one citrate molecule can donate three electron pairs to one metal ion. However, the experimental results showed that trisodium citrate has a faster plating rate. The bigger molecular structure of sodium citrate might be responsible for the high plating rate. There are

many factors such as temperature, copper concentration and pH affecting the plating rate, though most of these factors are carefully controlled, at present no reasons are known to explain the difference in plating rates of structurally similar chelating agents. Therefore, further analysis of the electroless copper plating solution is required.

4.4.2   Variation of electrolessly plated copper surfaces during the plating process

The plated copper surfaces at various stage of electroless plating for each respective chelating agent namely: sodium potassium tartrate, trisodium citrate and potassium sodium salt of malic acid were examined using scanning electron microscope (SEM) and atomic force microscope (AFM). The changes on the surface of the plated copper of various chelating agents are discussed in the following sections.

4.4.2.1   Sodium potassium tartrate as the main chelating agent

Figures 4.10a-e shows the 3-dimensional surface image generated by AFM at different plating times. Fig. 4.11 shows the corresponding surface roughness from the roughness analysis. The other 2 chelating agents surface roughness were also included in Fig. 4.11. At the beginning stage of plating, the plated copper surface is relatively flat (surface roughness of 41.34nm) and contains very few 'cone' structures as seen in Fig. 4.10a. The number of 'cone' structures increases with the plating time and also the size tends to increase as well. Comparing Figures 4.10b and c, it is clearly seen that some of the 'cone' structures lump together to form larger ones when the plating time increase from 10 to 15 minutes. At the last investigated plating time of 25 minutes, several large 'cone' structures which are not closely packed are found, resulting in high surface roughness of 126.20 nm.

Fig 4.10 Atomic force microscope 3-dimensional surface images (15 x 15 μm) with sodium potassium tartrate as the chelating agent at a plating time of a)5 min b)10 min c)15 min d)20 min e)25 min (Z axis 250 nm/div)

Fig 4.11 Variation of surface roughness with plating time for various chelating agents

Figures 4.12a-e show the scanning electron microscope images at 5000 magnification at different plating times. The grain structure of the plated copper is not clearly seen at 5 minutes of plating time, this is probably due to the thin layer of plated copper. The fine grain structure of copper is clearly seen when the plating time is above 10 minutes. As the plating time increases, clusters of copper grain structures of 4-5 µm are more common. Fig. 4.11 shows that the surface roughness of the plated copper increases with the plating time. The AFM surface image and SEM image agree well with each other.
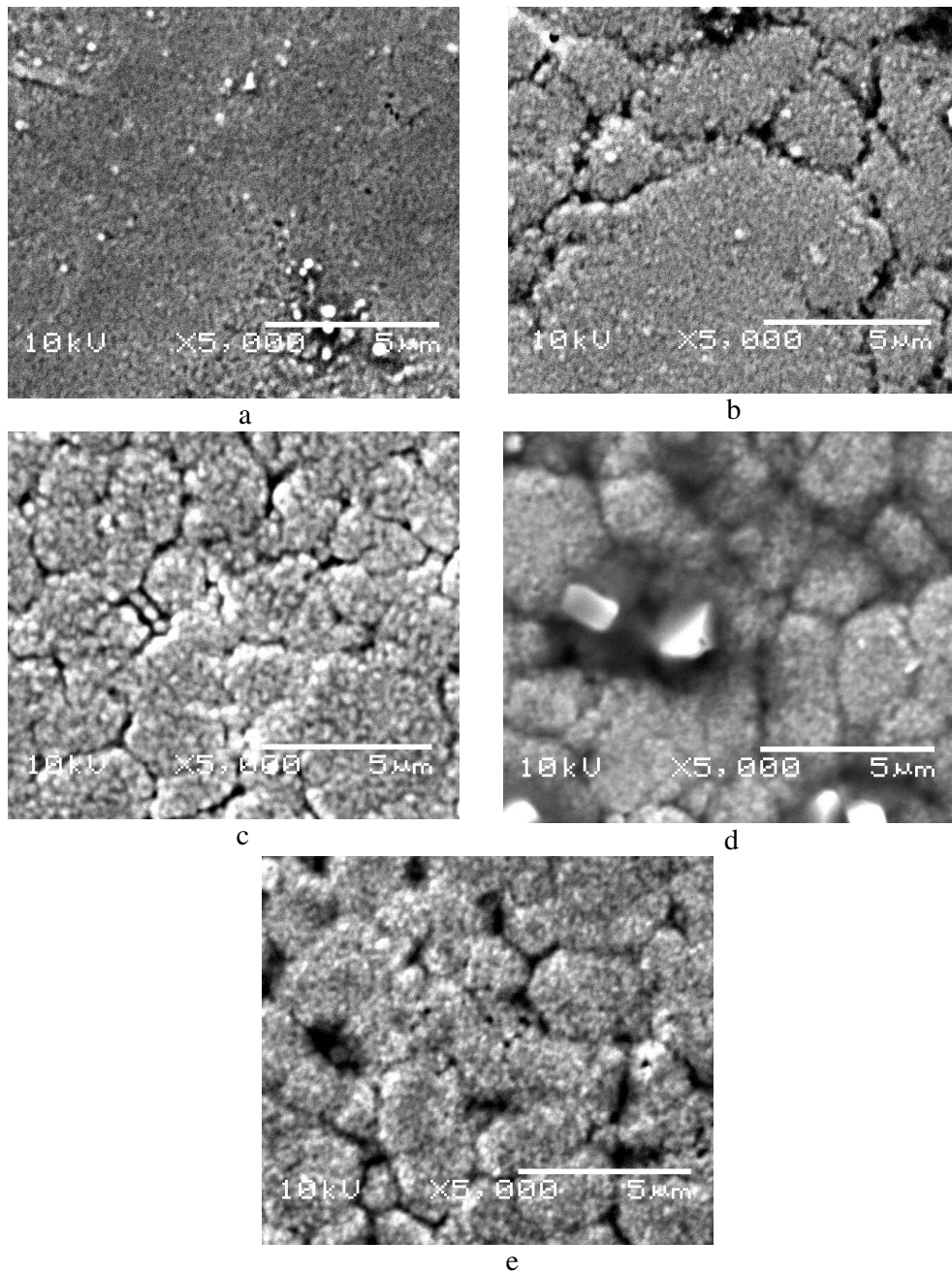
Fig 4.12 Scanning electron microscope images with sodium potassium tartrate as the chelating agent at a plating time of a)5 min b)10 min c)15 min d)20 min e)25 min. Magn. X 5000

4.4.2.2   Trisodium citrate as the main chelating agent

The 3-dimensional surface images generated by AFM at different plating times are shown in Figures 4.13a-e and the corresponding roughness results from the surface roughness analysis are shown in Fig. 4.11. At the first investigated plating time of 10 minutes, many thin 'cone' structures together with a few thicker 'cone' structures are formed. When the plating time increased to 15 minutes, these thin 'cone' structures disappear as they are lumped together to form larger ones of about 2-3 µm. The thin 'cone' structures reappear at the plating time of 20 minutes, but from the AFM surface image, the larger copper structures are still quite dominant. Similar to sodium potassium tartrate, the copper structures tend to increase in size with the plating time. At the last investigated plating time of 30 minutes, the scan area consists mostly of large 'cone' structures of about 2-4 µm in size.
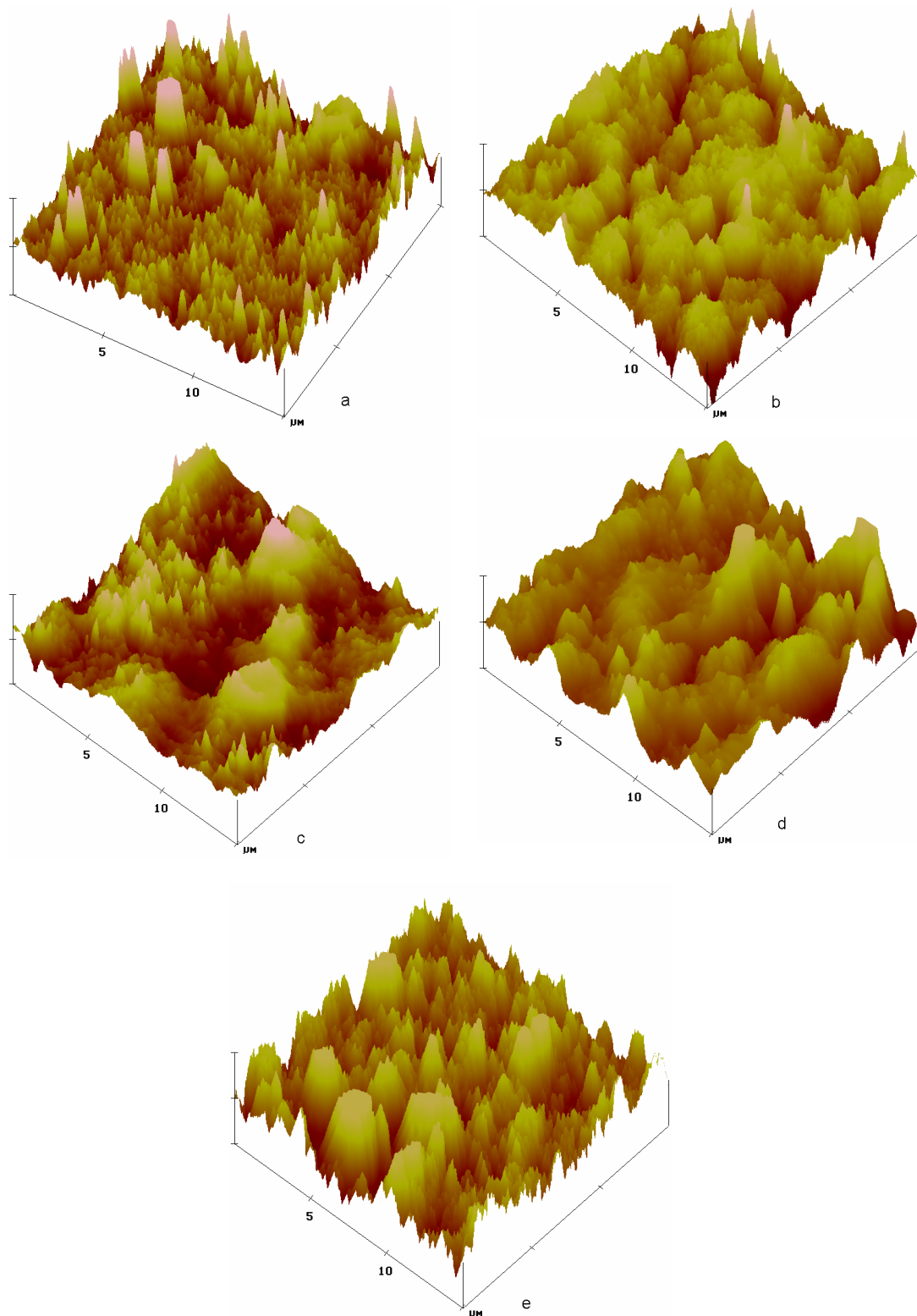
Fig 4.13 Atomic force microscope 3-dimensional surface images (15 x 15 µm) with
trisodium citrate as the chelating agent at a plating time of a)10 min b)15 min c)20 min
d)25 min e)30 min (Z axis 250 nm/div)

The scanning electron microscope images at 5000 magnification at different plating times are shown in Figures 4.14a-e. The SEM image at 10 minutes of plating time agrees extremely well with its AFM counterpart, in which many discrete copper structures of about 0.6 µm are observed. These discrete copper structures are probably covered by additional copper deposited at longer plating times. Clusters of copper structures of about 3-6 µm in size are also formed when the plating time exceeds 15 minutes. At a final plating time of 30 minutes, the SEM image show a rough surface made up of discrete copper structure of 0.5-1.0 µm. Fig. 4.11 shows a roughness of about 103.60 nm. Generally, the surface roughness increases with the plating time and the AFM and SEM image do not contradict each other.
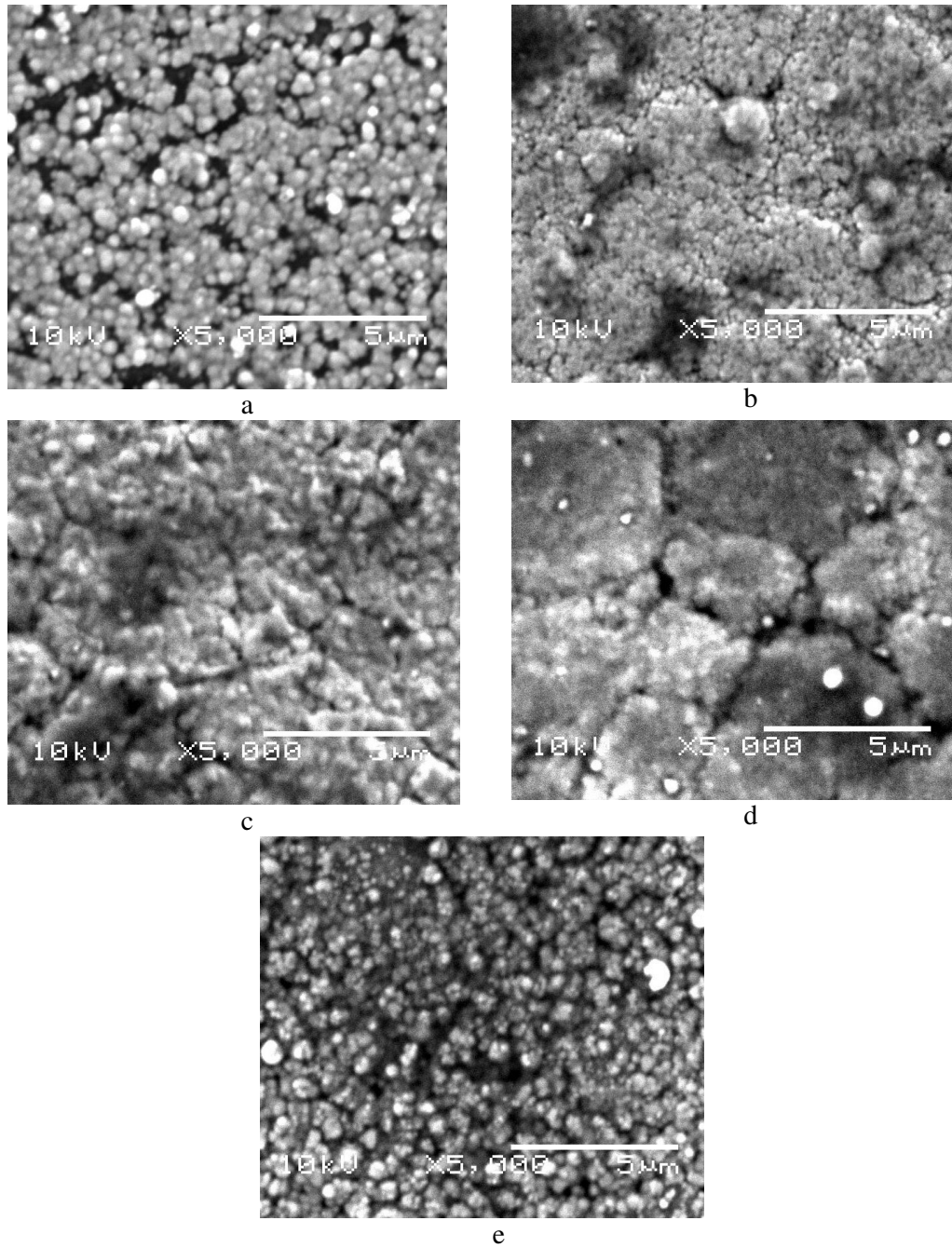
Fig 4.14 Scanning electron microscope images with trisodium citrate as the chelating agent at a plating time of a)10 min b)15 min c)20 min d)25 min e)30 min. Magn. X 5000

4.4.2.3   Potassium sodium salt of malic acid as the main chelating agent

Figures 4.15a-e show the 3-dimensional surface image generated by AFM at different plating times. Fig 4.11 shows the corresponding selected results from the roughness analysis. The initial plating time of 10 minutes shows that many thin 'cone' structures are formed. These 'cone' structures are lumped together when the plating time increases to 15 minutes. However, the lump 'cone' structures do not seem to dominate as the plating time continues to increase and the roughness fluctuates with the plating time.
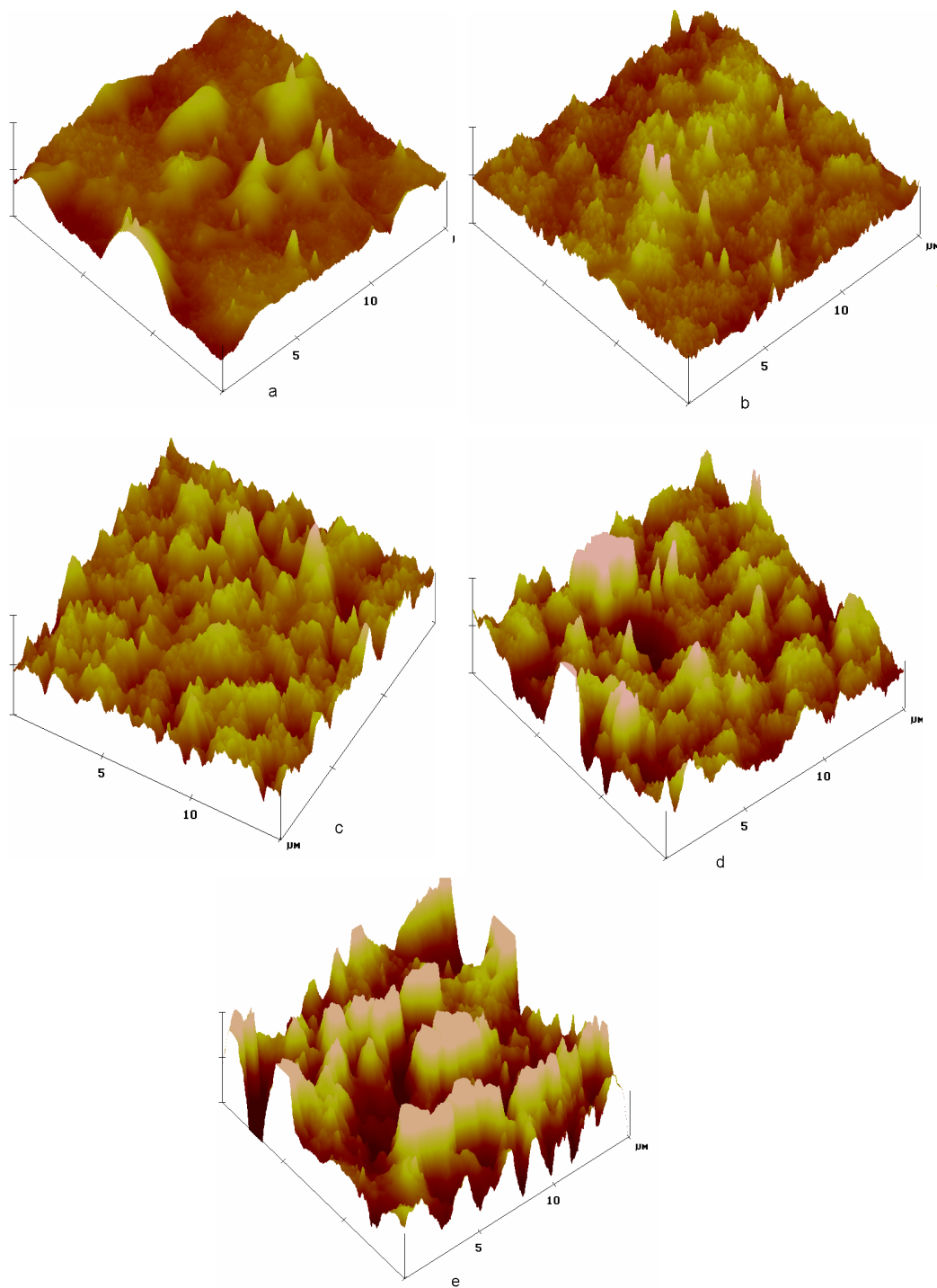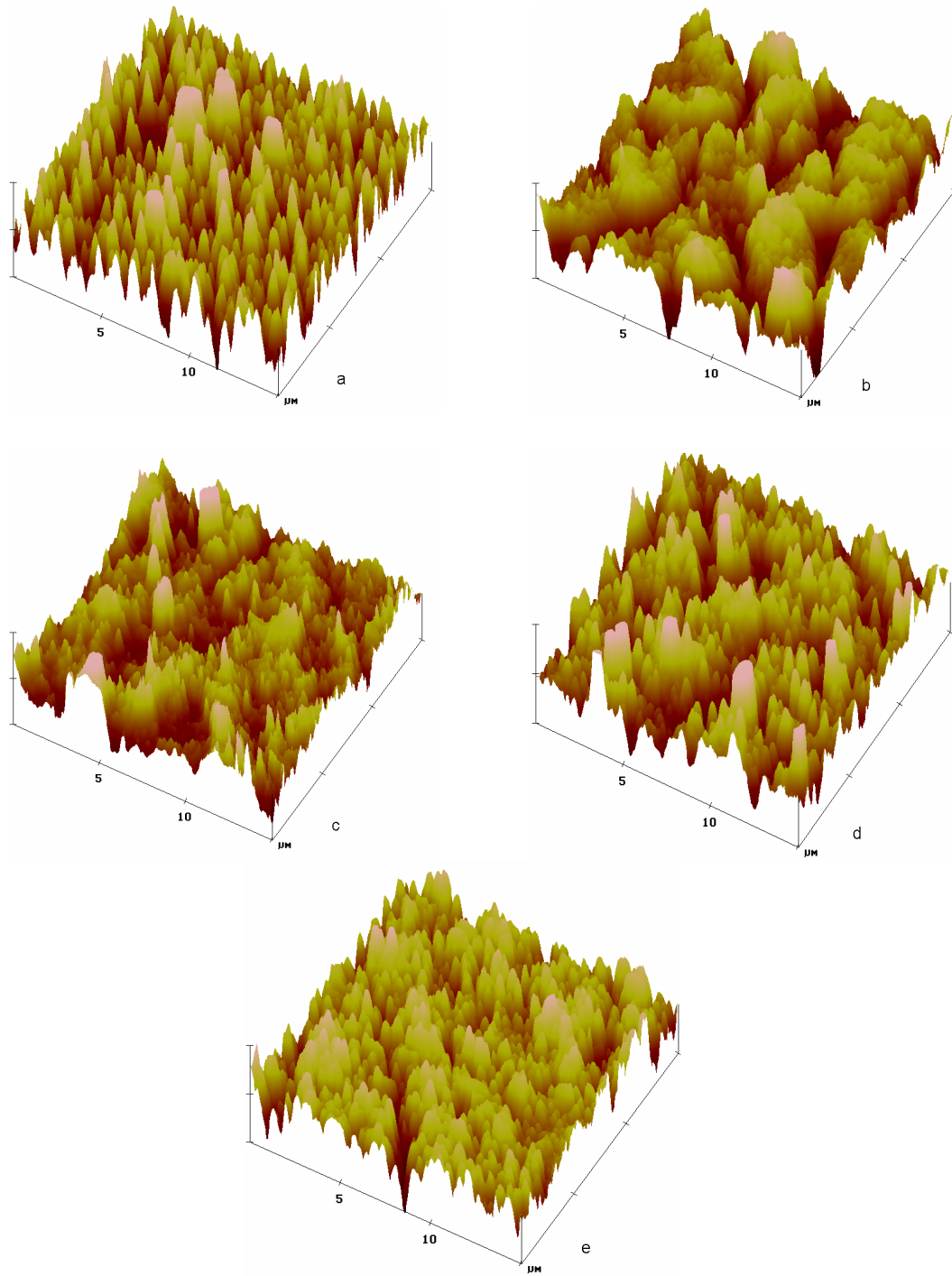
Fig 4.15 Atomic force microscope 3-dimensional surface images (15 x 15 μm) with potassium sodium salt of malic acid as the chelating agent at a plating time of a)10 min b)15 min c)20 min d)25 min e)30 min (Z axis 250 nm/div)

Figures 4.16a-e show the scanning electron microscope images at 5000 magnification at different plating times. The SEM image at 10 minutes of plating time corresponds well with the AFM surface image, in which discrete copper structures of about 0.6 µm are formed. As the plating time further increases from 15 to 25 minutes, the size of the copper grains noticeably increase and start to overlap each other. Finally, at the last investigated plating time of 30 minutes, the copper grains are at the largest at about 1 µm in size. The potassium sodium salt of malic acid tends to produce rougher and less uniform copper surfaces compared to tartaric and citric salts. Therefore, the malic acid is not a suitable chelating agent for electroless copper deposition.
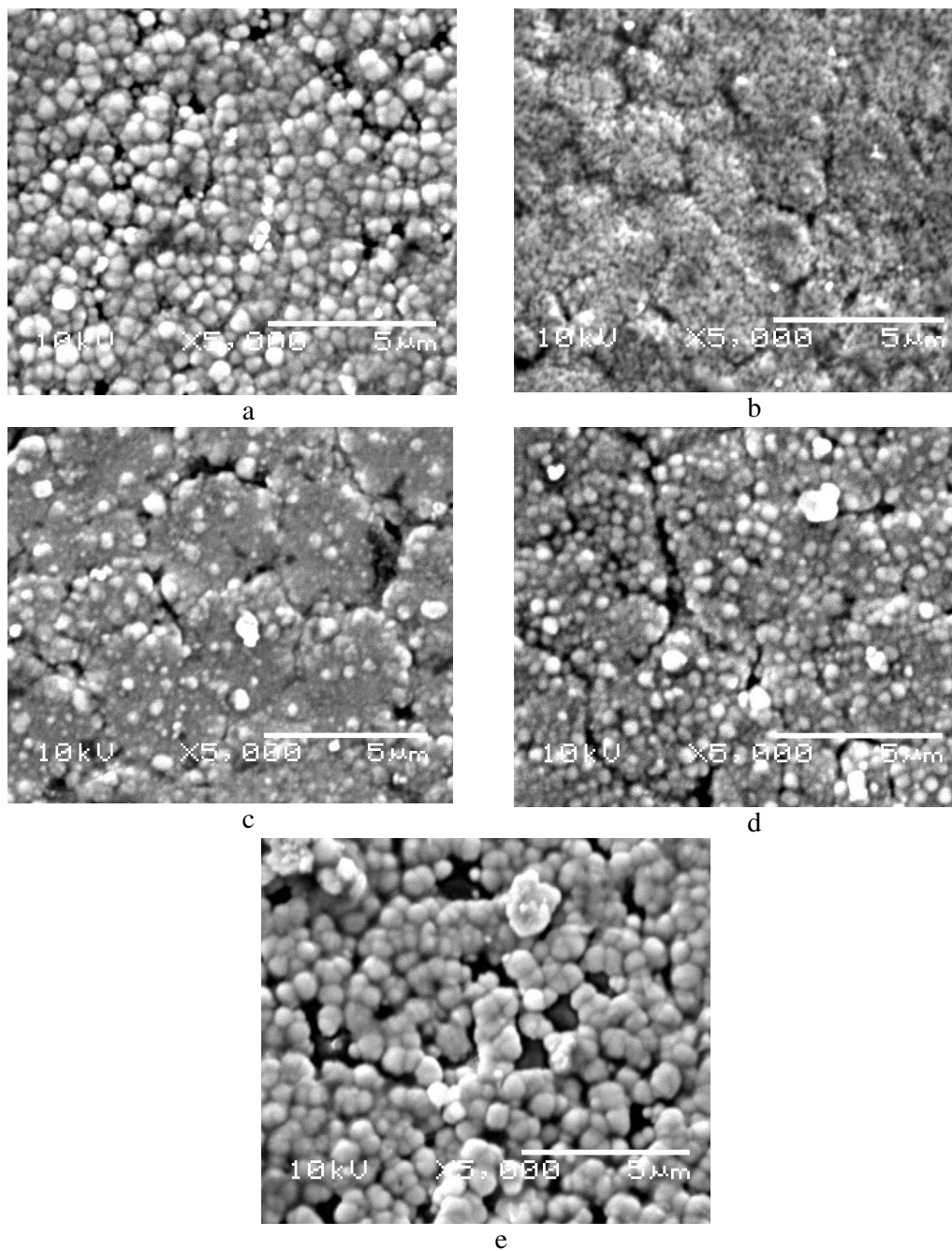
Fig 4.16 Scanning electron microscope images with potassium sodium salt of malic acid as the chelating agent at a plating time of a)10 min b)15 min c)20 min d)25 min e)30 min. Magn. X 5000

4.5   X-ray diffraction (XRD) studies on the effect of structurally similar chelating agents in electroless copper plating solution

XRD studies were conducted on three copper samples electrolessly plated on acrylonitrile-butadiene-styrene (ABS) film using potassium sodium tartrate, trisodium citrate and potassium sodium salt of malic acid as the main chelating agent in each plating solution. The optimized mole ratios of the chelating agents to copper ions are 3.5 for both the potassium sodium tartrate and trisodium citrate, and 2.5 for potassium sodium salt of malic acid. The copper concentration in the electroless copper plating solution was held constant at 0.1161M.

The XRD patterns of each chelating agent used in electroless copper plating solution are shown in Figures 4.17-4.19. The scanning range of the XRD is set at 25 to 75° and each distinct peak represents a particular plane orientation. Within the scanning range, all the three chelating agents reveal a strong (111) plane orientation and a relatively weak (200) plane orientation. However, the (111)/(200) intensity ratios are slightly different. Table 4.7 gives the values of the (111)/(200) intensity ratios of each chelating agent. Tri-sodium citrate dihydrate most favours the (111) plane orientation , while potassium sodium salt of malic acid least favours.

Lin and Yen. (2001) carried out XRD analysis of electrolessly plated copper on copper sheets employing ethylenediaminetetracetic acid (EDTA) and triethanolamine (TEA) as the dual chelating agent system. The reducing agent used was formaldehyde. Crystalline planes of (111), (200) and (220) are found with (111) and (220) as the major crystallographic orientation. XRD analysis performed on plated copper from an electroless plating solution containing copper ions, EDTA, formaldehyde and bi-pyridine revealed a (111) and (200) crystallographic orientation (Oita et al., 1997).

Therefore, the crystalline structure obtained from our plating solutions is comparable to other electrolessly deposited copper from similar plating solutions.

Table 4.7 (111)/(200) Intensity ratios of structurally similar chelating agents

Chelating agent	(111)/(200) Intensity ratio
Sodium potassium tatrtrate	2.375
Trisodium citrate	2.731
Potassium sodium salt of malic acid	1.992

XRD Pattern of Mole Ratio of Sodium Potassium Tartrate to $CuSO_4$=3.5
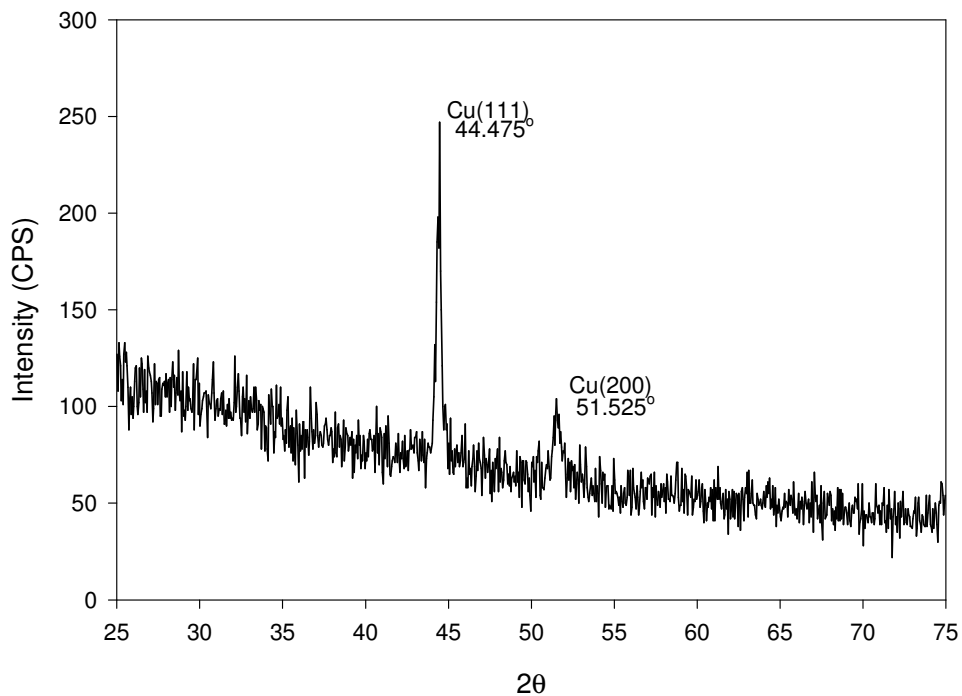
Fig 4.17 XRD pattern of electrolessly plated copper using sodium potassium tartrate as the main chelating agent. The mole ratio of sodium potassium tartrate to copper is 3.5

XRD Pattern of Mole Ratio of Trisodium Citrate to $CuSO_4$=3.5
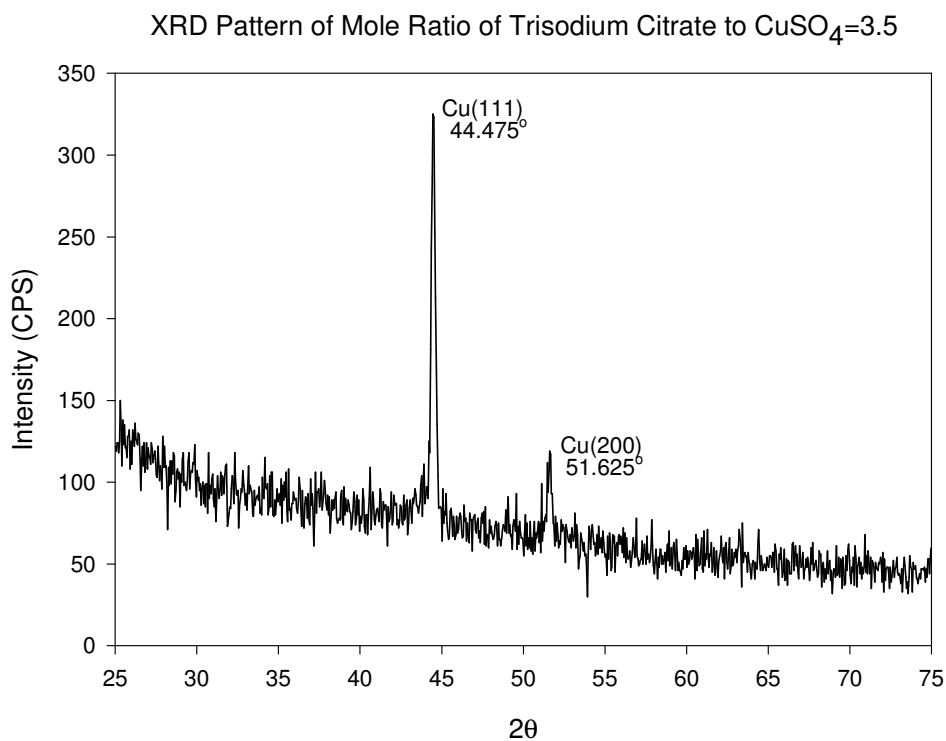
Fig 4.18 XRD pattern of electrolessly plated copper using trisodium citrate as the main chelating agent. The mole ratio of trisodium citrate to copper is 3.5

XRD Pattern of Mole Ratio of Potassium Sodium Salt of Malic Acid to $CuSO_4$=2.5
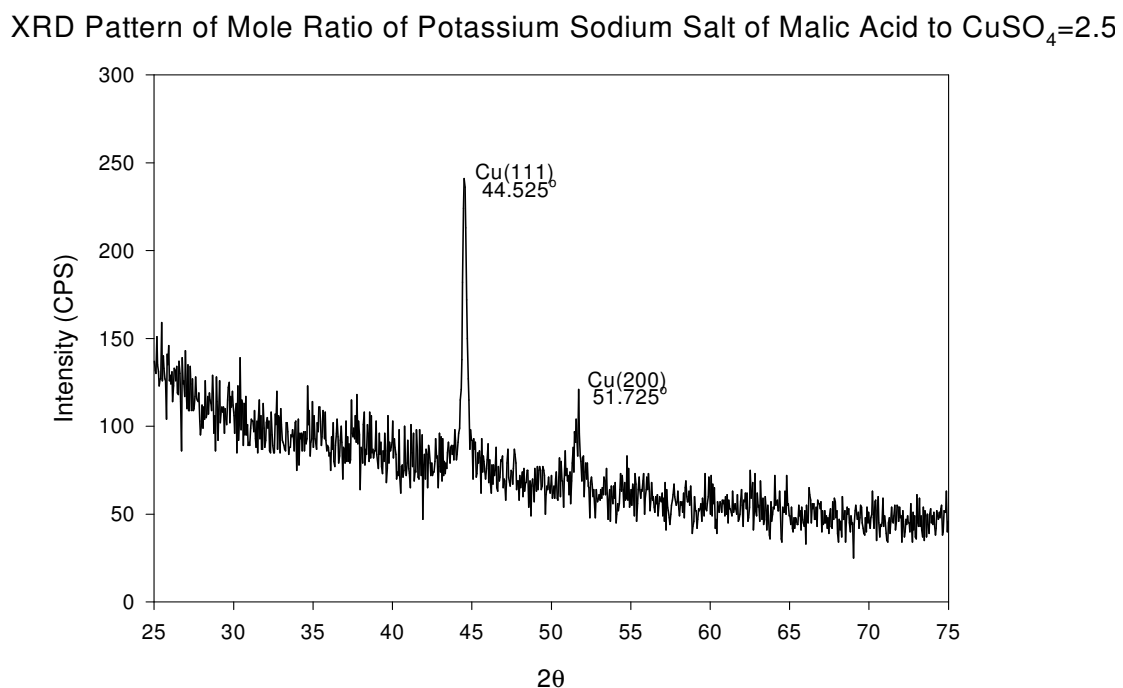
Fig 4.19 XRD pattern of electrolessly plated copper using potassium sodium salt of malic acid as the main chelating agent. The mole ratio of potassium sodium salt of malic acid to copper is 2.5

Chapter 5

Influence of Stabilizer on the Electroless Copper Plating Solution

The primary role of stabilizers is to prevent decomposition of the plating solution during the electroless deposition process as the electroless plating solution is inherently thermodynamically unstable. This chapter seeks to explore possible stabilizer candidates with special attention given to amino acids. Plating rates employing various stabilizers were obtained by weight gain method as described in Section 3.3 and 3.5. The scanning electron microscopy (SEM) and atomic force microscopy (AFM) were used extensively to observe the surface morphology.

5.1 Removal of bi-pyridine from the electroless plating solution

The electroless copper plating employs the sodium potassium tartrate as the main chelating agent in optimized concentration determined in Section 4.1. The rest of the components are stated in Table 3.3. The only difference is the omission of bi-pyridine. Kinetic analysis and surface morphology of the plated copper were investigated.

5.1.1 Calculated plating rates in the absence of bi-pyridine

Fig 5.1 shows the graph of the increase of plated copper with plating time in the absence of bi-pyridine. The pH of the plating solution was maintained at a close range of 12.10 to 12.30. A plating rate of 21.78 µm/hr was obtained, which was about 14.5 times faster when bi-pyridine was included.

Copper Thickness with Plating Time
(No Stabilizer: without Bi-pyridine)
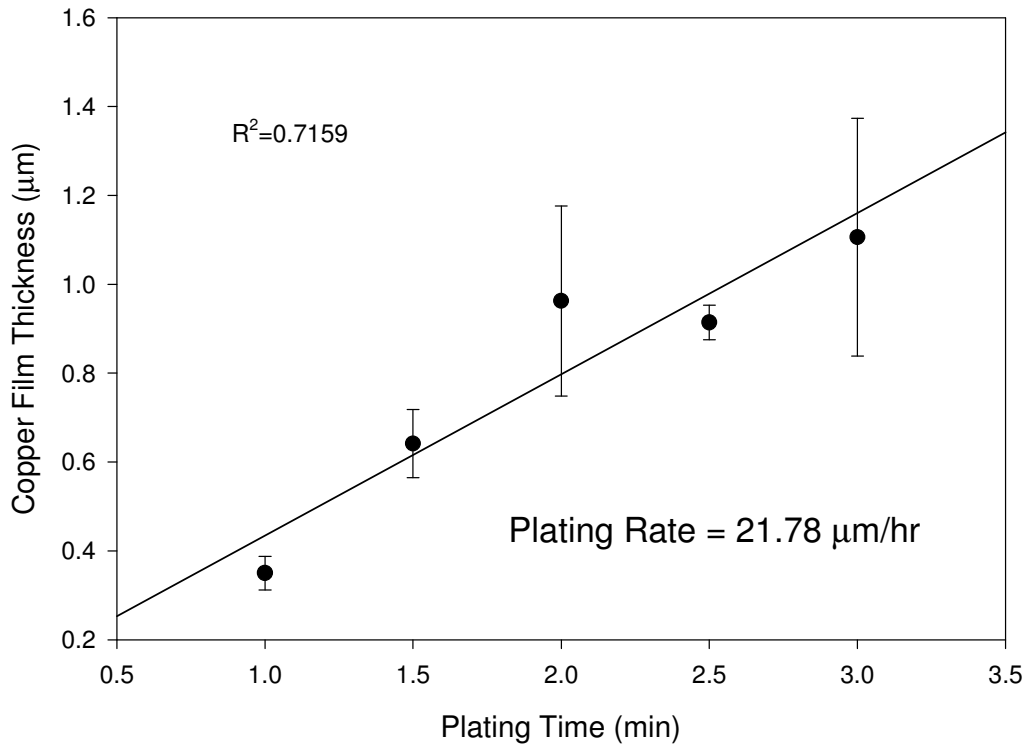
Fig 5.1 Plated copper thickness with time with no bi-pyridine

5.1.2   Variation of electrolessly plated copper surface during the plating process

The surface image (15x15 µm) of the plated copper taken by AFM in the absence of bi-pyridine at various plating times are shown in Figures 5.2a-e. The roughness analysis of the plated copper surface at various plating times is shown in Table 5.1. It is obvious from Fig. 5.2 that the surface roughness increase with the plating time and the roughness measurements shown in Table 5.1 verifies this. At the early stage of plating, the surface area is relatively even with few 'cone' like structures. When the plating time increases to 1.5 minutes, many 'cone' structures were formed on the thin layer of ABS plastics, and those structures lumped together to form larger ones as plating proceeds. At the last investigated plating time of 3.0 minutes, an uneven

surface made up of big 'cone' structures surrounded by small copper structures were formed. The associated surface roughness was 168.6 nm.
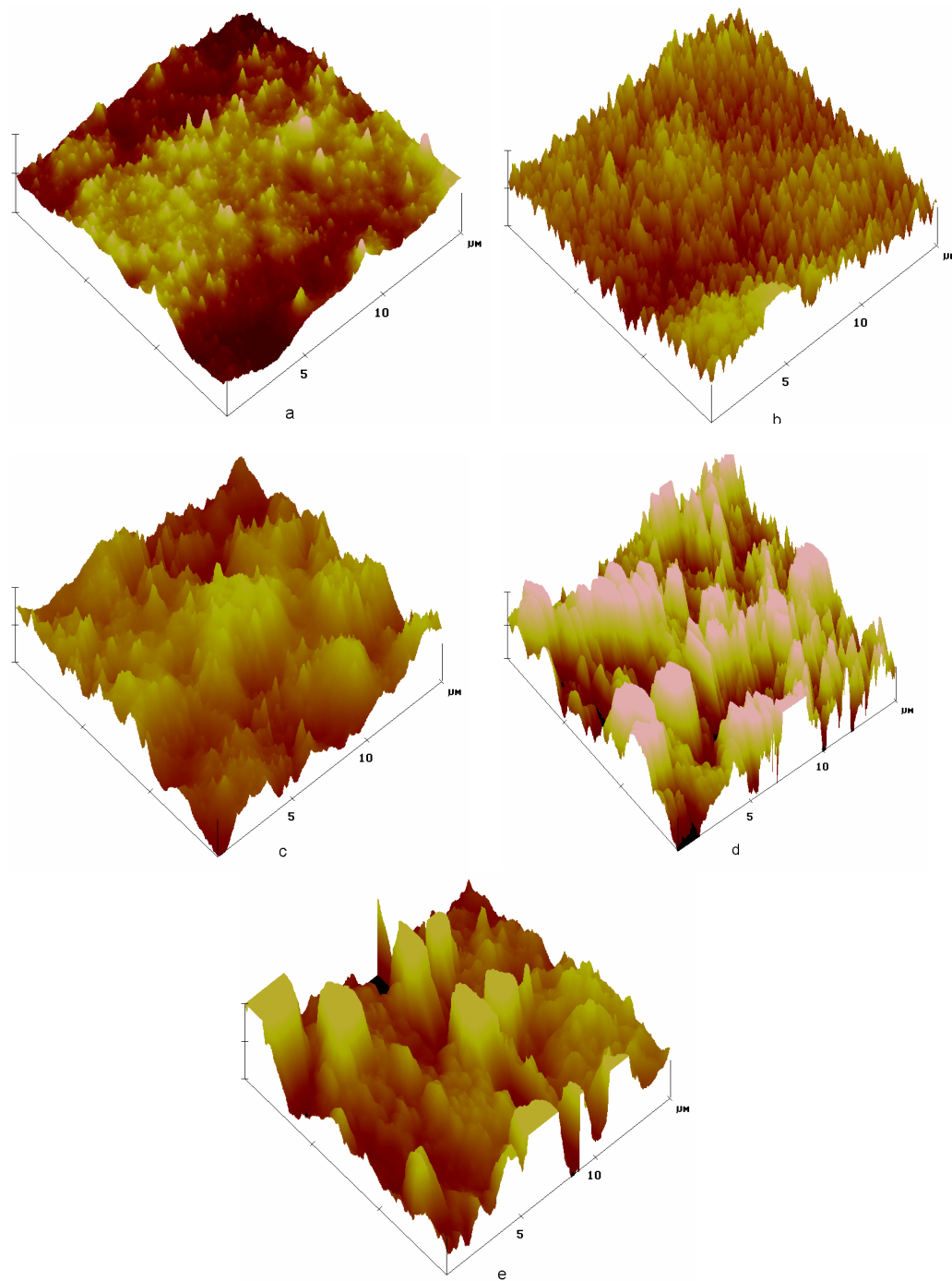
Fig 5.2 Atomic force microscope 3-dimensional surface images (15 x 15 μm) without bi-pyridine as the stabilizer at a plating time of a)1.0 min b)1.5 min c)2.0 min d)2.5 min e)3.0 min (Z axis 250 nm/div)

Table 5.1 Selected roughness analysis results at various plating times in the absence of bi-pyridine

Plating time/min	Img. RMS (Rq) /nm
1.0	48.2
1.5	73.0
2.0	100.5
2.5	157.9
3.0	168.6

Img. Rms (Rq) refers to the root mean square of height deviations taken from the mean data plane, expressed as $\sqrt{\dfrac{(Z_1^2 + Z_2^2 + Z_3^2 + ... + Z_n^2)}{N}}$

The SEM images at various plating times are shown in Fig. 5.3. At all the various plating times, grain structure of copper of about 0.4-0.6 µm in size is clearly seen. At the initial phase of plating (1-2 minutes), no clusters of copper grain are formed. The SEM image and the AFM surface image complement each other in a way that SEM reveals more information on the surface morphology of the copper grains, while AFM provides important height variations of the plated copper structures.
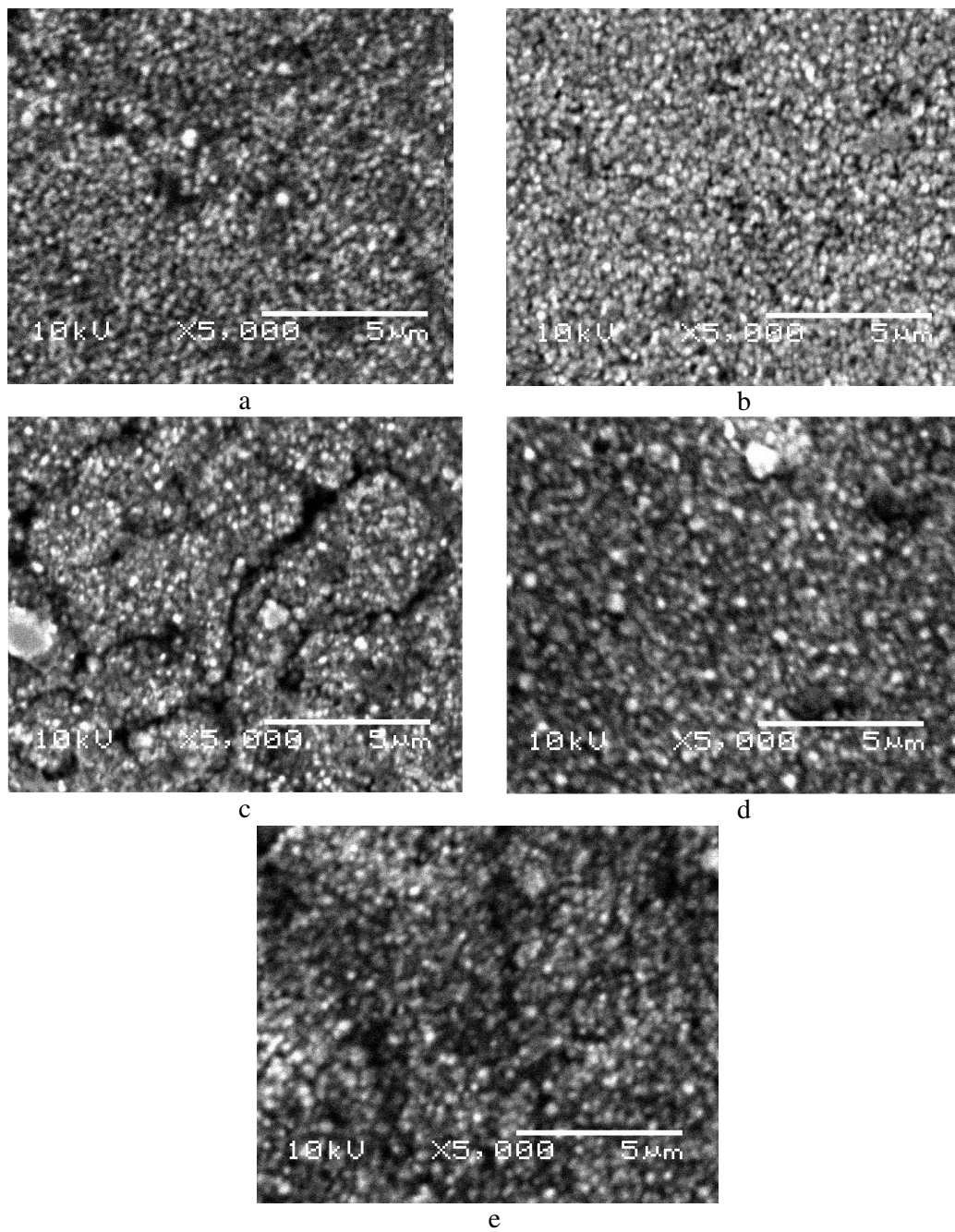
Fig 5.3 Scanning electron microscope images at a plating time of a)1.0 min b)1.5 min c)2.0 min d)2.5 min e)3.0 min in the absence of bi-pyridine. Magn. X5000

5.1.3 Discussion

Certain chemical properties of bi-pyridine make it a good choice for stabilizing the electroless copper plating solution. As mentioned in Section 2.1, Cu_2O is one of the main causes for bath decomposition, bi-pyridine are known to form complex with Cu(I) and prevent the formation of Cu_2O. Also, bi-pyridine can adsorb on the active nuclei in the bulk solution and block the growth of these active nuclei to prevent plate-out (Mallory and Haju, 1990). From the experimentally determined plating rates with and without bi-pyridine, it is obvious that bi-pyridine interferes with the plating process . The bi-pyridine could have possibly adsorb onto the activated ABS film and compete with the Cu^{2+} deposition process. Through this process, the grain structure of copper is more refined with the addition of bi-pyridine. This is shown by comparing the SEM images in Fig. 4.12 and Fig. 5.3. However, the surface roughness of the plated copper samples does not change drastically. Thus, the concentration of bi-pyridine is effective in controlling the deposition rate and grain structure of the plated copper.

5.2 Replacement of bi-pyridine with L-methionine in the electroless plating solution

The electroless copper plating employs sodium potassium tartrate as the main chelating agent at optimized concentration determined in Section 4.1. The rest of the components are listed in Table 3.3. The only difference is the replacement of bi-pyridine with L-methionine. The mole concentration of L-methionine in the plating solution is the same as bi-pyridine. Later, the concentration of L-methionine was doubled. Kinetic analysis and the surface morphology of the plated copper were investigated.

5.2.1 Calculated plating rates with L-methionine as stabilizer

Fig. 5.4 shows the graph of the increase of plated copper with plating time with L-methionine as stabilizer. The pH of the plating solution was maintained at 12.60-12.90. A plating rate of 34.01 µm/hr was obtained, which was about 22.6 times faster when bi-pyridine was used as the stabilizer.

Copper Thickness with Plating Time
(Stabilizer: L-Methionine)

R^2=0.9024

Plating Rate = 34.01 µm/hr

Copper Film Thickness (µm)

Plating Time (min)
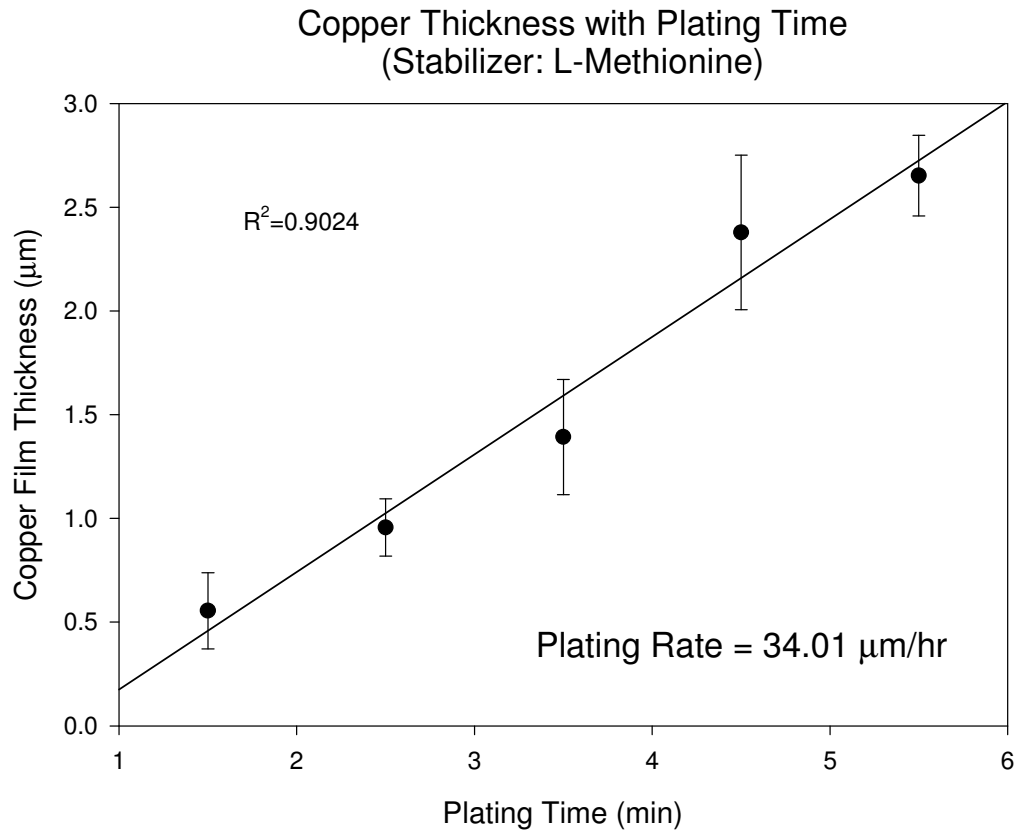
Fig 5.4 Plated copper thickness versus time with L-methionine as the stabilizer

5.2.2 Variation of electrolessly plated copper surface during the plating process

The surface image (15 x 15 µm) of the plated copper taken by AFM with L-methionine as stabilizer at various plating times are shown in Figures 5.5a-e. The roughness analysis of the plated copper surface at various plating time are shown in Table 5.2. During the early stages of plating, the plated copper surface is relatively even with few

'cone' structures. When the plating time was increased to 2.5 minutes, the surface image looks to be rougher with more protruding copper structures. The surface roughness increases from 48.9 to 58.9 nm. From Table 5.2, the surface roughness of the plated copper appears to be at its peak at a plating time of 3.5 minutes. The AFM surface image at 3.5 minutes shows a mixture of 'cone' structures of various heights, and it seems to have the roughest surface from observation. At a further plating time of 4.5 minutes, many smaller copper 'cone' structures are seen together with two much larger structures and finally the small 'cone' structures were lumped together to form larger ones as shown in Fig. 5.5e.

Table 5.2 Selected roughness analysis results at various plating times with bi-pyridine as the stabilizer

Plating time/min	Img. RMS (Rq) /nm
1.5	48.941
2.5	58.899
3.5	75.176
4.5	60.402
5.5	46.696

Img. Rms (Rq) refers to the root mean square of height deviations taken from the mean data plane, expressed as $\sqrt{\dfrac{(Z_1^2 + Z_2^2 + Z_3^2 + ... + Z_n^2)}{N}}$
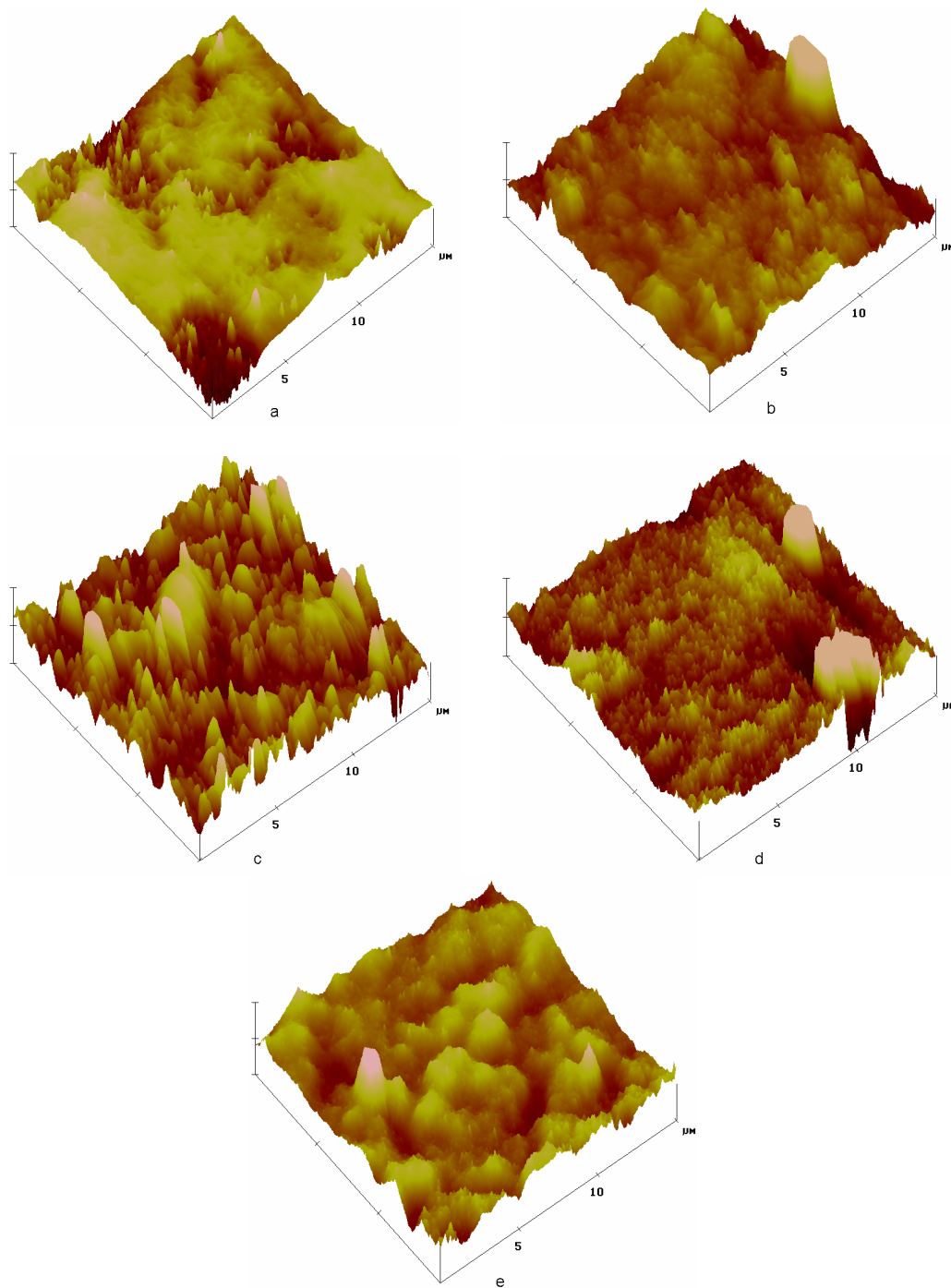
Fig 5.5 Atomic force microscope 3-dimensional surface images (15 x 15 μm) with L-methionine as the stabilizer at a plating time of a)1.5 min b)2.5 min c)3.5 min d)4.5 min e)5.5 min (Z axis 250 nm/div)

The corresponding SEM images at various plating times are shown in Figures 5.6a-e. All the SEM images exhibit fine grain structures except in Fig. 5.6c, which is not taken clearly. These fine grain structures are similar to those utilising bi-pyridine as the stabilizer (shown in Fig. 4.12). This is totally different from those SEM images of electrolessly plated copper samples omitting bi-pyridine, which reveal a coarse grain structure. The clusters of grain structure of copper of about 4-6 µm in size are formed at longer plating times. The SEM images are consistent with the AFM surface images.
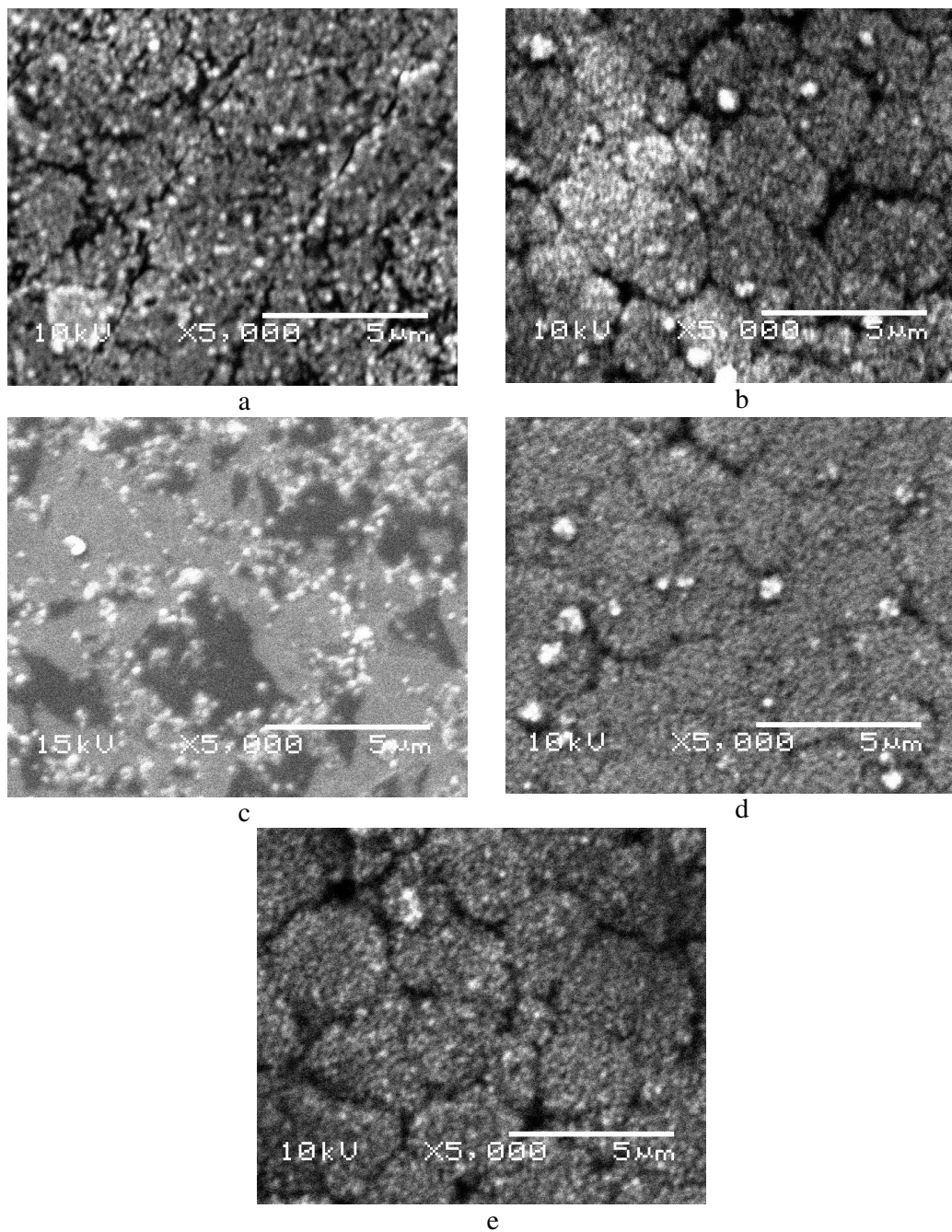
Fig 5.6 Scanning electron microscope images at a plating time of a)1.5 min b)2.5 min c)3.5 min d)4.5 min e)5.5 min with L-methionine as the stabilizer. Magn. X5000

5.2.3   Discussion

When the bi-pyridine was used as the stabilizer in the plating solution, the electroless plating solution does not decompose within 30 minutes. When bi-pyridine was

replaced by L-methionine at the same concentration, the electroless copper plating solution was found to have decomposed within 30 minutes of plating. This shows that L-methionine is not a strong stabilizing agent as compared to bi-pyridine.

High plating rate was observed with L-methionine employed as the stabilizer. This plating rate of 34.01 µm/hr is even higher than when bi-pyridine was omitted. The presence of L-methionine accelerates the electroless copper plating process. The stability constant of Cu^{2+} to L-methionine is 7.87 (Martell and Smith, 1989). This stability constant of Cu^{2+} to L-methionine is much higher than sodium potassium tartrate, trisodium citrate and malic acid given in Table 4.6. The L-methionine could have adsorbed onto the activated ABS film and attracts the Cu^{2+} ions since its affinity to Cu^{2+} is even higher than tartaric acid, which is the main chelating agent. The structure of L-methionine is shown in Fig. 5.7. L-methionine, which is one of the natural amino acids, is a dipolar molecule. It exists as a negatively charged molecule in alkaline conditions as shown in Equation 5.1 (Morrison and Boyd, 1992). This will further increase its affinity towards Cu^{2+} ions.

$$^{+}H_{3}NCHRCOO^{-} + OH^{-} \Leftrightarrow H_{2}NCHRCOO^{-} + H_{2}O \qquad (5.1)$$
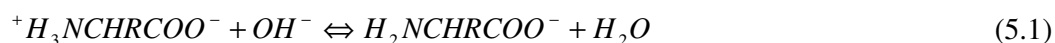
where R represents the organic group

The presence of low concentrations of L-methionine seems to have an effect on the copper grain structure. Fine grain structures, which are very similar to those obtained with bi-pyridine, were observed. At this stage, the exact reason to explain how the L-methionine could have contributed to the formation of fine grain structures is still unknown. However, it is obvious that plating speed does not affect the morphology of the copper structures.
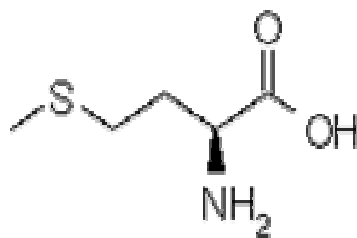
Fig 5.7 The structure of L-methionine

5.2.4   Calculated plating rates at a double concentration of L-methionine

Fig. 5.8 shows the graph of the increase of plated copper with plating time with a
double concentration of L-methionine as the stabilizer. The pH of the plating solution
was maintained at 12.60-12.90. A plating rate of 23.66 µm/hr was obtained, which
was much slower as compared to half of the L-methionine concentration used earlier.
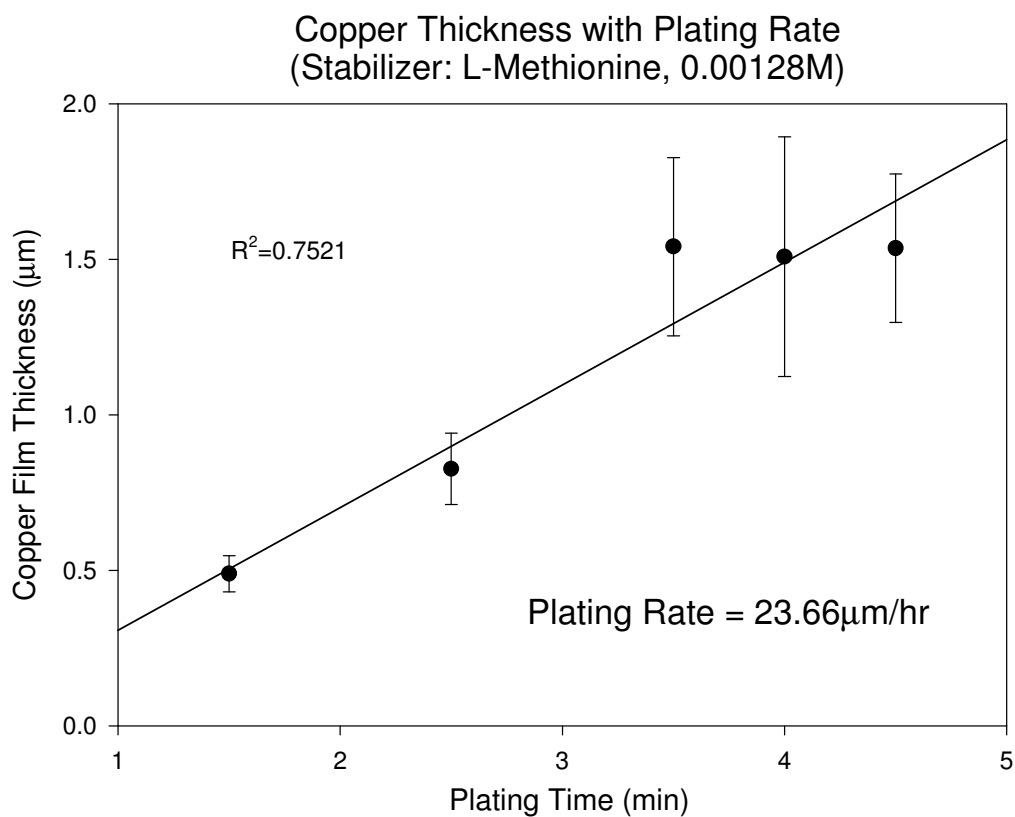
Fig 5.8 Plated copper thickness versus time with double of the concentration of L-
methionine as the stabilizer

5.2.5   Variation of electrolessly plated copper surface during the plating process
         with double the concentration of L-methionine

The surface images (15 x 15 µm) of the plated copper taken by AFM with double the

concentration of L-methionine as the stabilizer at various plating times are shown in

Figures 5.9a-e. The roughness analysis of the plated copper surface at various plating

times are shown in Table 5.3. At the first investigated plating time of 1.5 minutes, the

surface of the plated copper is the smoothest with small 'cone' structures covering

about 85% of the scan area. At the next plating time of 2.5 minutes, larger 'cone'

structures are formed and the surface roughness increased from 25.4 to 35.9 nm. The

'cone' copper structures lumped together over the subsequent plating time at 3.5

minutes and 4.0 minutes. Lastly, at the final investigated plating time of 4.5 minutes,

an uneven surface was formed with many large 'cone' structures. The surface

roughness from Table 5.3 showed that the surface roughness increases with the plating

time.

Table 5.3 Selected roughness analysis results at various plating times with double the
concentration of bi-pyridine as the stabilizer

Plating time/min	Img. RMS (Rq) /nm
1.5	25.4
2.5	35.9
3.5	35.5
4.0	47.2
4.5	61.6

Img. Rms (Rq) refers to the root mean square of height deviations taken from the mean

data plane, expressed as $\sqrt{\dfrac{(Z_1^2 + Z_2^2 + Z_3^2 + ... + Z_n^2)}{N}}$

Fig 5.9 Atomic force microscope 3-dimensional surface images (15 x 15 µm) with double the concentration of L-methionine as the stabilizer at a plating time of a)1.5 min b)2.5 min c)3.5 min d)4.0 min e)4.5 min (Z axis 250 nm/div)

The corresponding SEM images at various plating times are shown in Figures 5.10a-e. Figures 5.10a-d show the plated copper is made up of fine grain structures similar to Fig. 5.6. However, at the last investigated plating time of 4.5 minutes, coarse grain structures of copper were observed. At the initial phase of plating, defects like cracks are more common.

5.2.6   Discussion

When the concentration of L-methionine in the electrolessly plating solution was doubled, the decomposition time does not vary much. Incremental addition of L-methionine does not prolong the decomposition time. A plating rate of 23.66 µm/hr was obtained when the concentration of L-methionine was increased to 0.00128 M. It is much slower than the plating rate of 34.01 µm/hr when the concentration of L-methionine was only 0.00064 M. Plating rate is not directly proportional to the concentration of L-methionine. It is certain that only a certain range of L-methionine produces a high plating rate. Changes in the concentration of L-methionine do not change the grain structure of the plated copper to a large extent within the investigated concentration range.
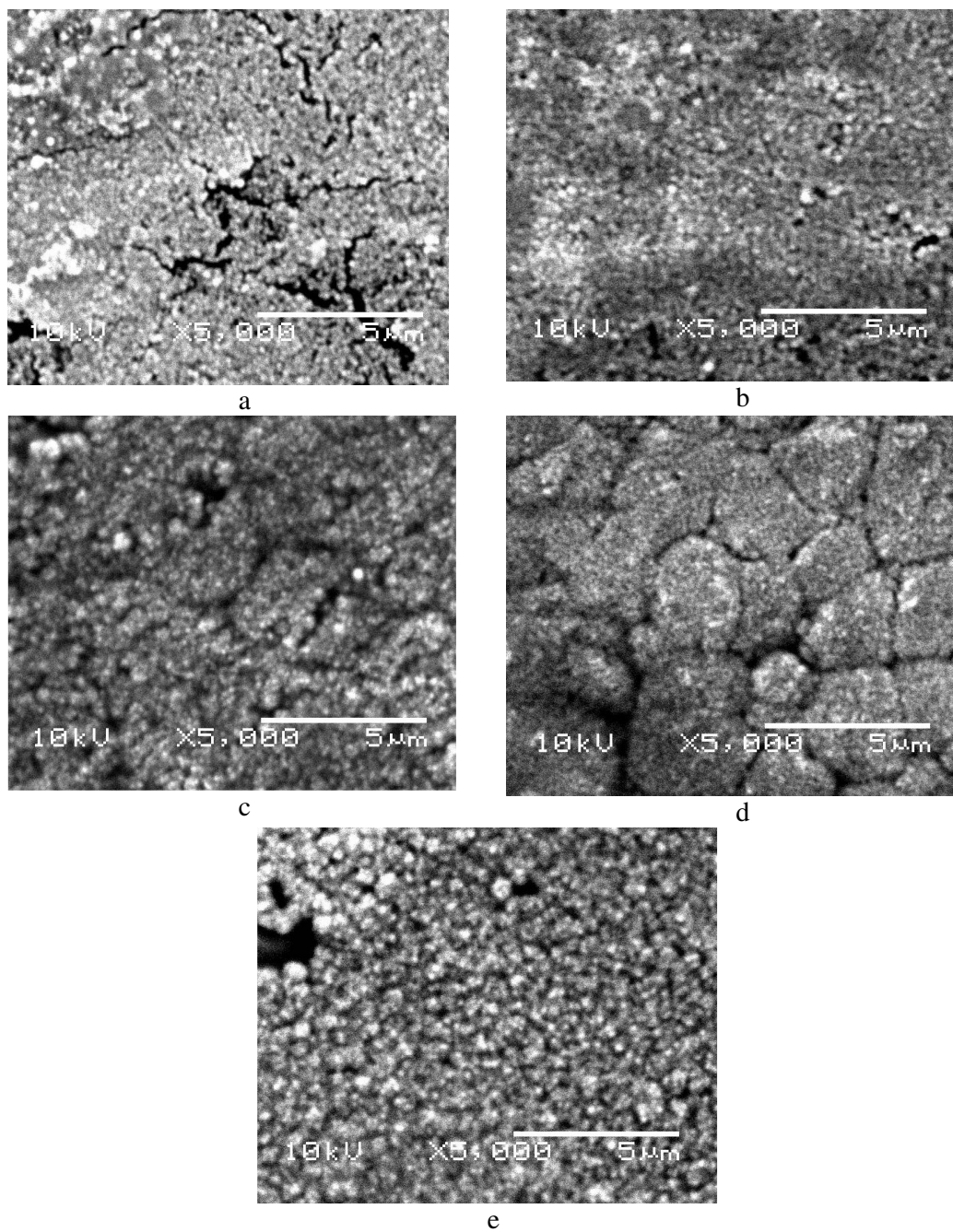
Fig 5.10 Scanning electron microscope images at a plating time of a)1.5 min b)2.5 min c)3.5 min d)4.0 min e)4.5 min with double the concentration of L-methionine as the stabilizer. Magn. X5000

5.3 Replacement of bi-pyridine with glycine in the electroless plating solution

The electroless copper plating employs the sodium potassium tartrate as the main chelating agent at the optimized concentration as determined in Section 4.1. The rest of the components are stated in Table 3.3. The only difference is the replacement of bi-pyridine with glycine. The molar concentration of glycine in the plating solution is the same as bi-pyridine. Kinetic analysis and surface morphology of the plated copper were investigated.

5.3.1 Calculated plating rates with glycine as the stabilizer

Fig. 5.11 shows the graph of the increase of plated copper with plating time with glycine as the stabilizer. The pH of the plating solution was maintained at 12.70-13.00. A plating rate of 20.17 µm/hr was obtained.
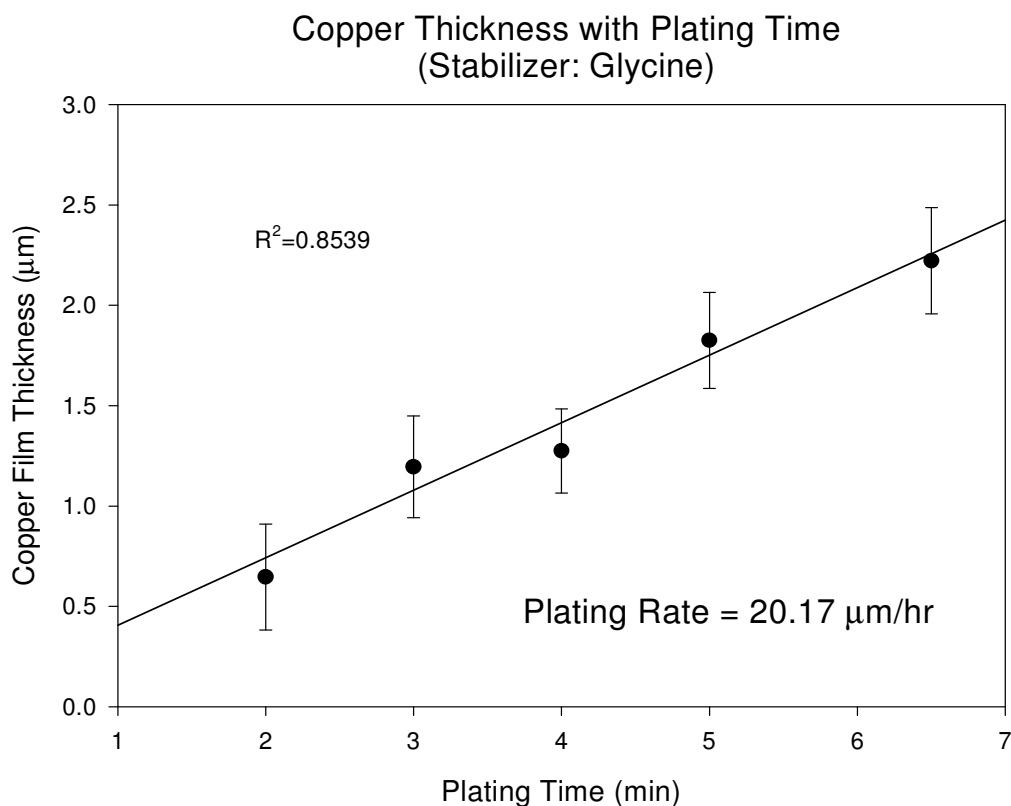
Fig 5.11 Plated copper thickness versus time with glycine as the stabilizer

5.3.2   Variation of electrolessly plated copper surface during the plating process

The surface images (15 x 15µm) of the plated copper taken by AFM with glycine as the stabilizer at various plating times are shown in Figures 5.13a-e. The roughness of the plated copper surface at various plating times is shown in Table 5.4. The initial plating is characterized by small 'cone' copper structures scattered around the scan area. When the plating time is increased to 4 minutes and beyond, the plated surface becomes uneven. A mixture of small and large copper 'cone' structures were observed. Table 5.4 shows that the surface roughness generally increases with the plating time.

Table 5.4 Selected roughness analysis results at various plating times with glycine as the stabilizer

Plating time/min	Img. RMS (Rq) /nm
2.0	54.0
3.0	52.8
4.0	70.7
5.0	82.3
6.5	94.7

Img. Rms (Rq) refers to the root mean square of height deviations taken from the mean data plane, expressed as $\sqrt{\dfrac{(Z_1^2 + Z_2^2 + Z_3^2 + ... + Z_n^2)}{N}}$
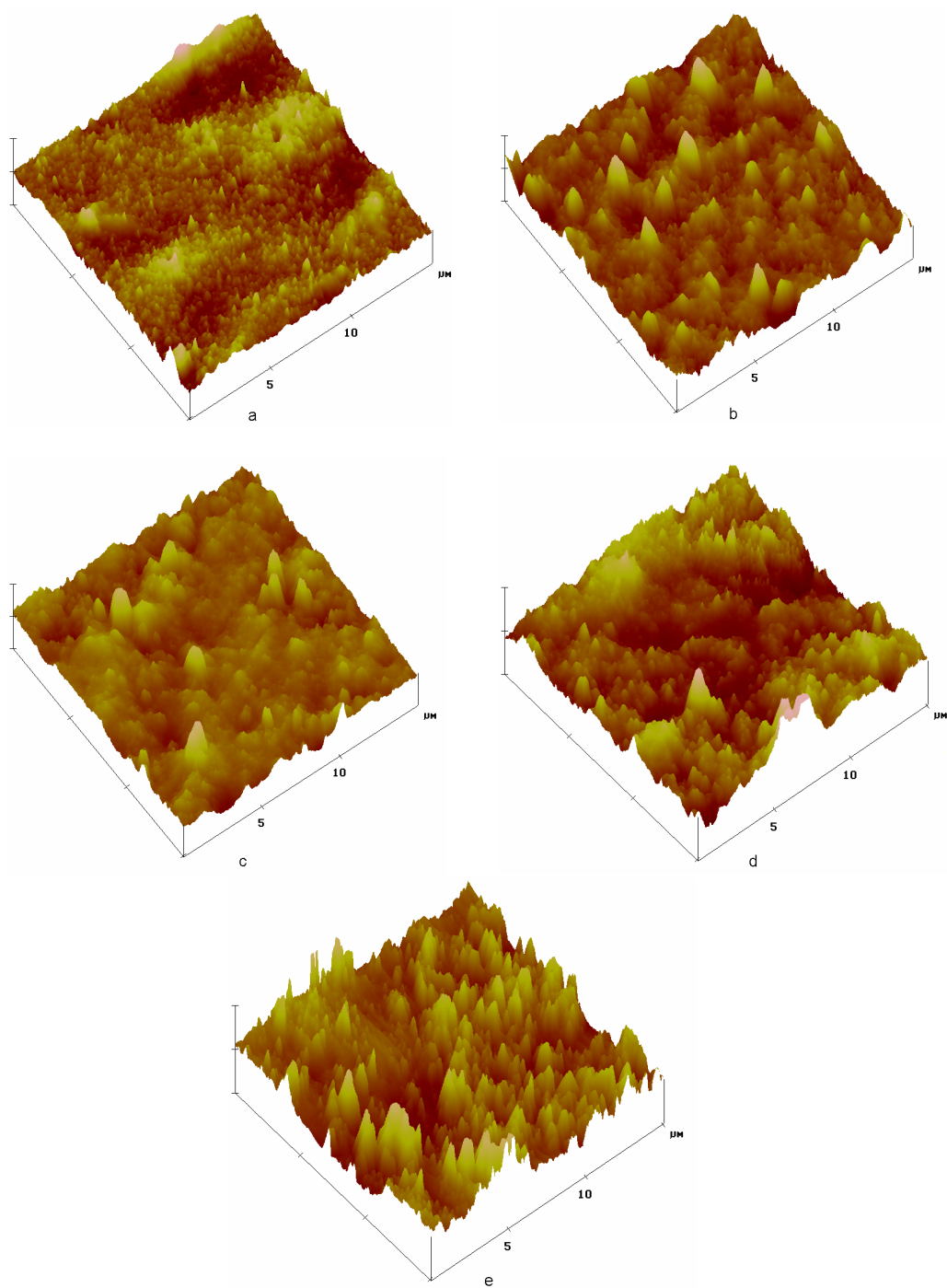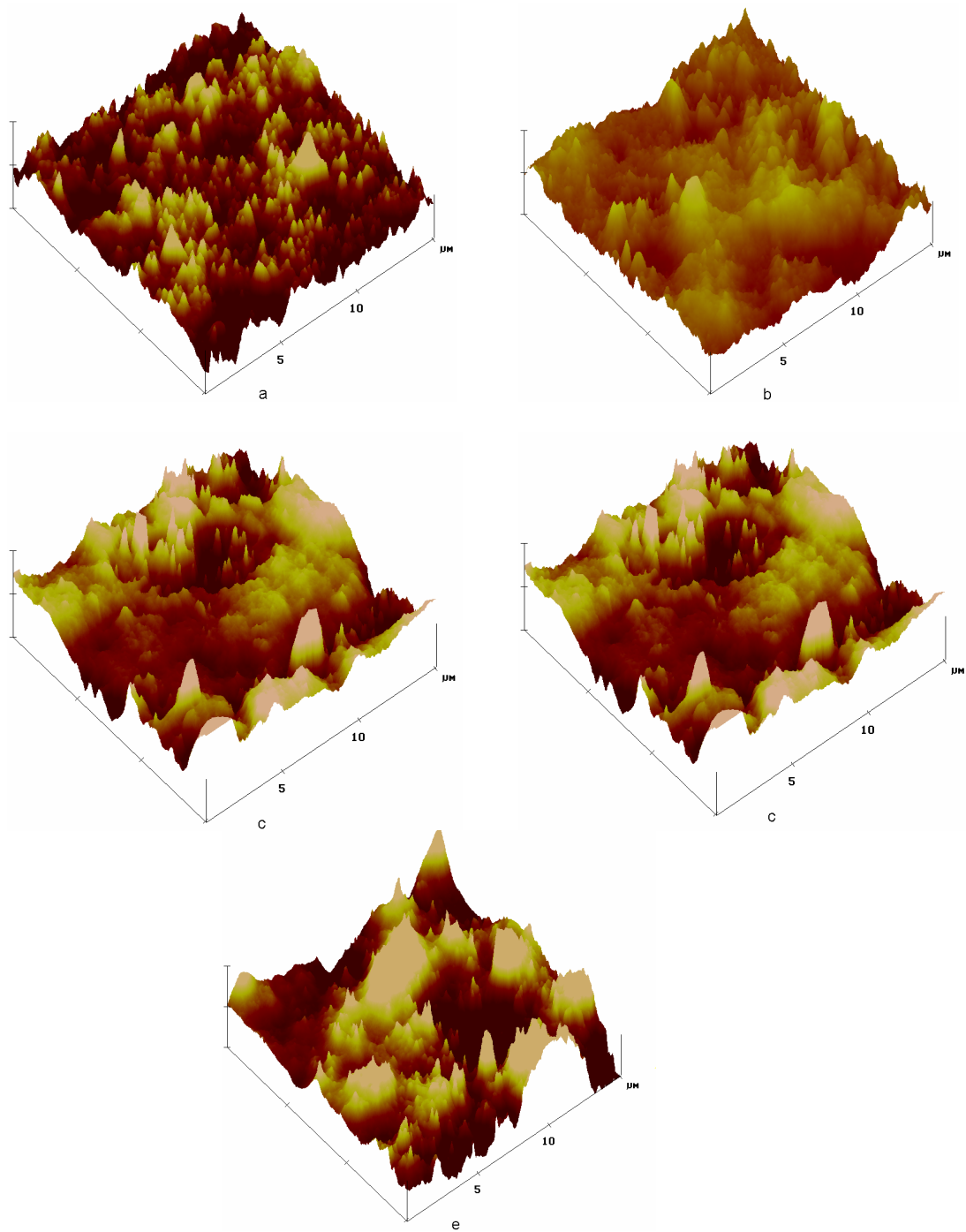
Fig 5.12 Atomic force microscope 3-dimensional surface images (15 x 15 µm) with glycine as the stabilizer at a plating time of a)2.0 min b)3.0 min c)4.0 min d)5.0 min e)6.5 min (Z axis 250 nm/div)

The corresponding SEM images at various stages of plating are shown in Figures 5.14a-e. All the SEM images reveal a coarse grain structure very similar to the ones obtained from the electroless plating solution omitting bi-pyridine. The grain size of the plated copper tends to increase with plating time. The grain size at 2.0 minutes of plating is around 0.4 µm, at the final investigated plating time of 6.5 minutes, the grain size increases to about 0.8 µm. The AFM surface images are quite consistent with the SEM images.
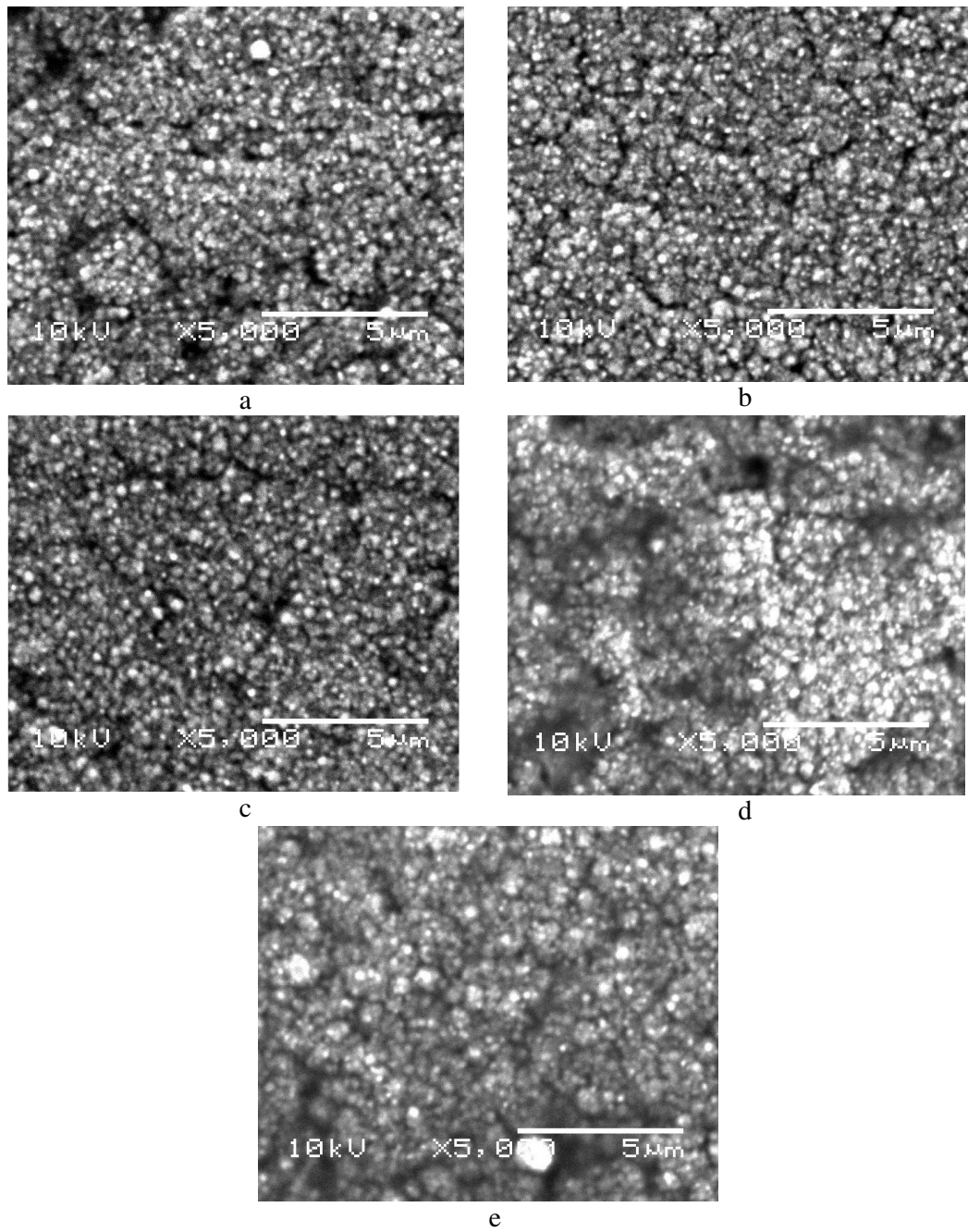
Fig 5.13 Scanning electron microscope images at a plating time of a)2.0 min b)3.0 min c)4.0 min d)5.0 min e)6.5 min with glycine as the stabilizer. Magn. X5000

5.3.3 Discussion

When glycine is used to replace bi-pyridine as the stabilizer of the electroless plating solution, the decomposition time of the plating solution shortens. The plating solution containing glycine decomposed within 10 minutes, which is even much faster comparing to L-methionine. Like L-methionine, glycine may not form complexes with Cu(I) easily.

A plating rate of 20.17 µm/hr was obtained using the weight gain method described in Section 3.4. This plating rate is similar to the plating rate without bi-pyrdine obtained in Section 5.1.1. Additional of glycine in the same concentration of bi-pyridine does not enhance the deposition rate, unlike L-methionine. The structure of glycine is shown in Fig. 5.12. L-methionine has a longer carbon chain than glycine and also contains an additional sulphur. The stability constant of Cu^{2+} to glycine is 8.15 (Martell and Smith, 1989). Since the stability constant of Cu^{2+} to glycine is slightly larger than L-methionine, one would expect a faster deposition rate. However, the reverse occurs. The glycine may not adsorb as easily as the L-methionine on the activated surface and the glycine does not contain sulphur. The presence of sulphur in amino acids seems to accelerate the plating rate, which may due to the its high affininty for copper ions.
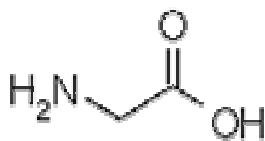
Fig 5.14 The structure of glycine

The presence of a low concentration of glycine does not result in a fine grain structure similar to Figures 5.6 and 5.10 when L-methionine was used as stabilizer. Instead, coarse grain structures are formed. This may imply that sulphur containing amino acids can result in the formation of fine grain structures. The actual role of sulphur which leads to the formation of fine grain structure is still unknown at this stage. For the above reasons, glycine is not a suitable stabilizer compared to L-methionine and bi-pyridine.

Chapter 6

Effect of Additives on the Electroless Copper Plating Process

Generally, the electroless copper plating solution consists of copper ions, reducing agent, complexing agents, buffer, accerlerator and additives. The effect of additives on the type of copper plated is examined in this chapter. The term additives encompasses a wide range of compounds, ranging from cyanide or related nitrile compounds, organo-sulphur compounds, silicanes and surfactants (Mallory and Haju, 1990). Additives are frequently used to change the grain size and surface morphology of deposit as they are able to adsorb on the active surface nuclei (Kou and Hung, 2003). This chapter only focus on one particular class of additives, which is polyethylene glycol (PEG), primarily a surfactant. This is because up to present, not much work has been done on the influence of PEG on electroless copper deposits. Surface analysis were carried out by scanning electron microscopy (SEM), atomic force microscopy (AFM) and transmission electron microscopy (TEM). Lastly, differential scanning colorimetry (DSC) was used to quantify the effect of PEG on the physical properties of the acrylonitrile-butadiene-styrene (ABS) film.

6.1   Surface analysis of electrolessly plated copper using polyethylene glycol

As usual, the electroless copper plating employs the sodium potassium tartrate as the main chelating agent in optimized concentration determined in Section 4.1. The rest of the components are stated in Table 3.3. The only difference is the addition of PEG having the concentration of 2.0 g/L. Four different molecular weights (600, 4000, 10000, 35000 g/mol) of PEG were used in each set of the plating experiment. The plating time for each individual molecular weight of PEG is different due to the

difference in plating rate. A minimum thickness of plated copper is needed in order for surface analysis to perform successfully. Surface morphology of the plated copper was investigated for each molecular weight of PEG.

6.1.1 Electrolessly plated copper for various molecular weights of polyethylene glycol

Figures 6.1a-d shows the SEM images taken at 5000 magnification for the molecular weight of PEG ranging from 600 - 35,000 g/mol. Almost spherical copper grain structures of less than 0.5 µm in diameter are seen clearly when the molecular weights of PEG is 600 and 4,000 g/mol. For the higher molecular weights of PEG, much smaller grain structures are formed. The size of these grain structures cannot be determined from the SEM images.
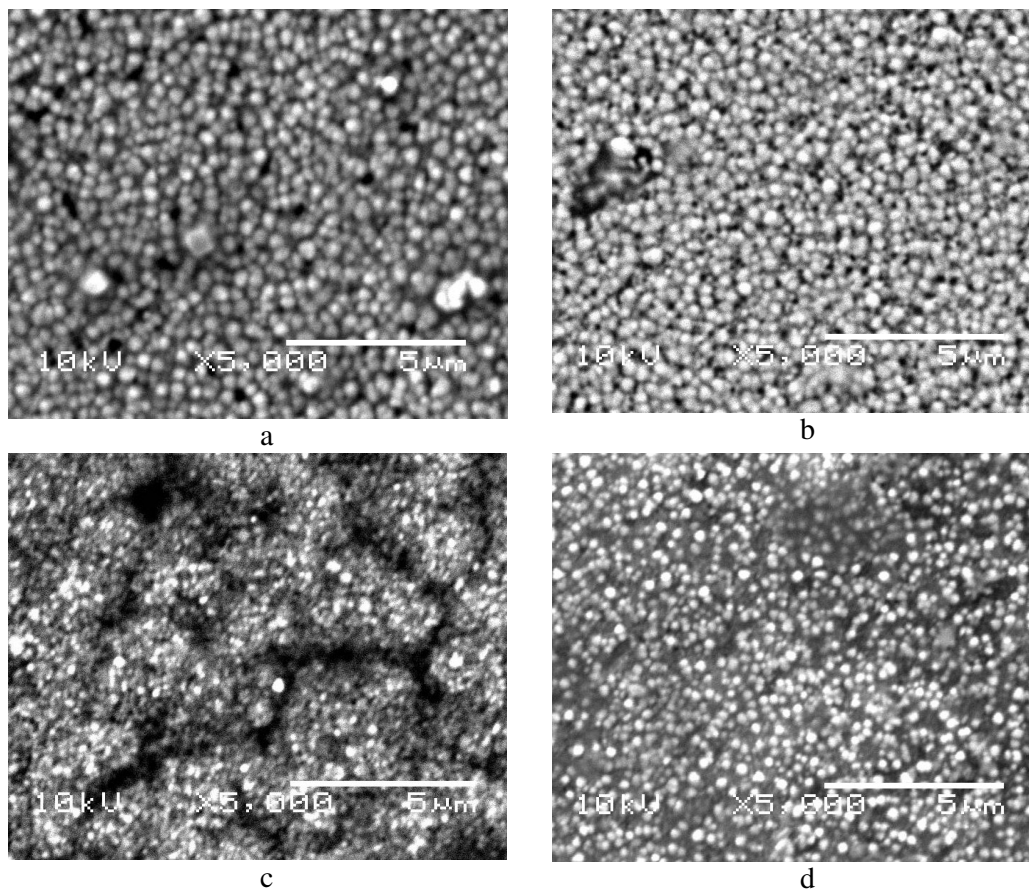
Fig 6.1 Scanning electron microscope images with PEG a) 600 b) 4,000 c) 10,000 d) 35,000 g/mol as the surfactant. Magn. X5000

Figures 6.2a-d show the corresponding AFM surface images for the molecular weights of PEG ranging from 600 to 35,000 g/mol. The surface roughness of the various plated copper surfaces is given in Table 6.1. Small 'cone' copper structures are seen on the scan area when the molecular weight of PEG is 600 and 4,000 g/mol. This is quite consistent with SEM images. At a larger molecular weight of 10,000 g/mol, non-distinctive 'cone' structures are formed, it could be due to the small individual grain structure. For the highest molecular weight of 35,000 g/mol, the familiar small 'cone' structures are formed. Results from the surface roughness analysis do not reveal any relationship with the molecular weights of PEG.
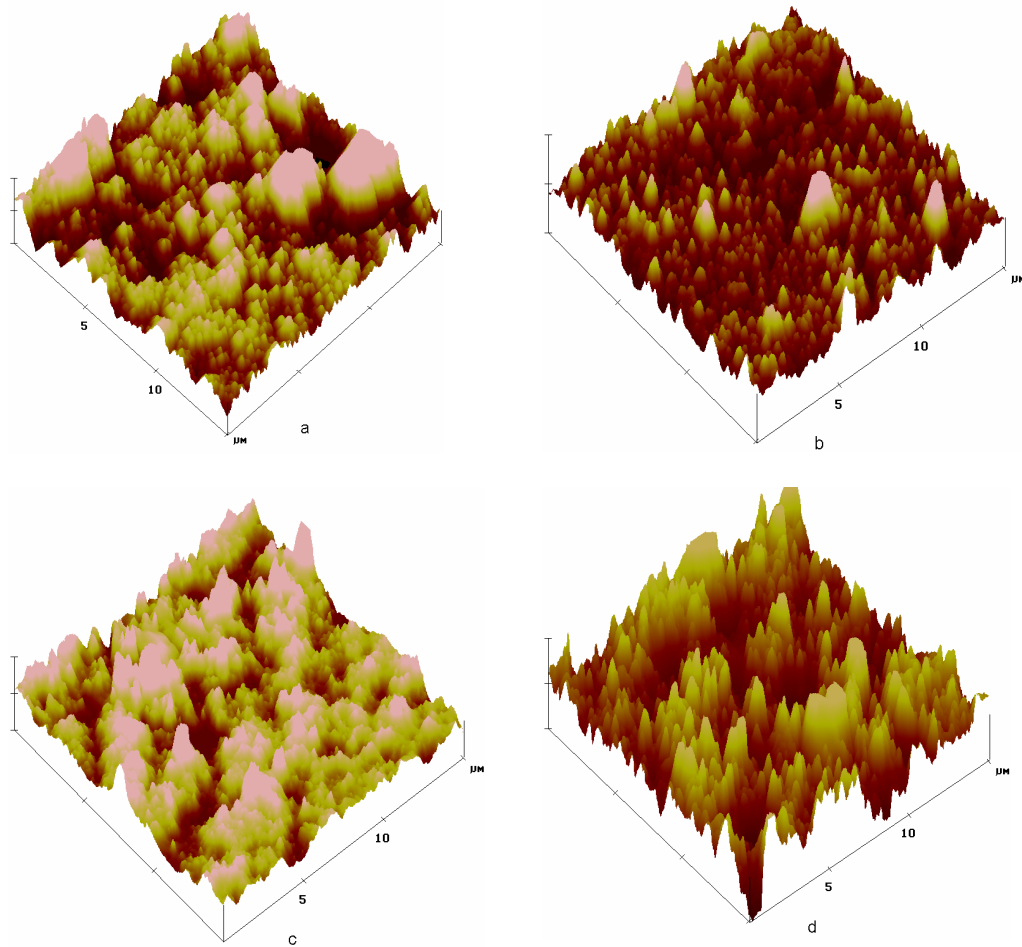
Fig 6.2 Atomic force microscope 3-dimensional surface images (15 x 15 µm) with PEG a) 600 b) 4,000 c) 10,000 d) 35,000 g/mol as the surfactant (Z axis 250 nm/div)

Table 6.1 Selected roughness analysis results for various molecular weights of PEG in the electroless plating solution

Molecular weight of PEG g/mol	Img. RMS (Rq) /nm
600	90.740
4000	48.752
10000	58.365
35000	100.60

Img. Rms (Rq) refers to the root mean square of height deviations taken from the mean

data plane, expressed as $\sqrt{\dfrac{(Z_1^2 + Z_2^2 + Z_3^2 + ... + Z_n^2)}{N}}$

From the above SEM and AFM surface images, the addition of PEG seems to produce highly oriented copper structures. Higher magnification is needed to examine the copper structures at a closer level. Figures 6.3a_b show the surface image of PEG 600 and 4,000 generated by AFM at a higher magnification. The AFM surface images confirmed that the grain structure of copper is roughly spherical in size and ranges from 100 - 200 nm. In addition, TEM was also used to examine the copper particles deposited from the electroless plating solution employing PEG 600. The TEM image is shown in Fig. 6.4. The dark area represents the grain structure of a single copper particle, where the particle seems to make up of even smaller particles of about 20 nm in size.
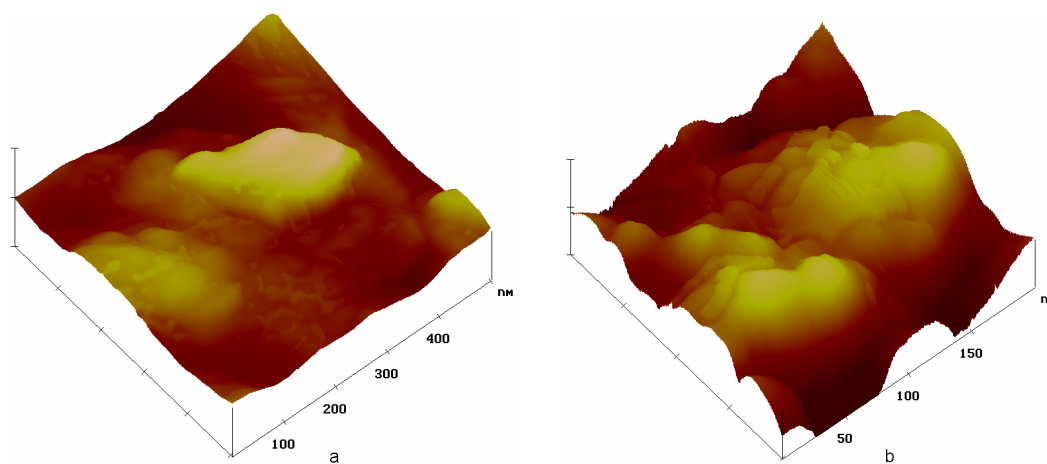
Fig 6.3 Atomic force microscope 3-dimensional surface images with PEG a) 600 [0.5 x 0.5 µm][Z axis 250 nm/div] b)4,000 g/mol as the surfactant [0.2 x 0.2 µm][Z axis 10 nm/div]
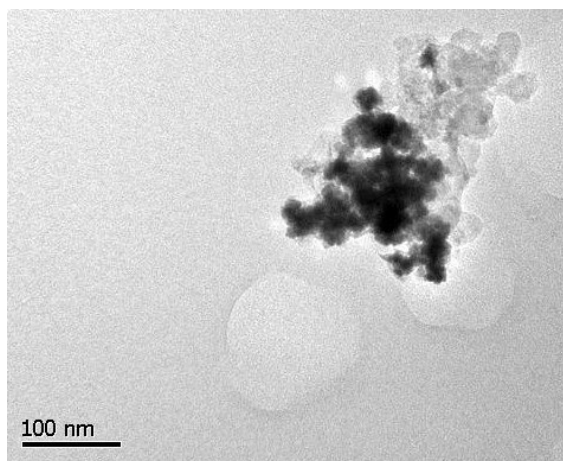
Fig 6.4 Transmission electron microscope image with PEG 600 g/mol as the surfactant

6.1.2 Discussion

Polyethylene glycol (PEG) is an non-ionic surfactant, which do not have a charged group. The structure of PEG is shown in Fig. 6.5. From Fig. 6.5, it can be seen that the higher the molecular weight, the longer is the PEG molecule. Its solubility generally decreases with increasing molecular weight (Porter, 1994).
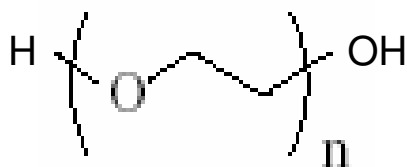
Fig 6.5 The structure of polyethylene glycol

From the above SEM, AFM and TEM images, the presence of trace amount of PEG in the electroless plating solution creates highly uniform and compact copper grain structures as compared to the SEM images in Fig. 4.2b where PEG was not included. It is reported that PEG can easily adsorb on highly catalytically active sites

on the plated surface, this has prevented hydrogen inclusion in the deposit (Veleva, 1986). This adsorption ability probably alters the morphology of the copper deposits. Also, the plating rate will decrease as well, however this was not experimentally verified because the morphology of the plated copper apparently is more important. The various molecular weights of PEG was maintained at the same concentration for comparison purposes. Fig. 6.1 clearly shows the distinct differences among them. The size of the PEG molecule affects the surface morphology. High molecular weights of PEG induce very compact copper grain structures as shown in Figures 6.1c and 6.1d. At the molecular weight of 35,000 g/mol, no visible copper grain structures (underneath the white spots) are seen at 5,000 magnification as they are probably too small. The white spots look to be the secondary deposited copper layer. At the next lower molecular weight of 10,000 g/mol, the grain structures are finer compared to the lighter PEG. TEM is a better alternative of observing the plated copper structures due to its higher magnification power. However, it is difficult and time consuming to take good and accurate images which explain why the TEM image taken is not sufficient to draw any conclusion. From these preliminary findings, it seems that electroless copper plating solution that contains PEG 10,000 produces the smallest copper grain structures.

6.2   Effect of polyethylene glycol on the physical properties of acrylonitrile-butadiene-styrene film

From Section 6.1, the effect of polyethylene glycol (PEG) on the surface morphology of the plated copper was seen clearly by the SEM micrographs in which highly uniform copper particles of around 100 - 200 nm are deposited on the acrylonitrile-butadiene-styrene (ABS) film. This section further investigates the changes made to the ABS film after it was plated with electroless plating solution containing PEG at

various molecular weights. The ABS is generally a thermoplastic polymers that soften when heated (and eventually liquefy) and harden when cooled. The other details of the ABS used are given in Section 3.1.1.

6.2.1 Unplated acrylonitrile-butadiene-styrene film

.

Fig. 6.6 shows the heat evolved of the unplated ABS film versus the temperature generated from differential scanning colorimetry (DSC). ABS is mixture of three different polymers: acrylonitrile, butadiene and styrene in a certain percentage. The ABS used in this research has a acrylonitrile/butadiene/styrene mole ratio of 2:1:2. From Fig. 6.5, the first glass transition temperature (Tg) occurs at around 100 ^{o}C. This is probably due to the combined effect of the acrylonitrile and styrene polymers as butadiene has a very low Tg. The product information also states that the Tg of this particular grade of ABS is 103 ^{o}C (Section 3.1.1), which is close to the experimentally determined value. When the temperature increased from 120 to 150 ^{o}C, some heat fluctuations were seen. This may due to the change in local composition of the ABS under increasing heat application. The ABS polymer chains become less orderly packed and decrease the percentage of crystallinity. The second Tg occurs at around 200 ^{o}C. The second Tg is actually is mixture of melting and Tg. For consistency, it is referred to Tg for all other following sections.

Fig 6.6 Graph of heat evolved of unplated ABS film versus temperature

6.2.2   Acrylonitrile-butadiene-styrene film with polyethylene glycol (600 g/mol)

Fig. 6.7 shows the heat evolved of the copper plated ABS film with PEG 600 enhanced versus the temperature generated from DSC. The first Tg occurs at around 105 ^{o}C. This shows the plated copper with PEG 600 does not significantly influence the first Tg. Similar to unplated ABS, from the temperature range of 120 to 150 ^{o}C, heat fluctuations were seen. The second Tg was observed at around 225 ^{o}C, which is hgher compared to the unplated ABS film.

ABS with PEG 600

Fig 6.7 Graph of heat evolved of plated PEG 600 enhanced ABS film versus temperature

6.2.3   Acrylonitrile-butadiene-styrene film with polyethylene glycol (4,000 g/mol)

Fig. 6.8 shows the heat evolved of the copper plated ABS film with PEG 4,000 enhanced versus the temperature generated from DSC. The first Tg occurs at around 100 ^{o}C, which is the same as the unplated ABS. For the second Tg, it occurs at around 230 ^{o}C. This confirms that plated copper ABS film has a higher second Tg. This may be due to the strong Cu-CN bonding on the surface of ABS film, since the plating solution contains trace amounts of cyanide. These bonding between Cu-CN at the copper-ABS interface result in more orderly structure of the ABS polymer, which probably increases the second Tg.
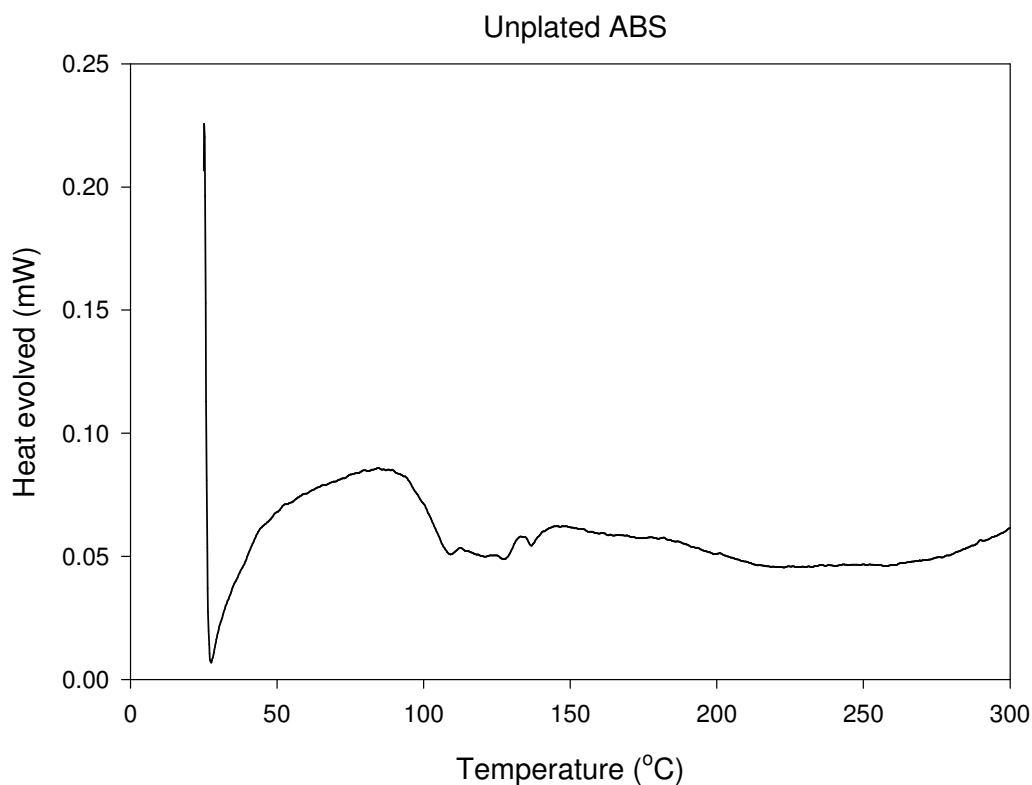
ABS with PEG 4000

Fig 6.8 Graph of heat evolved of plated PEG 4,000 enhanced ABS film versus temperature

6.2.4 Acrylonitrile-butadiene-styrene film with polyethylene glycol (10,000 g/mol)

Fig. 6.9 shows the heat evolved of the copper plated ABS film with PEG 10,000 enhanced versus the temperature generated from DSC. The first Tg occurs at around 100 $^{\circ}$C, which is same as unplated ABS and ABS with PEG 600, 4000 respectively. The familiar heat fluctuations occur along the temperature range of 130 to 230 $^{\circ}$C. The second Tg occurs at around 265 $^{\circ}$C, which is the highest temperature so far. This is accompanied by an obvious endothermic adsorption. This interesting observation could be related to the grain size of the plated copper. The smallest copper grain occurs when PEG 1,000 was added to the plating solution as shown in Fig. 6.1. The smaller the grain size, the higher the percentage of coordination-unsaturated copper bonds is. In other words, a decrease in grain size will make the copper more reactive, as more

copper atoms in a grain are exposed. As such, the copper atoms at the metal-polymer interface are reactive and possibly form strong bonds with the CN on the polymer (described in Section 6.2.3). The small size of the copper grain also allows it to penetrate deeper into the polymer matrix. These changes can cause the polyacrylonitrile segment to be more orderly than before, and results in the high Tg of 265 ^{o}C.
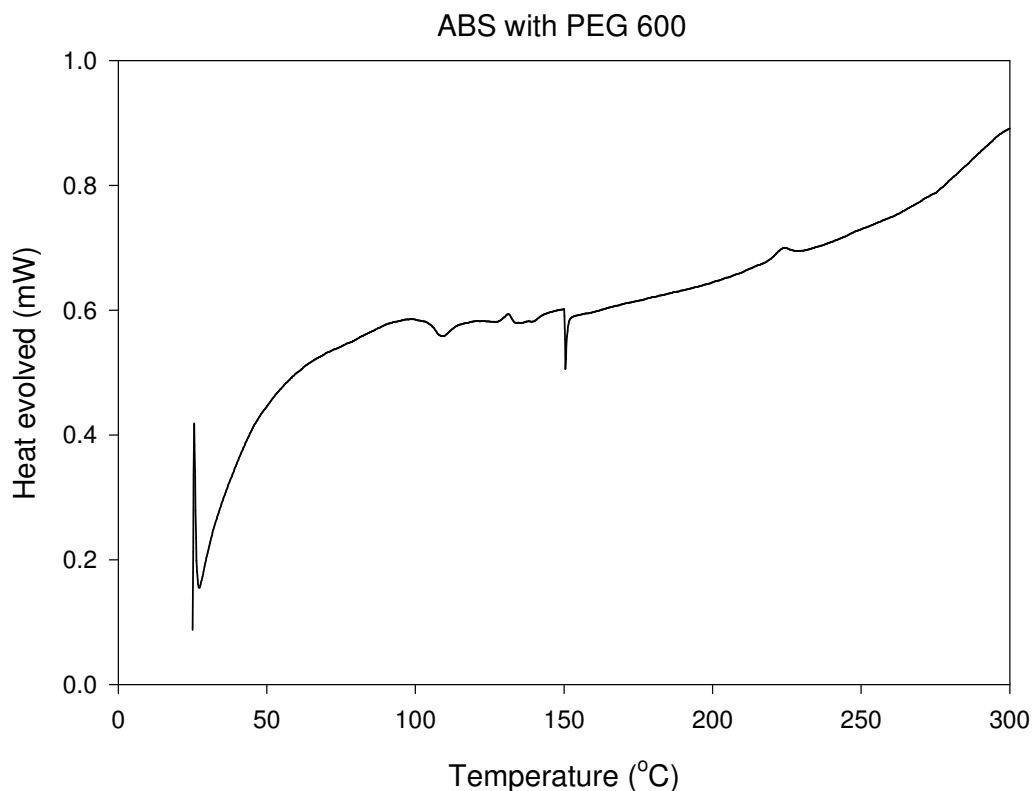

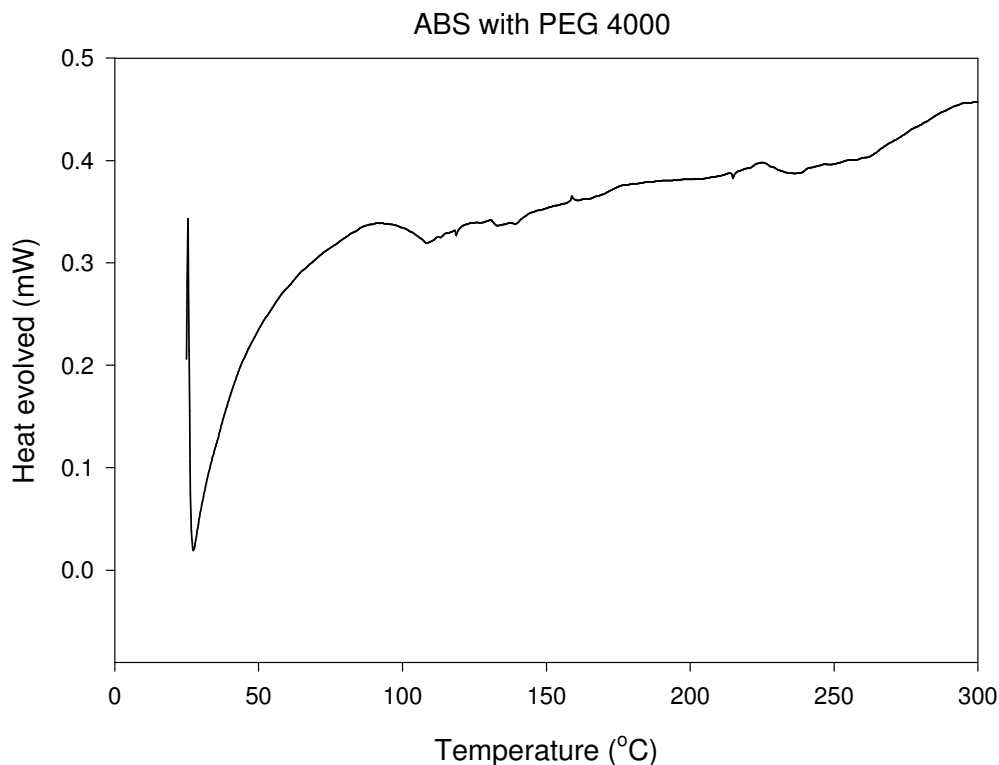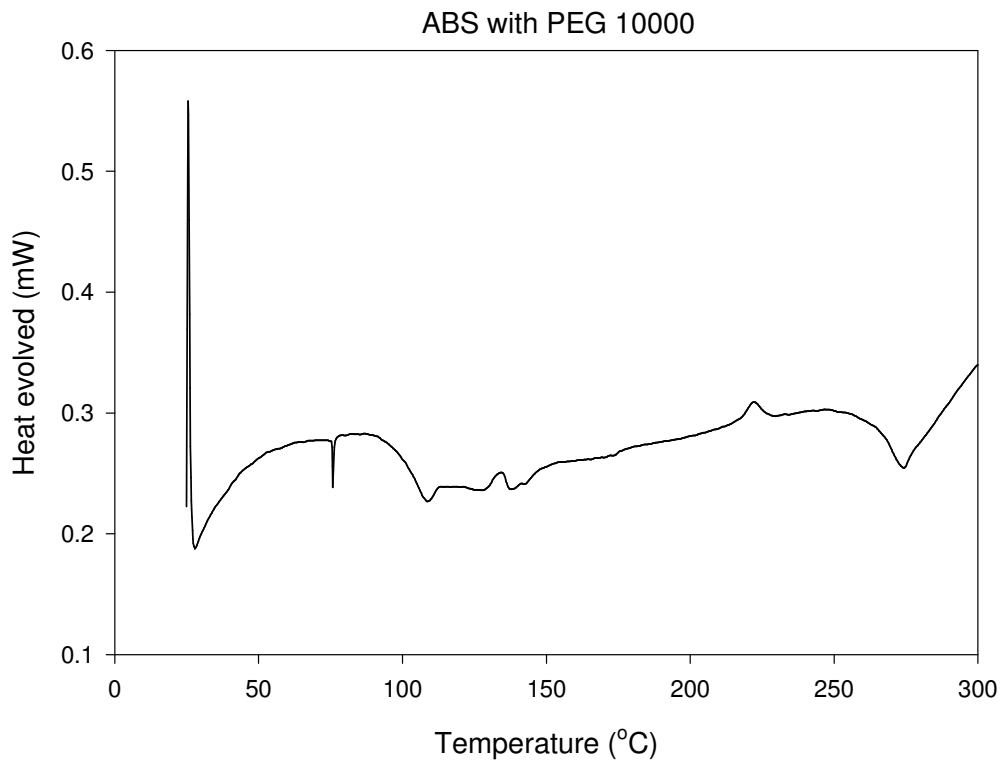Fig 6.9 Graph of heat evolved of plated PEG 10,000 enhanced ABS film versus temperature

6.2.5 Acrylonitrile-butadiene-styrene film with polyethylene glycol (35000 g/mol)

Fig. 6.10 shows the heat evolved of the copper plated ABS film with PEG 35,000 enhanced versus the temperature generated from DSC. This time, the first Tg increase remarkably to 130 ^{o}C. However, no second Tg was seen within the investigated

temperature range of 25 - 300 ^{o}C. Fig. 6.1 shows that the grain size of copper plated ABS film with PEG 35,000 (Fig. 6.1d) is much larger than PEG 10,000 (Fig. 6.1c). This increase probably affects the metal-polymer interactions as described above. The structure of ABS is actually core shell of butadiene surrounded by polymer chains of acrylonitrile and styrene. The plated copper grains seem to make the polystyrene and polyacrylonitrile segment more orderly, which increase the Tg by about 30 ^{o}C.

.

ABS with PEG 35000
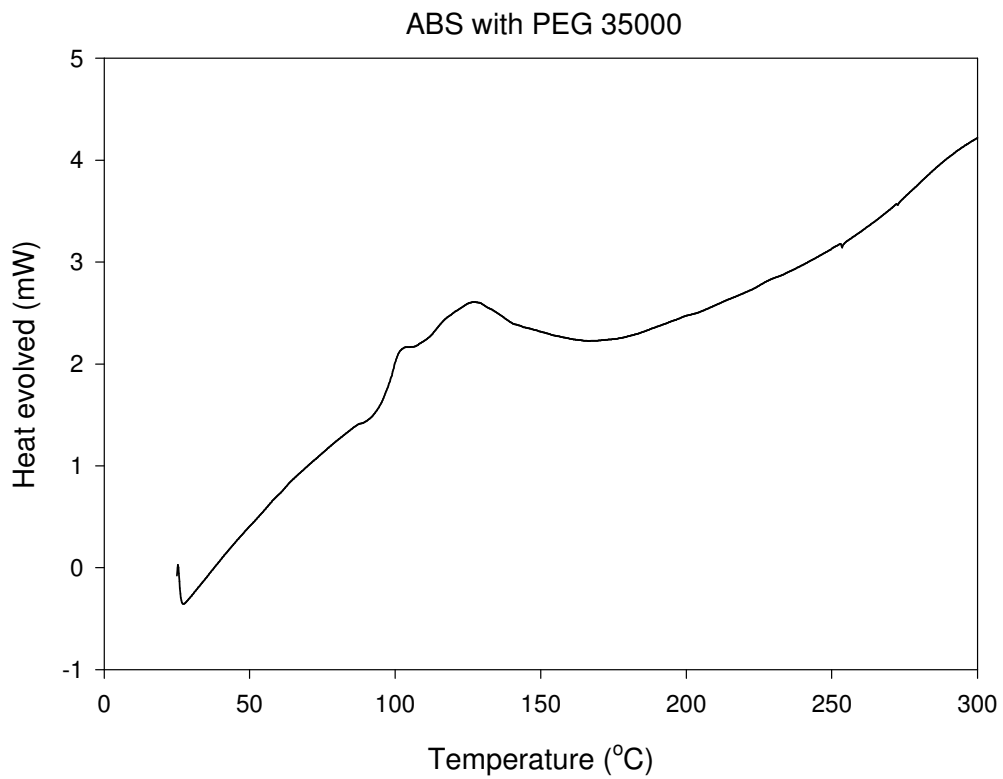
Fig 6.10 Graph of heat evolved of plated PEG 35,000 enhanced ABS film versus temperature

Chapter 7

Electrochemical Analysis of Electroless Plating Solution

Potentiommetry and voltammetry are two of the common methods used for electrochemical analysis. The measured variable in potentiommetry is potential and the measured variable in voltammetry is current. Within voltammetry, there are sub methods which include polargraphy, single-sweep, cyclic-sweep, rotated-disk and ring-disk electrodes, and pulse (Sawyer et al., 1995). This chapter deals with the cyclic voltammetry (CV) analysis of various simplified electroless copper plating solution as CV is one of the commonly used method. The primary event in CV experiments is the oxidation or reduction of a solution chemical species at an electrode. Through the series of experiments, important aspects of electroless copper deposition like ease of deposition and effect of additives were explored in greater depth. However, the kinetic aspects of the electroless plating process due to composition changes cannot be determined.

7.1 Cyclic voltammetry analysis of electroless plating solution

Cyclic voltammetry analysis was performed on three main groups of electroless copper plating solution, in which each group focusing on a different component of the plating solution. Group 1 is on the effect of chelating agents, group 2 is on the effect of additives and lastly group 3 focuses on surfactants. There is a total of ten plating solutions of different compositions undergoing CV analysis. The composition of the various plating solutions are given in the subsequent sections.

7.1.1 Effect of chelating agents

Fig. 7.1 shows the cathodic scans of the three various electroless plating solution (Group 1a, 1b, 1c) employing different chelating agents. The compositions of the plating solution are given in Table 7.1. These plating solutions represent the simplified version of the electroless copper plating solution used in this research (Table 3.3). The purpose is to examine the effects of sodium potassium tartrate and disodium EDTA on the electroless copper deposition process.

Effect of chelating agents (Cathodic scan)

Fig 7.1 Cyclic voltammetry of various chelating agents in the electroless plating
solution (Cathodic scan, scan rate = 0.008 V/S)

Table 7.1 Composition of simplified electroless plating solutions employing various chelating agents

	Group 1a	Group 1b	Group 1c
$CuSO_4.5H_2O$ mol/L	0.1161	0.1161	0.1161
Na_2CO_3 mol/L	0.2359	0.2359	0.2359
NaOH mol/L	1.048	1.048	1.048
Sodium potassium tartrate $[KNaC_4H_4O_6.4H_2O]$ mol/L	0.4065	0	0.4065
Disodium EDTA $[C_{10}H_{14}N_2Na_2O_8.2H_2O]$ mol/L	0	0.4065	0.03351

Group 1a exhibits one cathodic peak at -1.16 V and the corresponding current density peak is -12.2 mA/cm^2. The cathodic peak represents Cu^{2+} reduction. Group 1b has a cathodic peak occurring at -1.47 V, the associated current peak of -21.2 mA/cm^2 is larger in magnitude. The potential shift shows that Cu^{2+} ions are bounded more strongly to disodium EDTA than the sodium potassium tartrate. This phenomena is verified by looking at the values of the formation constants of Cu-EDTA and Cu-tartrate complex. The formation constant of Cu-EDTA is $10^{18.7}$, which is higher than Cu-tartrate of $10^{3.39}$ (Martell and Smith, 1989). For Group 1c, copper reduction occurs at -1.19V and the corresponding current density is -12.5 mA/cm^2. This Cu reduction potential occurs between -1.17 and -1.47 V, which represents the reduction potential of group 1a and 1b respectively. This is expected as group 1c consists of both chelating agents and tends to group 1a as the solution contains a higher concentration of sodium potassium tartrate. The magnitude of the corresponding current density is similar to group 1a. The higher cathodic peak value of group 1b also indicates disodium EDTA favours Cu^{2+} reduction.

Fig. 7.2 shows the corresponding anodic scans of the solutions of group 1a-c. All the anodic scans show two distinct peaks around -0.4 V and 0 V respectively. Equation 7.1 and 7.2 shows the standard electrochemical potential of copper reduction (Dean, 1979).

$$Cu^+ + e \leftrightarrow Cu \quad E^o = 0.52 \text{ V} \tag{7.1}$$
$$Cu^{2+} + e \leftrightarrow Cu^+ \quad E^o = 0.153 \text{ V} \tag{7.2}$$
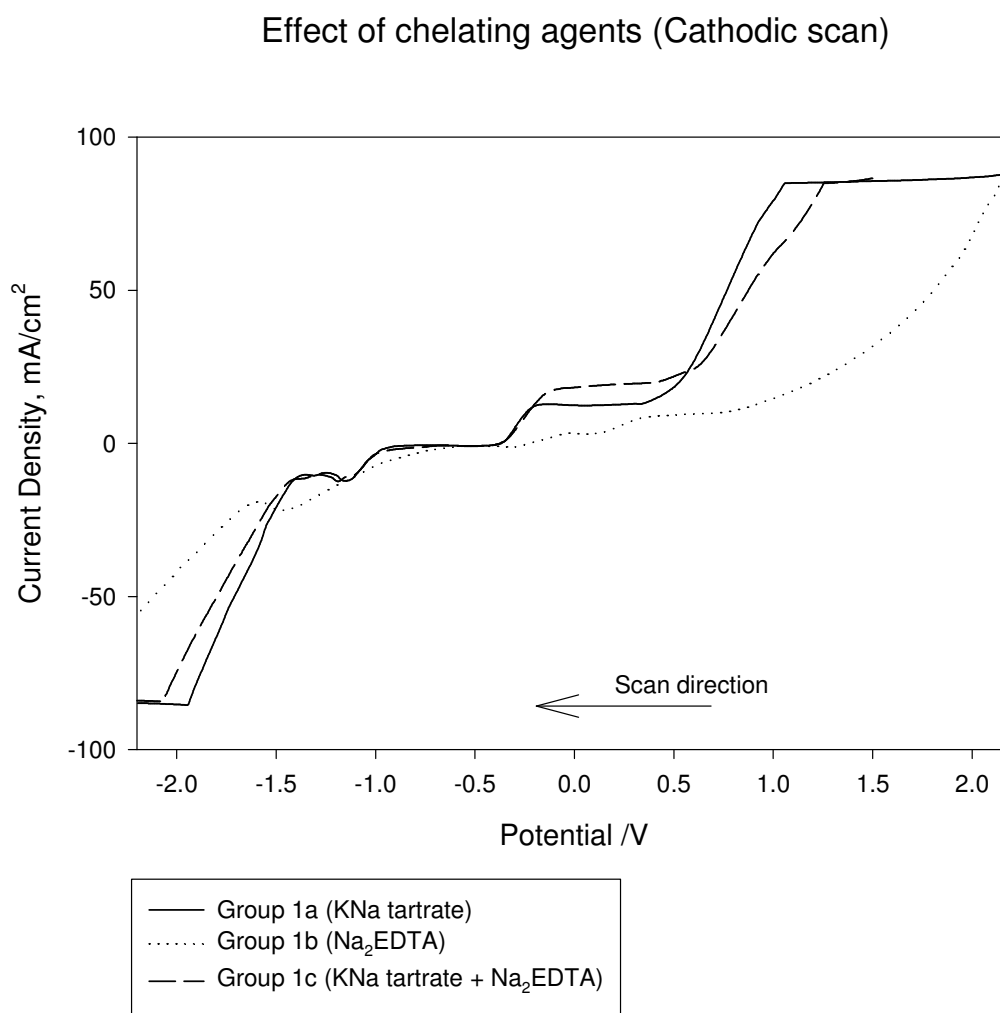
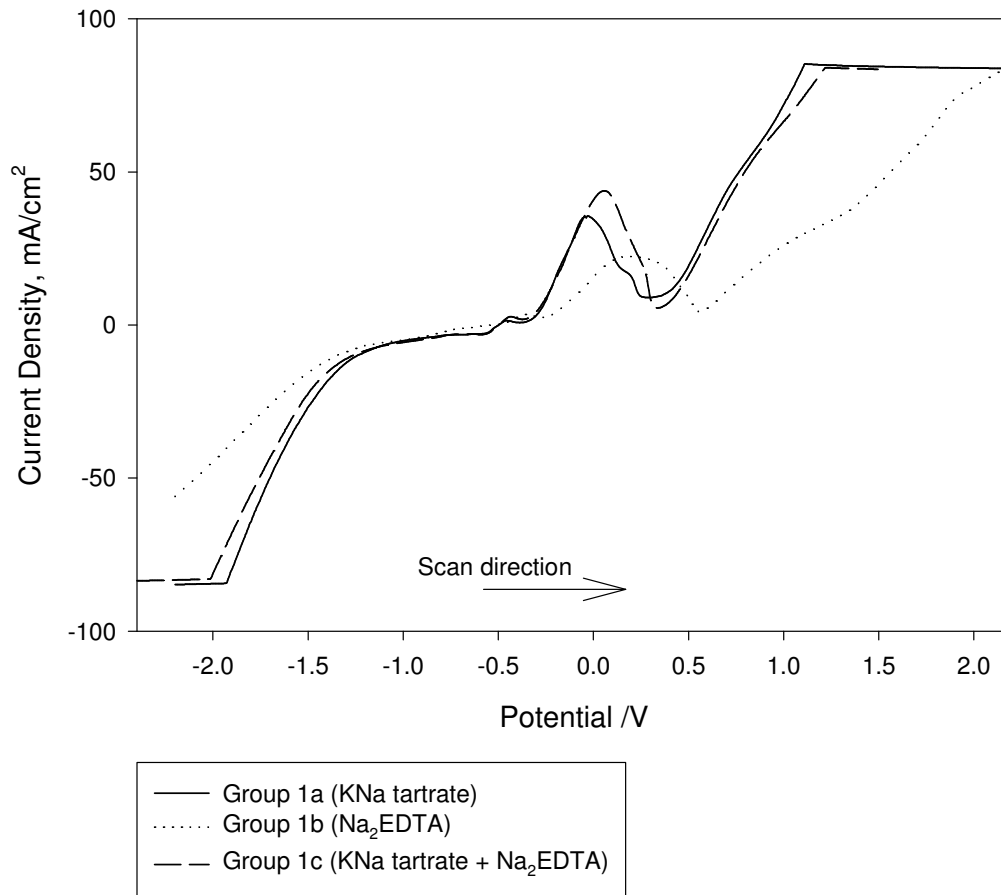### Effect of chelating agents (Anodic scan)

Fig 7.2 Cyclic voltammetry of various chelating agents in the electroless plating solution (Anodic scan, scan rate = 0.008 V/S)

From these 2 equations, formation of Cu^+ probably occurs at the first small peak in the 0 V region. The second larger peak represents the oxidation of Cu^+ to Cu^{2+} and also some of the elemental copper which is directly oxidised to Cu^{2+}. Comparing the anodic scans of group 1a and 1b, the first peak occurs at -0.46 V and -0.35 V from group 1a and 1b respectively. The corresponding current densities are 1.41 mA/cm^2 and 3.53 mA/cm^2. Thus, the selection of sodium potassium tartrate or disodium EDTA does not really affect the formation of Cu^+. However, for the second peak, group 1a has a larger current density of 35.3 mA/cm^2, compared to 21.6 mA/cm^2. The potential for formation of Cu^{2+} also differs. Group 1b requires a larger potential at 0.19 V, as compared to -0.029 V. This reinforced the fact that the formation constant of Cu(II)-EDTA complex is larger than the Cu(II)-tartrate complex. Also the high current density indicates that formation of Cu(II)-tartrate is more favourable. When both sodium potassium tartrate and disodium EDTA are combined with the former as the majority component as shown in group 1c, the first peak is about the same as group 1a and 1b. But for the second peak, a resultant higher current density was observed at a similar potential of around -0.45 V. This suggests that a combination of two chelating agents is more electrochemically desirable to one.

7.1.2 Effect of additives

The triethanolamine, potassium ferrocyanide and bi-pyridine are used in trace amount in the electroless copper plating solution. Their influence on the electroless plating process was investigated by CV analysis. Fig. 7.3 shows the cathodic scans of four different electroless plating solution (Group 2a, 2b, 2c, 2d) employing various additives. Three of the curves were deliberately shift along the current density axis because the curves are too close together. The current densities corrections are shown

in the box directly below the graph. The composition of the plating solutions are given in Table 7.2. The bulk of the four electroless plating solutions is the same as group 1c, the minor difference is the type of additives added.

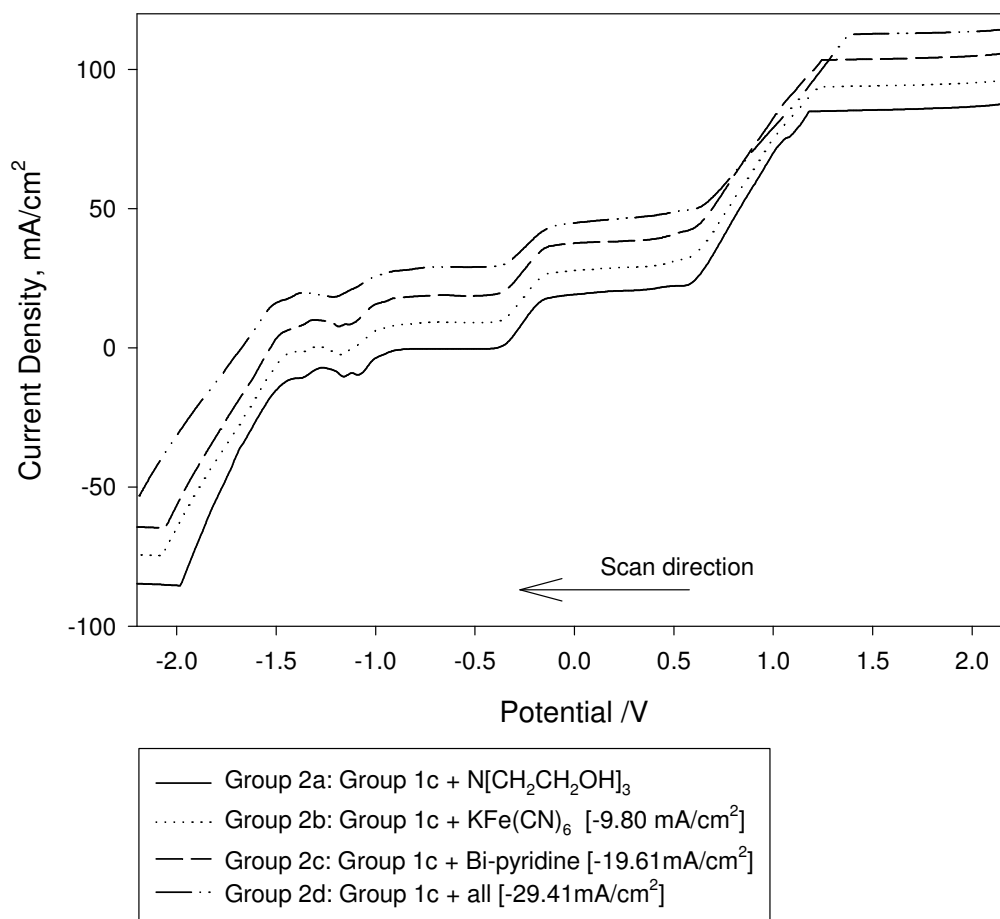## Effect of additives (Cathodic scan)

Fig 7.3 Cyclic voltammetry of various additives in the electroless plating solution
(Cathodic scan, scan rate = 0.008 V/S)

Table 7.2 Composition of simplified electroless plating solutions employing various additives

	Group 2a	Group 2b	Group 2c	Group 2d
$CuSO_4.5H_2O$ mol/L		0.1161		
Na_2CO_3 mol/L		0.2359		
NaOH mol/L		1.048		
Sodium potassium tartrate [$KNaC_4H_4O_6.4H_2O$] mol/L		0.4065		
Disodium EDTA [$C_{10}H_{14}N_2Na_2O_8.2H_2O$] mol/L		0.03351		
Triethanolamine { $N[CH_2CH_2OH]_3$} mol/L	0.03351	0	0	0.03351
Potassium ferrocyanide $K_4Fe[CN]_6.3H_2O$ mol/L	0	0.000118	0	0.000118
Bi-pyridine ($C_{10}H_8N_2$) mol/L	0	0	0.00064	0.00064

In group 2a, the cathodic scan is very similar to that of group 1c. There are two closely cathodic peaks at -1.09 V and -1.16 V. The corresponding currents are -9.80 mA/cm^2 and -10.4 mA/cm^2 respectively. These two peaks are very similar to group 1c in terms of potential and current density. The only difference is the addition cathodic peak. Low concentration of triethanolamine probably does not play a significant role in the copper reduction. For group 2b, the triethanolamine was replaced by potassium ferrocyanide of another composition stated in the reference plating solution. The cathodic scan shows only one peak (-1.18 V, -12.4 mA/cm^2). This peak follows very closely to the cathodic peak in group 1c. This probably implies that the addition of trace amount of cyanides does not affect the Cu reduction process. Similarly in group 2c, the additive used is bi-pyridine in the composition stated in Table 3.3. Only one cathodic peak was observed and occurs at -1.19 V, with a corresponding current density of -12.0 mA/cm^2. This cathodic peak also follows closely to group 1c. Bi-

pyridine probably did not affect the copper reduction process from the electrochemical view. Lastly, all the above additives: triethanolamine, potassium ferrocyanide and bi-pyridine, maintaining the same composition are added to form group 2d. The observed cathodic scan features 1 cathodic peak at -1.22 V and the current density is -11.2 mA/cm^2. There is slight potential shift of 0.3 V compared to group 1c which implies that copper reduction becomes mildly unfavourable, but not to a large extent. The corresponding current density decreases by about 10%, which means the same as the potential shift. This is expected as these additives slow down the plating process.
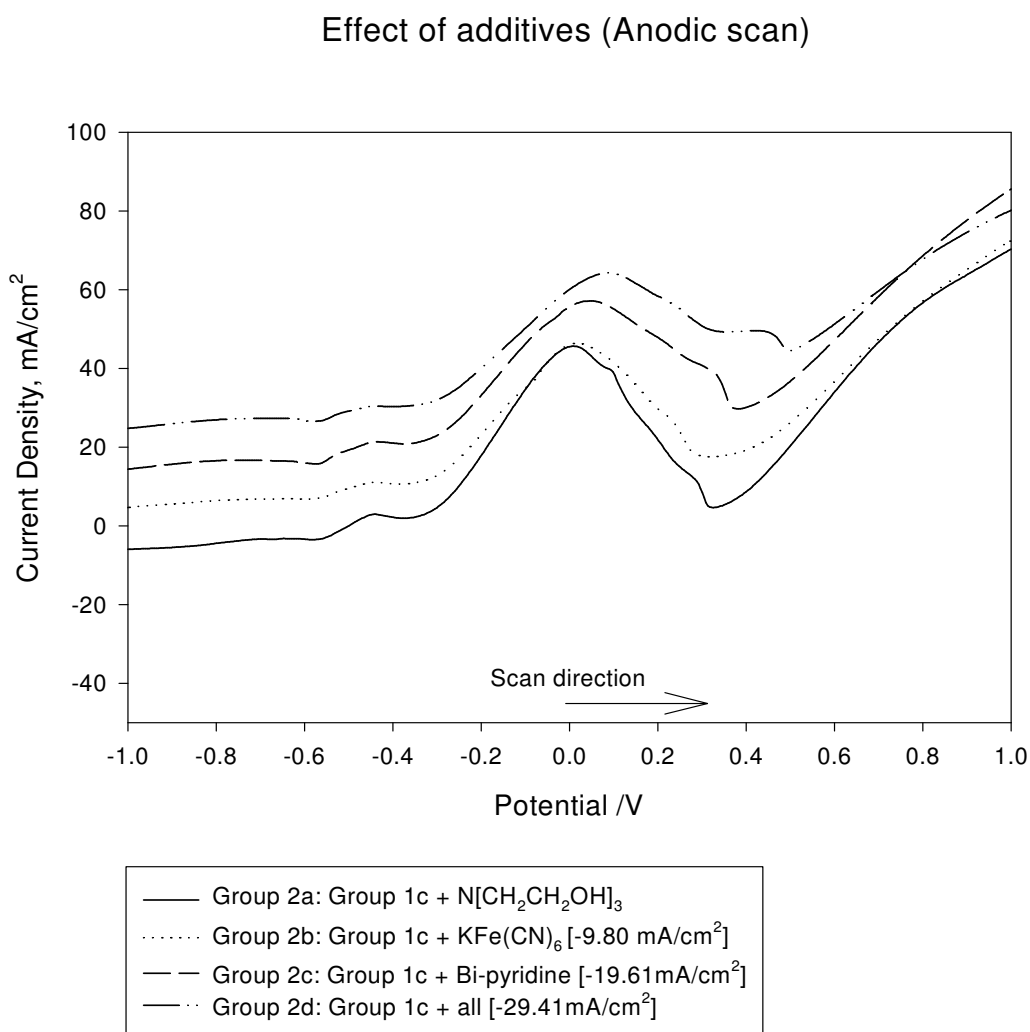
Effect of additives (Anodic scan)

Fig 7.4 Cyclic voltammetry of various additives in the electroless plating solution
(Anodic scan, scan rate = 0.008 V/S)

The anodic scans of the four different electroless plating solution: Group 2a, 2b, 2c, 2d are shown in Fig. 7.4. Three of the curves were deliberately shift along the current density axis because the curves are too close together. The current densities correction are shown in the box directly below the graph. In group 3a, there are two anodic peaks observed at -0.44 V and 0.0082 V and the corresponding current densities are 2.94 mA/cm^2 and 45.1 mA/cm^2 respectively. As mentioned earlier, the first peak (-0.44 V) represents the oxidation of Cu to Cu$^+$. Comparing with group 1c, this first peak is very similar in terms of potential and current density values. Formation of Cu$^+$ is not much affected by addition of triethanolamine. However, for the second peak, potential shift of minus 0.046 V and current density increases a little to 45.3 mA/cm^2 were observed. Therefore, Cu^{2+} formation is favourable in the presence of triethanolamine, since triethanolamine is also a chelating agent which can form copper complex. In the case for group 2b, the potential at which the first peak occurs is the same as group 2a. However, the associated current density is reduced by 58%. It seems like Cu$^+$ formation is slightly less favourable. The second peak reports a potential and current density value of 0.012 V and 37.3 mA/cm^2 respectively. Comparing with group 1c, potential shift of minus 0.042 V and current density decreases by about 16% to 37.3 mA/cm^2. Addition of cyanide ions possibly inhibits the formation of Cu^{2+} ions to a small extent. Cyanide ions are known to stabilize the electroless copper plating solution, this probably explains the above CV findings (Mallory and Haju, 1990). For group 3c, the first peak (-0.44 V, 1.76 mA/cm^2) is comparable to group 1c, 2a and 2b. As for the second peak (0.045 V, 37.3 mA/cm^2), smaller potential shift was observed and the current density also decrease by 16% to 37.3 mA/cm^2 when compared to group 1c. Addition of bi-pyridine seems to have a similar effect as cyanides ions as they both played the role of stabilizers in the plating solution. Lastly, in group 2d, the three

additives: triethanolamine, potassium ferrocyanide and bi-pyridine were added together. Three anodic peaks were observed instead of the usual two. The first peak at -0.44 V and 1.00 mA/cm^2 was similar to group 2a, 2d and 2c. For the second peak, it occurs at a higher potential of 0.087 V, which is even higher than group 2c. The corresponding current density is much lower at 35.3 mA/cm^2. It looks like the formation of Cu^{2+} is even more unfavourable when all the additives were included, this may due to the synergistic effect of potassium ferrocyanide and bi-pyridine.

7.1.3   Effect of surfactants

The effect of surfactants on the electrolessly plated copper has been discussed in great detail in chapter 6. This section focus on the electrochemical aspect, which uses cyclic voltammetry to generate response curves from the plating solutions.

Fig. 7.5 shows the cathodic scans of three electroless copper plating solutions employing different molecular weights of polyethylene glycol (PEG). The bulk of the electroless plating solution is the same as group 2d with additional PEG added at 2 g/L. One cathodic peak was observed for the all three curves. For group 3a, the reduction cathodic peak occurs at -1.17 V and the corresponding current density is -13.1 mA/cm^2. Comparing to the cathodic peak of group 2d (-1.22 V, -11.2 mA/cm^2), addition of PEG 600 seems favourable for Cu^{2+} reduction as the magnitude of current density is higher. For group 3b and 3c, the cathodic peaks occur at -1.17 V and -1.18 V respectively, and the corresponding current densities are -10.9 mA/cm^{2}and -12.1 mA/cm^2. These values again reflect that addition of PEG 4,000 and 10,000 do not hinder Cu^{2+} reduction.

Effect of PEG (Cathodic scan)

Fig 7.5 Cyclic voltammetry of various molecular weights of polyethylene glycol in the electroless plating solution (Cathodic scan, scan rate = 0.008 V/S)

The anodic scans of the three electroless copper plating solutions employing different molecular weights of PEG are shown in Fig. 7.6. All the three anodic scans exhibit two anodic peaks. The first anodic peak which relates to the formation of Cu^+, occurs at -0.44 V with the current density range from 1.29 - 1.57 mA/cm^2 for all the three curves. The first anodic peak is comparable with the group 2d. As for the second anodic peaks, which relate to the formation of Cu^{2+}, the various electroless plating solution exhibit slightly different results. For the plating solution employing PEG 600, the peak occurs at 0.041 V and 43.1 mA/cm^2. The second anodic peak for plating

solution employing PEG 4,000 occurs at 0.012 V and 41.2 mA/cm^2, and lastly for PEG 10,000, the peak occurs at 0.066 V and 43.1 mA/cm^2. The potential at which Cu$^+$ oxidation occurs is smaller in magnitude compared to group 2d. The corresponding current is notably higher by around 7.84 mA/cm^2. This suggests that addition of PEG favours Cu$^+$ oxidation and in turn affect the morphology of the plated copper.
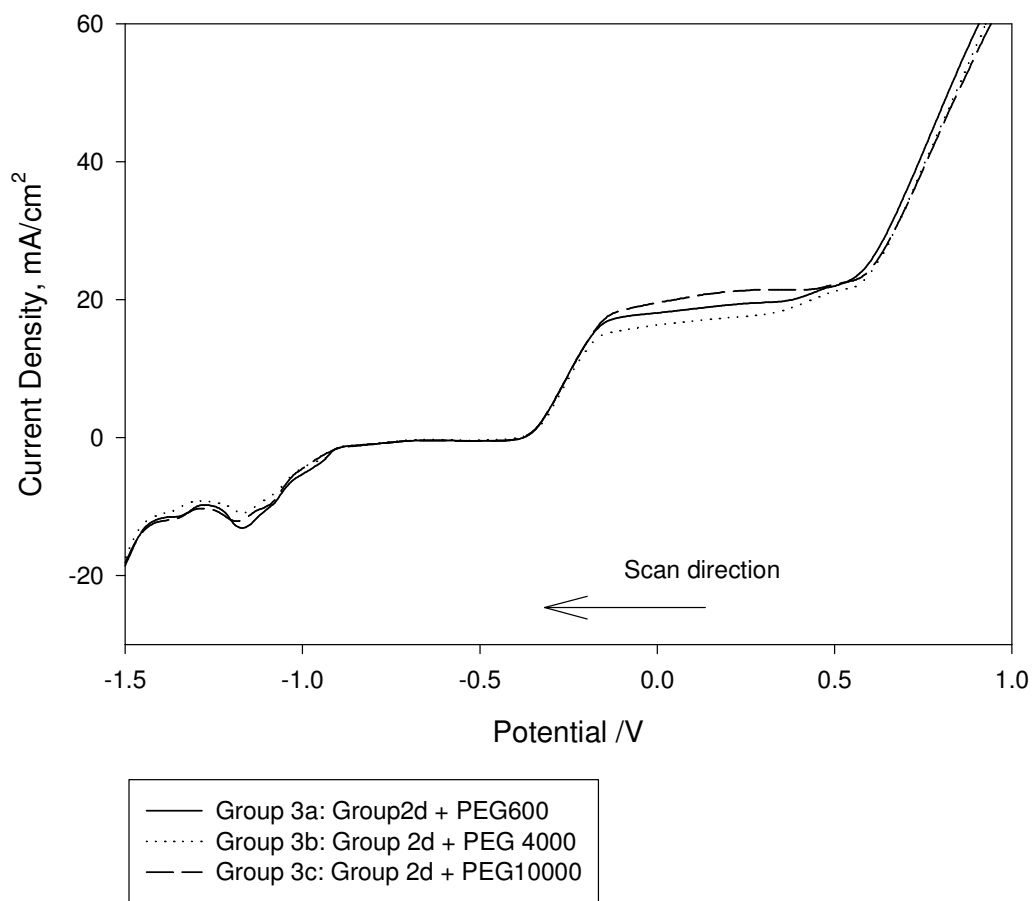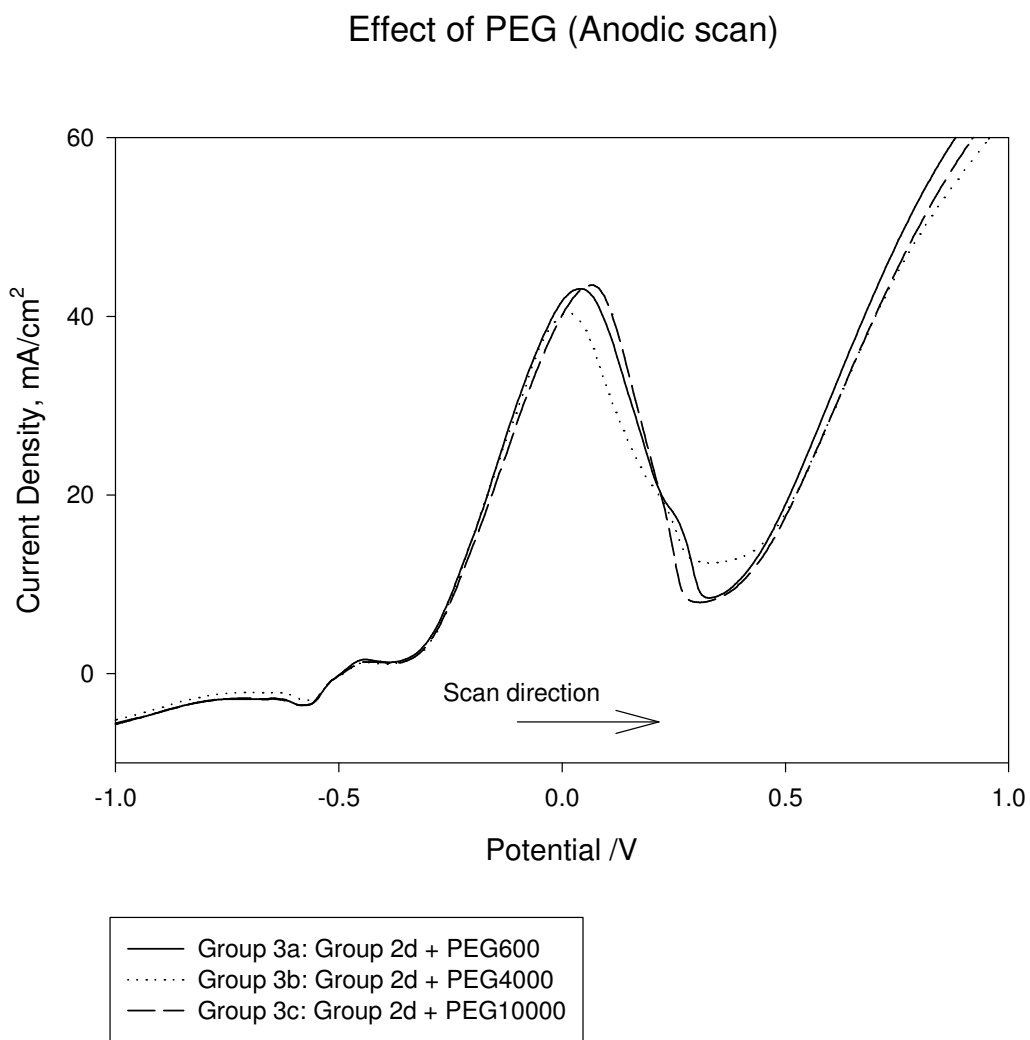
Effect of PEG (Anodic scan)

Fig 7.6 Cyclic voltammetry of various molecular weights of polyethylene glycol in the electroless plating solution (Anodic scan, scan rate = 0.008 V/S)

Chapter 8

Conclusions and Recommendations

8.1   Conclusions

Formaldehyde based electroless copper plating was successfully performed on acrylonitrile-butadiene-styrene (ABS) film. Electroless plating was carried out at 25 $^{\circ}$C and the plating solution was constantly stirred. The relationship between the deposited copper and the chelating agents, stabilizers and surfactants were investigated in detail.

The main chelating agents used include sodium potassium tartrate, trisodium citrate and potassium sodium salt of malic acid, which was used separately. They were selected because of their similar structures. Potassium sodium salt of malic acid produces the largest copper grain size and also the roughest surface. Kinetic analysis of the structurally similar chelating agents revealed the electroless copper plating solution employing trisodium citrate has the highest plating rate of 4.66 µm/hr, followed by potassium sodium salt of malic acid of 1.88 µm/hr. Sodium potassium tartrate has the lowest plating rate of 1.51 µm/hr. Crystallgraphic planes of (111) and (200) were found in all of the copper samples plated with various structurally similar chelating agents. Sodium potassium tartrate was found to be the preferred chelating agent. Cyclic voltammetry analysis revealed that the dual chelating agent system of sodium potassium tartrate and disodium EDTA electrochemically favours electroless copper deposition as compared to single chelating agent.

Selected amino acids were used to substitute bi-pyridine as the stabilizer of electroless plating solution. In the absence of bi-pyridine, the plating rate increases by about 14.5 times. When the plating solution was replaced with L-methionine (a sulphur

containing amino acid) having the same concentration, a high plating rate of 34.01 µm/hr was achieved. Double concentration of L-methionine lowers the plating rate to 23.66 µm/hr. This shows that certain range of L-methionine produces the highest plating rate. The inclusion of L-methionine produces fine grain copper structures similar to those obtained with bi-pyridine. The surface roughness generally increases with plating time. The other amino acid selected was glycine (a natural occurring amino acid). Fast decomposition of plating solution was observed and coarse grain structures of copper are formed. It seems that sulphur containing amino acids are related to the plating rate and grain size of deposited copper. Cyclic voltammetry analysis confirmed that stabilizers hinder the electroless copper deposition process.

The effect of additivies, in particular surfactants on the electrolessly plated copper was also examined. One particular class of surfactant: polyethylene glycol (PEG) was selected because they are known to modify the grain size and surface morphology. Various molecular weights of PEG were added separately to the plating solution containing sodium potassium tartrate as the main chelating agent. The concentration of PEG was set at 2.0 g/L. Highly uniform copper grain structures of about 100 - 200 nm in size were formed. Plating solution containing PEG 10,000 g/mol offers the smallest grain size. Thermal properties of ABS film were also changed with the addition of PEG. The second glass transition temperature (Tg) seems to increase with the molecular weight of PEG. Smaller copper particles are able to penetrate deeper into ABS polymer matrix and increase the order of crystallinity. Cyclic voltammetry shows that addition of PEG generally favours electroless copper deposition.

8.2   Recommendations

This fundamental research on the electroless copper plating chemistry can further elaborate on other areas as follows:

1) Replace formaldehyde with other less environmentally harmful chemicals such as hydrophosphite

2) Introduce more structurally similar chelating agents for purpose of comparison

3) The effects of pH and deposition temperature on the electroless plating process

4) More extensive application of transmission electron microscope on the uniform copper grains formed using polyethylene glycol

5) More in depth electrochemical analysis of the electroless plating process to complement the surface, kinetics analysis results

References

Baudrand, D. Electroless Processes. Plat. Surf. Finishing, v82, pp.57-81, Aug1995.

Bielinski, J. and Kaminski, K. Inorganic Compounds in Electroless Copper Deposition. Surf. Coat. Tech., v31, pp.223-233. 1987.

Bindra, P. and Roldan, J. Mechanisms of Electroless Metal Plating. Journal of Electrochemistry Society, v132, n11, pp.2581-2589, 1985.

Burke, L.D., Bruton, G.M. and Collins, J.A. The Redox Properties of Active Sites and the Importance of the latter in Electrocatalysis at Copper in Base. Electrochim. Acta, v44, pp.1467-1479, 1998.

Burke, L.D. and Ryan, T.G. The Participation of Interfacial Hydrous Oxide Species in Some Anodic Reactions at Copper Electrodes at Base. Journal of Electrochemistry Society, v137, n5, pp.1358-1364, 1990.

Coombs, C.F. Jr. Printed Circuits Handbook, 4th ed. pp.20.11, McGraw Hill, 1996.

Dean, J.A. Lange's Handbook of Chemistry, 12nd Edition, McGraw-Hill Book Company, 1979.

Decker, C.A. Electroless Copper Plating A Review: Part 1. Plat. Surf. Finishing, v82, pp.48-55, 1995.

Decker, C.A. Electroless Copper Plating A Review: Part 2. Plat. Surf. Finishing, v82, pp.58-64, 1995.

Donahue, F.M. Kinetics of Electroless Copper Plating. Journal of Electrochemcial Society, v127, n1, pp.51-55, 1980.

Dumesic, J, Koutsky, J.A. and Chapman, T.W. The Rate of Electroless Copper Deposition by Formaldehyde Reduction. Journal of Electrochemical Society, v121, n11, pp. 1405-1412, 1974.

El-Raghy, S.M. and Abo-Salama, A.A. The Electrochemistry of Electroless Deposition of Copper. Journal of Electrochemical Society, v126, pp.171-176, 1979.

Hajdu, J. Electroless Plating: The Past is Prologue. Plat. Surf. Finishing, v83, pp.29-33, 1996.

Hung, A. Electroless Copper Deposition with Hypophosphite as Reducing Agent. Plat. Surf. Finishing, v75, pp.62-65, 1988.

Hung, A. and Chen, K.M. Mechanism of Hypophosphite-Reduced Electroless Copper Plating. Journal of Electrochemical Society, v136, n1, pp.72-75, 1989.

Kissinger, P.T. and Heineman, W.R. Cyclic Voltammetry. J. Chem. Educ., v60, n9, pp. pp.702-706, 1983.

Kou, S.C. and Hung, A. Effect of 2,2'-dipyridine on Borate-Buffered Electroless Copper Deposition. Plat. Surf. Finishing, v90, n3, pp.44-47, 2003.

Lin, Y,M. and Yen, S.C. Effects of Additives and Chelating Agents on Electroless Copper Plating. Appl. Surf. Sci., v178, pp.116-126, 2001.

Lowenheim, F.A. Modern Electroplating, 3th Edition. pp.710, John Wiley & Sons, Inc, 1974.

Mallory, G.O. and Haju, J.B. Electroless Plating: Fundamentals and Applications. pp.289-322, American Electroplaters and Surface Finishers Society, 1990.

Martell, A.E. and Smith, R.M. Critical Stability Constants, vol 3: Other Organic Ligands. pp1-50, Plenum Press, New York & London, 1989.

Morrison, R.T. and Boyd, R.N. Organic Chemistry, 6th Edition, pp. 1210, Prentice Hall,1992.

Muller, G. and Baudrand, D.W. Plating on Plastics: A Practical Handbook, 2nd Edition. pp. 15-87, Robert Drapper Ltd, 1971.

Murphy, O.J., Srinivasan, S and Conway, B.E. Electrochemistry in Transition: From the 20th to the 21st Century. pp.479, Plenum Press, 1992.

Nuzzi, F.J. Accelerating the Rate of Electroless Copper Plating. Plat. Surf. Finishing, v70, pp.51-54, 1983.

Oita, M., Matsuoka, M. and Iwakura, C. Deposition Rate and Morphology of Electroless Copper Film from Solutions containing 2,2'-Dipyridyl. Electrochim. Acta, v42, n9, pp.1435-1440, 1997.

Paunovic, M. Ligand Effects in Electroless Copper Deposition. Electrochemical Society Journal, v124, n3, pp. 349-354, 1977.

Porter, M.R. Handbook of Surfactants, 2nd Edition. pp169-248, Blackie, London, 1994.

Sawyer, D.T., Sobkowiak, A. and Roberts, J.R. Electrochemistry for Chemists. pp. 68-69, John Wiley, New York, 1996.

Sawyer, D.T., Sobkowiak, A. and Roberts, Jr. J.L. Electrochemistry for Chemists, pp.1-23, John Wiley & Sons, 1995.

Schmacher, R, Pesek, J.J and Melroy, O.R. Kinetic Analysis of Electroless Deposition of Copper. J. Phys. Chem-US., v89, n20, pp.4338-4342, 1985.

Shacham-Diamand, Y., Dubin, V. and Angyal, M. Electroless Copper Deposition for ULSI. Thin Solid Films, v262, pp. 93-103, 1995.

Sze, S.M. Physics of Semiconductor Devices, 2nd Edition. pp. 392, John Wiley & Sons, 1981.

Vaskelis, A., Stalnionis, G. and Jusys, Z. Cyclic Voltammetry and Quartz Crystal Microgravimetry Study of Autocatalytic Copper (II) Reduction by Cobalt(II) in Ethylenediamine solutions. J. Electroanal. Chem., v465, pp.142-152, 1999.

Veleva, R. Role of Potassium Ferrocyanide in Electroless Copper Baths. Surf. Coat. Tech., v29, pp.87-93, 1986.

Vitkavage, D and Paunovic, M. Maximum Rate of the Cathodic Reaction in Electroless Copper Deposition, Plat. Surf. Finishing, v70, pp.48-50, 1983.

Tseng, W.T., Lo, C.H. and Lee, S.C. Electroless Deopsition of Cu Thin Films with $CuCl_2$-HNO_3 Based Chemistry. Journal of Electrochemical Society, v148, n5, pp. C327-C332, 2001.